UNCOVERING THE ROLE OF MICRORNA-206 IN DUCHENNE MUSCULAR DYSTROPHY

Karen Jennifer Bulaklak

A dissertation submitted to the faculty at the University of North Carolina at Chapel Hill in partial fulfillment of the requirements for the degree of Doctor of Philosophy in the Department of Pharmaceutical Sciences in the Eshelman School of Pharmacy.

Chapel Hill
2017

Approved by:

Xiao Xiao

Leaf Huang

Shawn Hingtgen

Joan Taylor

Charles Gersbach

ABSTRACT

Karen Jennifer Bulaklak: Uncovering the role of microRNA-206 in Duchenne muscular dystrophy
(Under the direction of Xiao Xiao)

Duchenne muscular dystrophy (DMD) is a severe muscle wasting disorder for which there is no cure. It is caused by a defect in the *dystrophin* gene, which encodes an important structural and regulatory protein at the muscle membrane. In DMD, the absence of dystrophin protein renders the muscle fragile and susceptible to damage. Patients gradually lose muscle mass and die prematurely from cardiac or respiratory complications. Current treatments are palliative and do not address the underlying cause.

Gene therapies that replace or correct mutated genes have shown promise for DMD. Recombinant adeno-associated viruses (rAAVs) are popular gene delivery vehicles because of their non-pathogenic nature and ability to establish long-term and efficient gene transfer. Still, restoring dystrophin is challenging and cannot completely alleviate motor deficits. While DMD is caused by a single gene defect, many secondary disease mechanisms are involved, such as ischemia and fibrosis. Thus, a strategy addressing multiple pathological mechanisms may be beneficial.

MicroRNAs (miRs) are small, regulatory RNA molecules that inhibit target gene expression. A skeletal muscle-restricted microRNA, miR-206, is highly upregulated in dystrophic muscle. Although its role in DMD is unclear, several miR-206 targets have

shown benefit for DMD, including vascular endothelial growth factor A (VEGFA) and utrophin. Counteracting miR-206 thus presents a viable treatment for DMD.

The goal of this study was to determine if downregulation of miR-206 would increase therapeutic gene expression, inhibiting secondary disease mechanisms and improving dystrophic symptoms. I demonstrated that a rAAV carrying antisense sequences against miR-206, AAV-anti-miR-206, can ameliorate motor deficits in dystrophic *mdx* mice. To understand its therapeutic mechanism, I focused on two prominent disease pathways.

Functional ischemia is a major contributor to the dystrophic phenotype and exacerbates muscle damage. Decreasing miR-206 appears to increase proangiogenic VEGFA expression, improving vascularization in *mdx* muscle. Also, overexpression of utrophin, a dystrophin paralog, can improve membrane stability and impede DMD progression. I observed increased utrophin in *mdx* muscle with miR-206 reduction, along with improved pathology, reduced fibrosis and delayed disease progression.

Altogether, this study characterizes a novel therapeutic strategy for DMD and sheds light on a contributing factor in secondary pathology.

ACKNOWLEDGEMENTS

Over the course of my studies, I have been extremely fortunate to have the support and guidance of my professors, peers, friends and family. I would first like to thank my committee members, Dr. Joan Taylor, Dr. Shawn Hingtgen, Dr. Charles Gersbach and Dr. Leaf Huang. I feel honored to be in the company of these exceptional scientists, who provided invaluable input for my project and also encouraged me to approach scientific questions critically, creatively and to always keep the broader impact of my work in mind. I would also like to thank my undergraduate mentor at Stony Brook University, Dr. Laurie Krug. I do not think I would have pursued my Ph.D. or have been admitted to the University of North Carolina if not for her constant support, patience and her faith in my ability to be a scientist.

I would like to thank my lab and especially my Ph.D. advisor, Dr. Xiao Xiao. I am very grateful that I was able to train in the Xiao laboratory and be amongst experts in the AAV gene therapy field. While my Ph.D. journey was not always easy, I had great co-workers who helped and encouraged me along the way. I would like to express my gratitude to Dr. Xiao, who has always believed in me and what I am capable of. His unending support inspired me to persevere through every failure during graduate school and will continue to be a major motivator throughout my career.

I would like to thank my friends in New York and in North Carolina, who have always been there to listen and comfort me during times of stress, happiness, loneliness

and everything in between. I thank my family and especially my parents, Cecilia and Cesar Bulaklak, who nurtured my love for science from the start and gave me everything I ever needed to pursue my dreams. I would like to thank my best friend and sister, Kristine. Even though she is younger than me, she is more of a grown up than I will ever be and I am amazed by all of her accomplishments. Lastly, I want to thank my boyfriend, Dr. Jonathan Clark, whom I look to for advice and encouragement, and to share every setback as well as every success in my life. Thank you for not charging me a consultation fee and for brightening each day with love and laughter.

TABLE OF CONTENTS

LIST OF TABLES

LIST OF FIGURES

LIST OF ABBREVIATIONS

AAV	Adeno-associated virus
ALS	Amyotrophic lateral sclerosis
AON	Antisense oligonucleotide
BCA	Bicinchoninic acid
BMD	Becker muscular dystrophy
bp	Base pair
cDNA	Complementary DNA
CK	Creatine kinase
CRISPR	Clustered regularly interspaced short palindromic repeats
DAPC	Dystrophin-associated protein complex
DIA	Diaphragm
DMD	Duchenne muscular dystrophy
DNA	Deoxyribonucleic acid
EBD	Evans blue dye
ECM	Extracellular matrix
F-actin	Filamentous actin
FBS	Fetal bovine serum
GAS	Gastrocnemius
GFP	Green fluorescent protein
GOI	Gene of interest
GRMD	Golden retriever muscular dystrophy

gRNA	Guide RNA
HAM	Hamstring
HGF	Hepatocyte growth factor
IGF-1	Insulin-like growth factor 1
ITR	Inverted terminal repeat
kDa	Kilodalton
MD	Muscular dystrophy
MEF2	Myocyte enhancer factor-2
mRNA	Messenger RNA
miR	MicroRNA
MOI	Multiplicity of infection
nNOS	Neuronal nitric oxide synthase
NMJ	Neuromuscular junction
NO	Nitric oxide
nt	Nucleotide
ORF	Open reading frame
PACT	Protein activator of the interferon-induced protein kinase
PBS	Phosphate-buffered saline
PCR	Polymerase chain reaction
PDE5	Phosphodiesterase inhibitor 5
qPCR	Quantitative polymerase chain reaction
QUAD	Quadricep
rAAV	Recombinant adeno-associated virus

RNA	Ribonucleic acid
SEM	Standard error of the mean
SMA	Spinal muscular atrophy
SRF	Serum response factor
TA	Tibialis anterior
TRBP	TAR RNA binding protein
UTR	Untranslated region
VEGFA	Vascular endothelial growth factor A
vg	Vector genome
WT	Wild-type

CHAPTER 1: INTRODUCTION

I. Muscular dystrophy

The muscular dystrophies (MDs) are a heterogenous group of rare genetic diseases characterized by progressive skeletal muscle degeneration and weakness. The MDs vary greatly in age of disease onset, severity, inheritance pattern, as well as muscle groups affected (Dalkilic and Kunkel 2003, Wallace and McNally 2009). Over 30 types of muscular dystrophy have been identified to date, which are classified into several major groups according to predominant distribution of symptoms (summarized in Table 1). These include: Duchenne and Becker MD, Emery-Dreifuss MD, congenital MD, limb girdle MD, facioscapulohumeral MD, distal MD and oculopharyngeal MD (Emery 2002). Despite sharing similar patterns of muscle weakness, MDs within each group can vary drastically in both clinical presentation and genetic etiology. For example, limb girdle muscular dystrophy can be further subdivided into 15 unique diseases (Guglieri, Straub et al. 2008). While the symptoms and causative genes for many MDs are known, current treatments are palliative and cannot prevent further muscle deterioration (Emery 2002).

Muscular dystrophies have been linked to mutations in 29 distinct genetic loci (Dalkilic and Kunkel 2003, Wallace and McNally 2009). These mutations lead to the loss of function in genes encoding components of individual muscle cells, or myofibers, such as the membrane (sarcolemma), cytoskeleton, extracellular matrix and nuclear

membrane. Defects in gene products involved in muscle membrane repair, such as dysferlin, have also been found (Cohn 2000, Dalkilic and Kunkel 2003, Wallace and McNally 2009). The majority of these genes encode constituents of the dystrophin-associated protein complex (DAPC), which spans across the sarcolemma and serves as a critical linkage between the extracellular matrix (ECM) and cytoskeletal actin fllaments (F-actin) that mediate movement (Figure 1). The DAPC provides mechanical stability to the sarcolemma by anchoring the cytoskeleton to the ECM as well as transmitting contractile force to the basement membrane to minimize stress on the lipid bilayer (Campbell and Stull 2003, Wallace and McNally 2009). Several proteins also participate in signaling cascades important for muscle development and maintenance (Jarmin, Kymalainen et al. 2014). The proteins within the DAPC can be classified into 3 distinct subcomplexes: the cytoskeletal proteins (dystrophin, syntrophins, α-dystrobrevin), sarcolemmal proteins (dystroglycan α and β subunits) and the sarcoglycans (α, β, γ and δ subunits) and sarcospan (Cohn 2000). The absence of any of these components renders the membrane fragile and susceptible to contraction-induced damage, eventually leading to muscle degeneration (Wallace and McNally 2009).

II. Molecular pathogenesis of DMD

Global muscle degeneration begins with myofiber necrosis caused by membrane permeability. Reduced membrane integrity results in high serum levels of muscle cytoplasm (sarcoplasm)-restricted enzymes, such as creatine kinase (Chargé and Rudnicki 2004). Membrane permeability and disorganization of structural components of the myofiber allow an unregulated influx of Ca^{2+} into the sarcoplasm, yet the mechanism

by which this occurs is not well-known. This event activates degenerative and well as reparative processes. Calcium-dependent proteases, such as calpains, degrade myofibrillar and cytoskeletal proteins, such as myosin, α-actinin, talin and vinculin. In addition, calpains can proteolytically cleave and thus activate other proteolytic enzymes, exacerbating injury. Raised intracellular calcium levels also stimulate dysferlin-mediated membrane repair; however, it cannot compensate for advanced muscle damage (Tidball 1995, Wallace and McNally 2009). The injured myofiber releases factors that activate and recruit resident and circulating inflammatory cells, predominantly neutrophils and macrophages. Following initial neutrophil infiltration (~1 to 6 hours post-injury), macrophages become more abundant (~48 hours later). These cells play complex roles in both promoting damage by releasing cytolytic factors and recruiting myogenic cells to initiate muscle repair (Chargé and Rudnicki 2004, Tidball 2005).

Following injury, myofibers release mitogens, such as hepatocyte growth factor (HGF), which activate muscle stem cells called satellite cells. Satellite cells are normally quiescent and reside in the basement membrane of the muscle. Once activated, satellite cells proliferate and are chemotactically drawn to the site of injury, where they produce muscle precursor cells, or myoblasts. Myoblasts then commit to the myogenic lineage, which is marked by myf5 and MyoD expression. Proliferating myoblasts continue to differentiate and fuse to existing fibers at the site of injury. In muscular dystrophy, normal regeneration may be impeded by defective muscle precursors, improper fusion or an unfavorable microenvironment (Wozniak, Kong et al. 2005, Wallace and McNally 2009). “Replicative aging,” which is defined as the premature senescence of muscle precursors, may also prevent regeneration due to telomere

shortening from constant proliferation (Wozniak, Kong et al. 2005, Wallace and McNally 2009).

In addition to muscle precursors, resident fibroblasts are stimulated in response to injury. Activated fibroblasts synthesize growth factors and extracellular matrix (ECM) components, including fibronectin, collagen I and III and proteoglycan, in order to promote cellular proliferation and provide a scaffold for infiltrating cells. Although fibroblast activity assists in proper regeneration in normal muscle, continuous damage and inflammation that are observed in muscular dystrophy results in permanent fibrotic deposition, ultimately replacing functional muscle (Serrano and Muñoz-Cánoves 2010). Satellite cells extracted from dystrophic mice have also been shown to overproduce collagen I and III (Alexakis, Partridge et al. 2007). Additionally, ECM components can sequester factors, such as insulin-like growth factor-1 (IGF-1), which are necessary for myoblast proliferation (Wallace and McNally 2009).

In summary, the dystrophic phenotype is marked by continuous muscle degeneration, usually initiated by genetic defects that impair the membrane, and the concurrent cellular processes, including inflammation, regeneration and fibrosis, which work to repair and exacerbate myofiber damage.

III. Duchenne muscular dystrophy

Originally described in 1851, Duchenne muscular dystrophy (DMD) is the most well-studied and common form of muscular dystrophy (~30% of MD cases), which affects about 1 in 3,500 male live births (Nonaka 1998). DMD is a sex-linked inherited muscle disorder that commonly affects young boys. The disease is characterized by progressive and debilitating weakness due to widespread degeneration in proximal

muscle (close to torso). Disease onset occurs in early childhood (~2 to 5 years of age) and initial symptoms include difficulties with walking, running and climbing stairs (Willmann, Possekel et al. 2009). About 20% of DMD patients also have some degree of mental impairment. Patients usually lose the ability to walk (non-ambulatory) in their early teens and cardiac and respiratory muscle failure are often observed in their late teens or early 20s. Presently available treatments, such as corticosteroid therapy, assisted ventilation and tracheostomy, have prolonged the lifespan of DMD patients. However, most eventually succumb to premature death in their 30s or 40s from pneumonia coupled with respiratory or cardiac insufficiency (Moser 1984, Emery 2002, Khurana and Davies 2003, Jarmin, Kymalainen et al. 2014). Becker muscular dystrophy (BMD) is a milder form of DMD that displays similar muscle distribution, but exhibits less severe symptoms and a slower rate of progression. Disease onset occurs later in life (~12 years of age) and patients survive well into their 40s and 50s (Blake, Weir et al. 2002, Emery 2002).

Duchenne and Becker muscular dystrophy are caused by mutations of the *dystrophin* gene, which encodes the 427 kDa dystrophin protein. In DMD, dystrophin is completely absent or greatly reduced in skeletal and cardiac muscle, while a truncated and partially functional dystrophin is present in BMD (Cohn 2000). Dystrophin was the first protein linked to muscular dystrophy pathogenesis and the recognition of its key role in muscle membrane integrity led to elucidation of other dystrophin-associated protein complex components. The full-length dystrophin protein can be organized into four major regions based on protein binding and sequence homology: the NH_2 terminal domain, central rod domain, cysteine-rich domain and the COOH terminal domain. At its

NH_2 terminus, dystrophin binds to cytoskeletal F-actin. The central rod domain contains 24 spectrin-like repeats interspaced by four proline-rich hinge regions that confer flexibility to the protein. Immediately following the central rod domain is the WW domain, which interacts with the dystroglycan and sarcoglycan DAPC subcomplex through binding β-dystroglycan. The cysteine-rich region is thought to bind intracellular cations (Ca^{2+} and Zn^{2+}) as well as calmodulin, a calcium-binding messenger protein that participates in calcium-dependent signal transduction. At its COOH terminus, dystrophin interacts with the cytoplasmic subcomplex of the DAPC by binding syntrophins and α-dystrobrevin (Blake, Weir et al. 2002). Due to its close interactions with these subcomplexes, the presence of dystrophin is essential for assembly of the entire DAPC. In muscle biopsies from dystrophic humans and mice, sarcolemmal localization of syntrophin β1, α-sarcoglycan, δ-sarcoglycan, α-dystroglycan and β-dystroglycan were dramatically reduced. Genetic defects in other sarcolemmal proteins, as in the case of certain limb girdle MDs and congenital MDs, did not affect normal distribution of other DAPC constituents (Ohlendieck and Campbell 1991, Ohlendieck, Matsumura et al. 1993). The loss of dystrophin also results in displacement of neuronal nitric oxide synthase (nNOS), which participates in signal transduction, at the sarcolemma (Wehling, Spencer et al. 2001, Kobayashi, Rader et al. 2008). Thus, the widespread and devastating muscle degeneration associated with DMD can be attributed to mutation of a single gene.

As previously stated, Duchenne muscular dystrophy is a recessive X-linked disorder, predominantly affecting males. The *dystrophin* gene can be mapped to the p21 locus on the X chromosome (Xp21). The gene is 2.5 Mbp in length and contains 79

exons, encoding a 14 kb transcript. Most mutations found in DMD patients are gross intragenic deletions of the dystrophin gene (~65% of cases). These deletions commonly occur in two “hotspots” that encompass exons 45 through 53 and exons 2 through 20. These regions encode part of the rod domain and actin-binding site along with part of the rod domain, respectively. About one-third of cases are due to small deletions or point mutations that result in non-sense or frame shift mutations, introducing a premature stop codon. The remaining cases of DMD result from duplications (1 to 5%), or intronic deletions (Blake, Weir et al. 2002, Muntoni, Torelli et al. 2003). No direct correlation between the size of the deletion and disease severity has been found. For example, missense mutations in the NH_2 terminal or cysteine-rich domain resulted in severe DMD phenotypes, while deletion of a large portion of the central rod domain (~46% of the dystrophin coding sequence) resulted in a mild case of BMD. As long as the normal open reading frame (ORF) is maintained, mutations in the dystrophin gene can be tolerated and in the case of BMD, produce a shorter, yet functional, protein.

IV. Animal models of DMD

Animal models of DMD have been used extensively to better understand disease pathology and develop new therapies. The most commonly used model is the dystrophin-deficient *mdx* mouse. The *mdx* mouse was first discovered in 1981 as a spontaneous mutant from a colony of C57BL/10 mice. These mice have a point mutation in exon 23 of the dystrophin gene that introduces a premature stop codon, which is found in about one-third of DMD patients. Unlike DMD patients who experience continuous muscle degeneration, *mdx* muscle pathology occurs in waves. An initial crisis of acute degeneration and regeneration is observed at 2 to 4 weeks, which is

marked by myofiber necrosis, centralized nuclei (actively regenerating fibers), variable myofiber sizes and elevated serum CK levels. By 8 weeks, muscle pathology returns to a chronic low level and fibrosis is not prominent in the hindlimb (Nonaka 1998, Grounds, Radley et al. 2008, Willmann, Possekel et al. 2009). In contrast, dystrophic pathology in the *mdx* diaphragm is severe and resembles the progressive degeneration, fibrosis and functional impairment found in DMD. By 6 months, a large number of diaphragm myofibers are necrotic and vary greatly in size. Also, the amount of connective tissue found in the *mdx* diaphragm is about 7 times greater than wild-type muscle and 10 times greater than the *mdx* hindlimb (Stedman, Sweeney et al. 1991). Overall, motor function deficits found in *mdx* mice are not as pronounced in those found in humans. Reduction in relative forelimb strength by ~50% has been observed at 4 months of age. Forced exercise regimes involving eccentric contraction, such as wheel running or treadmill running, have been utilized to aggravate dystrophic symptoms for better comparison of DMD treatments (Grounds, Radley et al. 2008). Finally, no respiratory or cardiac deficiencies are observed until later in life (6 and 16 months, respectively) and lifespan is only slightly shorter than wild-type mice (Willmann, Possekel et al. 2009).

Because of the milder phenotype of *mdx* mice, dystrophic murine models based on *mdx* have been generated by chemical and genetic manipulation informed by our understanding of dystrophin mutations present in DMD. For example, *mdx52* mice were created by disruption of exon 52 and have large deletions in the dystrophin gene, yet are histologically similar to *mdx* mice. Double knockout models have also been created to recapitulate muscle membrane fragility and exacerbate *mdx* pathology (Willmann, Possekel et al. 2009). Dystrophin/α-dystrobrevin (mdx; adbn$^{-/-}$) and dystrophin/α7

integrin (mdx; α7 integrin$^{-/-}$) are both examples of *mdx* mice lacking important structural membrane proteins. Another commonly used model is the dystrophin/utrophin double knockout (*mdx; utrophin*$^{-/-}$), which additionally lacks utrophin, an autosomal dystrophin paralog (Deconinck, Rafael et al. 1997). Compared to *mdx*, double knockout mice are extremely weak and skeletal and cardiac muscle display extensive necrosis and fibrosis. In addition, growth is stunted and spinal curvature (kyphosis) is observed. These mice also have a significantly lower body mass and dramatically reduced lifespan of 4 to 20 weeks (Deconinck, Rafael et al. 1997, Willmann, Possekel et al. 2009).

Dystrophin mutations have been identified in many dog breeds, including Rottweilers, Pembroke Welsh corgis, Labrador retrievers and most notably golden retrievers (Kornegay, Bogan Jr Fau - Bogan et al. , Nonaka 1998, Willmann, Possekel et al. 2009). The dystrophin-deficient golden retriever model (GRMD) is the most studied canine model. GRMD dogs possess a point mutation at the 3' splice site of intron 6, resulting in deletion of exon 7 and a frameshift in exon 8 (Nonaka 1998, Willmann, Possekel et al. 2009). Skeletal muscle lesions and cardiac pathology are more severe, which bears resemblance to DMD patients. In addition, GRMD dogs exhibit decreased respiratory capacity and motor function deficits, such as an uncoordinated, stiff gait and overall weakness. Death is usually caused by heart failure. Because of their similarities to human pathology, GRMD dogs have been extremely useful for evaluating potential therapies for muscular dystrophy (Khurana and Davies 2003, Willmann, Possekel et al. 2009).

V. Gene therapies for DMD

Gene therapy involves the use of nucleic acids (DNA or RNA-based) to improve cellular function. Gene-based strategies have successfully treated a plethora of diseases, including spinal muscular atrophy, hereditary blindness, hemophilia and metabolic enzyme deficiencies (Lu, Choi et al. 2006, Bainbridge, Smith et al. 2008, Burnett and Hooper 2009, Nathwani, Tuddenham et al. 2011, Bainbridge, Mehat et al. 2015, Chiriboga, Swoboda et al. 2016). Duchenne muscular dystrophy has been a popular focus for gene therapies due to a dearth of effective therapies and single gene defect. Multiple strategies targeted at the dystrophin gene have been employed: gene replacement, exon skipping and direct genome editing.

Gene replacement involves administration of a DNA sequence for the missing or defective protein. Viral vectors have been extremely useful for delivering the *dystrophin* sequence due to their prolonged transgene expression. Adenovirus-mediated delivery to the GRMD model resulted in moderate gene expression; however, a significant humoral and cellular immune response diminished dystrophin expression by 2 months post-treatment (Howell, Lochmuller et al. 1998). On the other hand, gene delivery attempts using recombinant adeno-associated viruses (rAAVs) were much more successful. To account for the small packaging size of AAVs (<5 kb), truncated dystrophin constructs ("mini-dysrophin" or "micro-dystrophin") were generated to include essential regions of the dystrophin protein (Wang, Li et al. 2000, Fabb, Wells et al. 2002, Sakamoto, Yuasa et al. 2002, Fairclough, Wood et al. 2013). In a notable example, mini-dystrophin constructs encoding the NH_2 terminal domain, cysteine-rich domain, central rod repeats (repeats 1 to 2 or 3 and 22 to 24) and variable hinge

regions were created (Wang, Li et al. 2000). These mini-dystrophin transgenes were packaged into the AAV2 capsid and injected intramuscularly into neonatal and adult *mdx* mice. Dystrophin and DAPC components at the sarcolemma were completely restored. As a result, dystrophic pathology was ameliorated, which was supported by normal myofiber morphology, increased membrane integrity, a reduction in centralized nuclei, decreased immune cell infiltration and absence of fibrosis. Greater improvements were observed with earlier intervention, but transgene expression was persistent at 6 months, regardless of age at treatment. A subsequent study reported that muscle from treated *mdx* mice showed increased contractile force, or the force generated by muscle (Watchko 2004).

In a following study performed in GRMD dogs, a mini-dystrophin construct was packaged into the AAV9 capid, which exhibits high transduction in striated muscle, and administered intravenously (Kornegay, Li et al. 2010). Dystrophin was present in nearly 100% of skeletal muscle and muscle from treated dogs largely mirrored murine histological findings. However, an innate immune response was detected. Coupled with transient immunosuppression, overall transgene expression was not affected and could be detected up to 2 years post-treatment. Studies using AAV6 to deliver a micro-dystrophin transgene to GRMD dogs have reported similar results, noting an immune response as well (Wang, Storb et al. 2012). Still, the immune responses reported did not adversely affect dystrophic pathology nor abrogate overall therapeutic value of these treatments. This response ultimately may be attributed to disease-associated inflammation and an animal model-specific reaction (ex. canine neutralizing antibodies). To this end, a Phase I clinical trial evaluating AAV-delivered mini-dystrophin found that

the humoral immune response could be minimized by AAV capsid modification (Bowles, McPhee et al. 2012). Further investigation has helped to clarify the contribution of the AAV vector in these responses and possible areas for improvement, which will be discussed in a later section (see *IV. Adeno-associated viruses*).

Exon skipping is another well-studied strategy that involves administration of antisense oligonucleotides (AONs), which hybridize to defective dystrophin precursor mRNA (premRNA) at specific splicing sites. Bound AONs would prevent splicing machinery from accessing these sites, effectively skipping certain exons to restore a normal open reading frame. The end product would be a truncated dystrophin protein to induce a milder phenotype as in BMD. Theoretically, most deletion, small and duplication mutations are amenable to skipping of one or two exons (79%, 91% and 73%, respectively) (Aartsma and Rus 2009). Due to the relatively short circulation time of AONs, chemical modifications have been made to increase oligonucleotide stability. Most preclinical and clinical phase studies have used 2'-O-methyl oligoribonucleotide and morpholino-based AONs (Lu, Mann et al. 2003, Aartsma and Rus 2009, Clement, Knop et al. 2009, Yokota, Lu et al. 2009, Cirak, Arechavala-Gomeza et al. 2011). In one particular study, adult and neonatal *mdx* mice were injected with morpholino-based AONs to skip exon 23 (Fletcher 2006). Sarcolemmal dystrophin expression was observed in 36% of fibers after intramuscular injection into the tibialis anterior muscle. Localized improvements were observed, with less centrally nucleated fibers and reduced mononuclear infiltration adjacent to the site of transgene expression. In a study with dystrophic dogs, a cocktail of morpholino AONs targeting exons 6 and 8 splice sites was evaluated (Yokota, Lu et al. 2009). Widespread dystrophin expression was

observed, which was accompanied by improvements in dystrophic pathology and stabilization of clinical symptoms.

Following promising preclinical results, several proof-of-concept clinical trials have been conducted in DMD boys (Kinali, Arechavala-Gomeza et al. 2009, Bowles, McPhee et al. 2012, Fairclough, Wood et al. 2013). A Phase I/II trial utilized a morpholino-based AON treatment targeted at exon 51, called Eteplirsen, which would be applicable to ~15% of patients. After treatment, patients expressed up to 32% of normal dystrophin levels. Results were dose-dependent and variable between patients, with some boys showing no changes in protein expression. In 2016, the FDA granted fast-track approval for Eteplirsen, which is contingent on evidence of functional improvements with treatment (Stein 2016). Nonetheless, the exon-skipping strategy faces major hurdles. AONs must be personalized for each mutation and each formulation would be considered an individual therapy subject to FDA approval. Oligonucleotides also suffer from poor uptake, which has been remedied by viral mediated delivery of exon-skipping sequences (Foster, Popplewell et al. 2012). Finally, the long-term effects associated with repeated oligonucleotide infusion are still unknown (Fairclough, Wood et al. 2013, Vila, Klimek et al. 2015). The recent approval of Nusinersen, an exon-skipping drug for spinal muscular atrophy, has strengthened hope in the field and may help to inform studies for future AON-based therapies for DMD (Dolgin 2017).

Genome editing has garnered a great deal of attention due to the development of new tools that increase specificity of gene correction. Adapted from prokaryotes, the CRISPR (clustered regularly interspaced short palindromic repeats)-Cas9 system has

been used by several groups to permanently excise defective dystrophin exons in the host genome. This approach is similar to exon skipping in that a shorter dystrophin protein is produced. The genome editing machinery consists of the Cas9 endonuclease, which cleaves the genome, and a guide RNA (gRNA) that directs Cas9 to a desired location. In one study, these components were delivered in separate AAV vectors to adult and neonatal *mdx* mice, which restored dystrophin expression in ~67% of myofibers. As a result, nNOS activity was restored and muscle function significantly improved (Nelson, Hakim et al. 2016). Another group showed that CRISPR/Cas9 could be used to correct dystrophin in the germ line of *mdx* mice. In progeny with 81% allele correction, dystrophin levels were indistinguishable from wild-type muscle and the dystrophic symptoms did not develop. Correction of 17% of alleles also displayed dystrophin expression in the majority of fibers and a milder pathology (Long, McAnally et al. 2014). Nevertheless, remaining obstacles with this strategy are low rate of correction, off-target cutting and a potential immune response to Cas9 (Calos 2016). Further study is necessary to find ways to overcome these limitations for treatment of DMD patients.

Vi. Surrogate therapies

Despite significant success with dystrophin-targeted therapies, remaining challenges have pointed to an incomplete understanding of disease pathobiology. After micro-dystrophin rescue, *mdx* mice still experienced fatigue after mild exercise (Kobayashi, Rader et al. 2008). Additionally, full restoration of mini-dystrophin expression in GRMD dogs failed to combat the progression of cardiomyopathy and joint contractures (Kornegay, Li et al. 2010). Several studies have shown that the profound

muscle degeneration observed in dystrophic muscle results from the contribution of secondary diseases pathways that exacerbate the primary genetic defect (Mendell, Engel et al. 1971, Deconinck and Dan 2007, Rosenberg, Puig et al. 2015). These findings have fueled investigation into surrogate therapies, which address aspects of DMD pathology aside from dystrophin loss. Gene therapies have utilized "booster genes" to ameliorate symptoms in the absence of dystrophin. Expression of booster genes targeting functional ischemia, inflammation, structural integrity, membrane instability, oxidative stress response and fibrosis have all shown impressive therapeutic benefit (Engvall and Wewer 2003). Two well-studied approaches will be discussed: improving muscle blood flow and increasing structural integrity.

Studies have indicated that dystrophic muscle is burdened by functional ischemia, or insufficient blood flow (Sander, Chavoshan et al. 2000, Nelson, Rader et al. 2014). Due to the displacement of nNOS at the sarcolemma, dystrophic muscle produces suboptimal levels of nitric oxide (NO), a potent vasodilator, in response to movement (Wehling, Spencer et al. 2001, Kobayashi, Rader et al. 2008). Reduced perfusion has been observed in DMD patients, which negatively impacted grip force (Nelson, Rader et al. 2014). Studies in rodents have also demonstrated that ischemia reproduced DMD lesions and was necessary for the development of the dystrophic phenotype (Mendell, Engel et al. 1971, Asai, Sahani et al. 2007). In one study, *mdx* mice were treated with rAAVs carrying the gene for vascular endothelial growth factor A (VEGFA) to increase capillary density. (Messina, Mazzeo et al. 2007). The VEGF family of growth factors serves as critical drivers of vascular formation during embryogenesis and post-natal growth. Binding of VEGFA with VEGF receptors is known to promote

endothelial cell migration, proliferation and survival, providing a framework for new vasculature. VEGFA also stimulates permeability, an effect that is dose-dependent and prominent in diseases such as cancer (Yancopoulos, Davis et al. 2000, Jain 2003). Localized expression of VEGFA increased capillary density in *mdx* muscle, particularly in regenerating regions, and reduced the number of necrotic fibers. Treatment also increased satellite cell activation and significantly improved forelimb strength (Messina, Mazzeo et al. 2007). The therapeutic value of increased muscle blood flow has been further supported by studies using pharmacological agents to induce vasodilation. Administration of phosphodiesterase 5 (PDE5) inhibitor, a potent vasodilator, improved cardiac function in *mdx* mice and also restored normal blood flow in DMD patients after exercise (Adamo, Dai et al. 2010, Nelson, Rader et al. 2014). While further investigation is necessary, mitigating functional ischemia appears to be a viable strategy for future DMD therapies.

Surrogate therapies have also aimed to increase structural integrity of the myofiber aside from dystrophin. One strategy is to increase the expression of utrophin, which is an autosomal paralog of dystrophin. Utrophin is found in all tissues and is normally localized at the neuromuscular and myotendinous junction of mature muscle. Utrophin is similar in size (395 kDa) and primary structure to dystrophin, especially at the NH_2, WW, cysteine rich and COOH terminal domains (Blake, Weir et al. 2002). Due to their structural homology, utrophin and dystrophin are believed to be functionally interchangeable, which may explain the milder phenotype of *mdx* (Deconinck, Rafael et al. 1997). While DMD patients also displayed utrophin increases in muscle, these levels were not sufficient for compensatory action (Khurana and Davies 2003).

Transgenic *mdx* mice that overexpressed full-length and a truncated utrophin at the sarcolemma did not develop any dystrophic symptoms. Furthermore, their muscle exhibited close to normal force generation (~80%) that persisted with repeated eccentric contractions, suggesting that utrophin and dystrophin are functionally redundant. Overexpression of utrophin also protected the myofiber from membrane damage and restored calcium homeostasis (Deconinck, Tinsley et al. 1997, Tinsley, Deconinck et al. 1998). To determine if utrophin-targeted gene therapy would be beneficial, a micro-utrophin construct was created encoding the NH_2, central rod repeats (1 to 3, 22) and cysteine-rich domains. The construct was packaged into an AAV6 vector and administered to *mdx; utrophin*$^{-/-}$ mice. Treatment increased utrophin and DAPC localization at the sarcolemma, which improved muscle fiber morphology and decreased central nucleation. Serum CK levels were also significantly reduced with treatment. Motor function deficits were also ameliorated; force generation increased and muscle injury from eccentric force was lessened with treatment (Odom, Gregorevic et al. 2008). Pharmacological interventions to increase endogenous utrophin levels have also been explored. A small molecule drug, SMT C110, increases utrophin transcription and provided therapeutic benefit in *mdx* mice (Tinsley, Fairclough et al. 2011). A clinical trial in DMD boys is currently underway (Tinsley, Robinson et al. 2014).

V. MicroRNA-206

Dysregulated microRNA profiles have been associated with a number of diseases, including schizophrenia, cardiac hypertrophy and cancer (Soifer, Rossi et al. 2007). MicroRNAs (miRNAs or miRs) are short (~21-24 bp) RNA molecules that serve as important regulators of gene expression. MicroRNA sequences are located in the

intronic region of protein encoding genes or in long non-coding RNAs. The majority of miRs are transcribed along with their respective protein encoding genes from a common promoter by RNA polymerase II (Pol II). Once transcribed, the miRNA hairpin within the primary mRNA (pri-mRNA) is recognized and cleaved by the nuclear microprocessor complex, composed of the ribonuclease enzyme Drosha and RNA-binding protein DGCR8. The resulting pre-miRNA (~60 nt) is recognized by exportin-5 and transported into the cytoplasm, where it is cleaved by Dicer into ~22 nt duplexes. One of the duplex strands is preferentially incorporated into the RISC complex with the help of cofactors such as TAR RNA binding protein (TRBP) and protein activator of the interferon-induced protein kinase (PACT). RISC will then cleave, degrade or preventing translation of hundreds of target transcripts, which is dictated by hybridization of the incorporated mature miRNA with complementary sequences in the 3' untranslated region (UTR) in the mRNA (Soifer, Rossi et al. 2007).

Four muscle-specific miRNAs, or myomiRs, have been identified: miR-1, miR-206, miR-133 and miR-208. These myomiRs play important roles in regulating gene expression in skeletal and cardiac muscle proliferation, differentiation and function. Expression of myomiRs is controlled by myogenic transcription factors (ex. SRF, MEF2 and MyoD) that direct transcription from gene clusters located on chromosome 20 (miR-1-1 and miR-133a-2), chromosome 18 (miR-1-2 and miR-133a-1) and chromosome 6 (miR-206 and miR-133b). Due to their involvement in multiple signaling pathways in muscle, strict control of myomiR expression is necessary (Williams, Liu et al. 2009).

A shared microRNA signature was discovered in DMD and *mdx* muscle, characterized by significant changes in 11 miRNAs. Levels of myomiRs miR-1 and miR-

206 were markedly decreased and increased, respectively, in dystrophic muscle compared to normal controls (Greco, De Simone et al. 2009). To ascertain whether dystrophin rescue normalized miRNA expression, *mdx* mice and DMD myotubes were treated with viral vectors encoding sequences to induce skipping of defective exons. In both cases, dystrophin rescue restored wild-type levels of all affected miRNAs, but not miR-206. Moreover, deregulation of miRs, such as miR-1 and miR-29, was linked to the abnormal oxidative stress response and fibrosis, respectively, typically observed in dystrophic muscle (Cacchiarelli, Martone et al. 2010). Thus, the miR-206 upregulation in DMD occurs independently of dystrophin loss and its contribution to disease pathology, if any, remains unclear.

Skeletal muscle-restricted miR-206 is highly expressed in regenerating muscle and serves as an important mediator of satellite cell differentiation via Pax7 inhibition (Chen, Tao et al. 2010). Transgenic miR-206 knockout mice develop normally, yet exhibit impaired regeneration in response to muscle damage. MicroRNA-206 gradually decreases with continued differentiation, but is relatively one of the most abundant miRs in adult skeletal muscle (McCarthy 2008). Compared to normal muscle, miR-206 levels are significantly upregulated in the *mdx* muscle and particularly in the diaphragm, which closely mirrors DMD pathology (McCarthy, Esser et al. 2007, Greco, De Simone et al. 2009). Elevated levels have also been discovered in myotonic dystrophy type I (DMI) patients (Gambardella, Rinaldi et al. 2010). Previous attempts have been made to elucidate the role of miR-206 in both DMD and amyotrophic lateral sclerosis (ALS) (Williams, Valdez et al. 2009, Liu, Williams et al. 2012). In these studies, *mdx* and ALS model mice were crossed with miR-206 knockout mice. Loss of miR-206 disrupted

skeletal muscle and neuromuscular synapse regeneration in each model, respectively. MicroRNA-206$^{(-/-)}$/*mdx* mice displayed a drastically worsened phenotype, suggesting a reparative role for miR-206. Since proper satellite cell functioning is necessary for adequate muscle regeneration in response to muscle damage, the additional loss of miR-206 may compound existing deficiencies in dystrophic muscle precursors. Still, these studies have only focused on myoblasts and do not address elevated miR-206 levels in mature muscle. Transgenic knockout also confound the possible contribution of other cell types present in the muscle. While miR-206 levels have been shown to be particularly high in the diaphragm compared to other muscle groups, the level myogenic proliferation in the diaphragm does not differ significantly from the hindlimb muscles (Anderson, Garrett et al. 1998, McCarthy, Esser et al. 2007). The notion that regenerating muscle is solely responsible for observed miR-206 levels is thus subject to question. Altogether, these findings denote a limited understanding of the function of miR-206 in dystrophic muscle overall, which warrants further study.

Interestingly, there is overlap between confirmed miR-206 targets and genes used for surrogate therapies. For example, studies in zebrafish have shown that miR-206 negatively regulates VEGFA and angiogenesis. Knockdown of miR-206 increased VEGFA expression and subsequently increased endothelial cell proliferation (Stahlhut, Suarez et al. 2012, Lin, Lee et al. 2013). Utrophin is another target of miR-206, which contains a miR-206 binding sequence that is shared between mice, humans and dogs. Induction of microRNA-206 expression *in vitro* has been shown to inhibit utrophin via its 3' UTR (Rosenberg, Georges et al. 2006). While elevated miR-206 levels are necessary for regulating differentiation-associated gene expression in muscle precursor cells, its

abnormal expression in dystrophic muscle may be detrimental by repressing proper responses to muscle damage. Altogether, miR-206 may be involved in downregulating beneficial gene expression, which points to a possible pathological role in DMD.

VI. Adeno-associated virus

Found ubiquitously in nature, the wild-type AAV is a small (~20 nm), non-enveloped Parvovirus with a DNA genome of about 4.8 kb. AAVs are naturally replication-defective, requiring helper virus functions for productive infection. Unlike other viruses commonly used for gene transfer, such as adenovirus and retroviruses, AAVs are non-pathogenic and have not been associated with any known disease. Recombinant adeno-associated viruses have been used extensively in basic research and therapeutics for their tissue tropism, favorable safety profile and ability to stably transduce tissue. These attributes have collectively made AAV-based gene therapies attractive for muscle diseases, such as DMD (Mezzina and Merten 2011).

The recombinant AAV genome is composed of an expression cassette containing a promoter, gene of interest (GOI) and poly-A signal, which is flanked on either side by inverted terminal repeats (ITRs). The ITRs are the only remnants of the wild-type AAV genome and are essential for proper orientation and packaging into the capsid (Mezzina and Merten 2011). To restrict expression to muscle, muscle-specific transcriptional regulatory elements have been utilized, such as the muscle creatine kinase (MCK) promoter and α-myosin heavy chain enhancer (Salva, Himeda et al. 2007). Gene therapies have also taken advantage of different AAV capsid variants, or serotypes, which display distinct receptor binding, tissue tropism and antigenicity. Twelve naturally-occurring serotypes, AAV1 through AAV12, have been isolated to date

(Asokan, Schaffer et al. 2012). AAV2 was the first identified serotype and has been used most frequently in muscular dystrophy trials. However, AAV1, AAV6, AAV7, AAV8 and AAV9 all display naturally high tropism in post-mitotic muscle, exceeding that of AAV2. These serotypes have demonstrated exceptional transduction in muscle (≥90%) after intravenous delivery, which would ensure efficient delivery to afflicted tissue (Qiao, Koo et al. 2011).

While rAAV gene therapies for DMD have many advantages, they still face vector- and disease-specific hurdles. AAV vectors have a limited packaging capacity of ~5 kb, which cannot accommodate the full-length dystrophin gene. Additionally, as many as 72% of the population has pre-existing neutralizing antibodies to the AAV2 serotype, which may obstruct AAV delivery to target tissue (Boutin , Calcedo, Vandenberghe et al. 2009). Employing an alternative serotype or mutant capsids are two strategies to avoid the Nab response, and can also work to reduce off-target effects and increase genetic payload (Kotterman and Schaffer 2014). Although the use of a mutant capsid minimized immunogenicity in a trial with DMD patients, there is also evidence of dystrophin-specific T cells present in some DMD patients (Mendell , Campbell et al. 2010, Bowles, McPhee et al. 2012). Thus, a greater understanding of DMD pathology and alternative strategies for treatment is necessary.

VII. Hypothesis & Specific Aims

As outlined in the previous sections, the lack of effective treatments for Duchenne muscular dystrophy warrants investigation into responsible pathological mechanisms and alternative therapeutic strategies. Challenges with dystrophin-targeted therapies have highlighted the role of secondary disease mechanisms, which

exacerbate dystrophic pathology. Surrogate therapies that address these mechanisms have significantly improved dystrophic symptoms. Studies have shown that microRNAs are dysregulated in dystrophic muscle and elevated microRNA-206 levels have been observed in muscle from both *mdx* mice and DMD patients compared to normal controls. However, the contribution of miR-206 in mature muscle to pathology is unknown. Overexpression of verified targets, VEGFA and utrophin, has demonstrated therapeutic benefit in animal models of DMD, pointing to pathological role for miR-206. Thus, I hypothesize that (1) miR-206 inhibits expression of therapeutic genes VEGFA and utrophin and (2) downregulation of miR-206 via an AAV9 vector ameliorates associated secondary disease pathways to improve dystrophic pathology. Focusing on two well-studied disease mechanisms, I will test these hypotheses in the following Aims:

(1) Deternine the role of miR-206 on muscle vascularization in *mdx* mice via VEGFA.

(2) Examine the role of miR-206 on muscle pathology in *mdx* mice via utrophin.

Disease	Inheritance pattern	OMIM number	Locus	Gene product
Dystrophinopathies				
Duchenne/Becker MD	Chromosome X	310200	Xp21.2	Dystrophin
Emery Dreifuss MD	Chromosome X	310300	Xq28	Emerin
Limb girdle MD (LGMD)				
Type 1A	Autosomal dominant	159000	5q31	Myotilin
Type 1B	Autosomal dominant	159001	1q21.2	Laminin A/C
Type 1C	Autosomal dominant	601253	3p25	Caveolin 3
Type 1D	Autosomal dominant	603511	7q	Not known
Type 1E	Autosomal dominant	603511	7q	Not known
Type 2A	Autosomal recessive	253600	15q15.1–q21.1	Calpain 3
Type 2B (Miyoshi myopathy)	Autosomal recessive	253601	2p13.3–p13.1	Dysferlin
Type 2C	Autosomal recessive	253700	13q12	γ-Sarcoglycan
Type 2D	Autosomal recessive	600119	17q12–q21.33	α-Sarcoglycan (adhalin)
Type 2E	Autosomal recessive	600900	4q12	β-Sarcoglycan
Type 2F	Autosomal recessive	601287	5q33	δ-Sarcoglycan
Type 2G	Autosomal recessive	601954	17q12	Telethonin
Type 2H	Autosomal recessive	254110	9q31–q34.1	E3-ubiquitin ligase
Type 2I	Autosomal recessive	606596	19q13.3	Fukutin-related protein
Type 2J	Autosomal recessive	Not available	2q24.3	Titin
Congenital MD (CMD)				
Merosin positive				
Rigid spine syndrome	Autosomal recessive	602771	1p36–p35	Selenoprotein N1
Ullrich syndrome	Autosomal recessive	254090	21q22.3	Collagen VI subunit α2
Merosin deficient without brain involvement				
Type 1A	Autosomal recessive	156225	6q22–q23	α2-Laminin (merosin)
Type 1B	Autosomal recessive	604801	1q42	Not known
Type 1C	Autosomal recessive	606596	19q13.3	Fukutin-related protein
CMD with brain involvement				
Fukuyama CMD	Autosomal recessive	253800	9q31	Fukutin
Walker-Warburg syndrome	Autosomal recessive	236670	9q34	*O*-Mannosyltransferase
Muscle–eye–brain disease	Autosomal recessive	253280	1p34–p33	POMGNT1

Table 1. Classification of the muscular dystrophies. Adapted from (Khurana and Davies 2003).

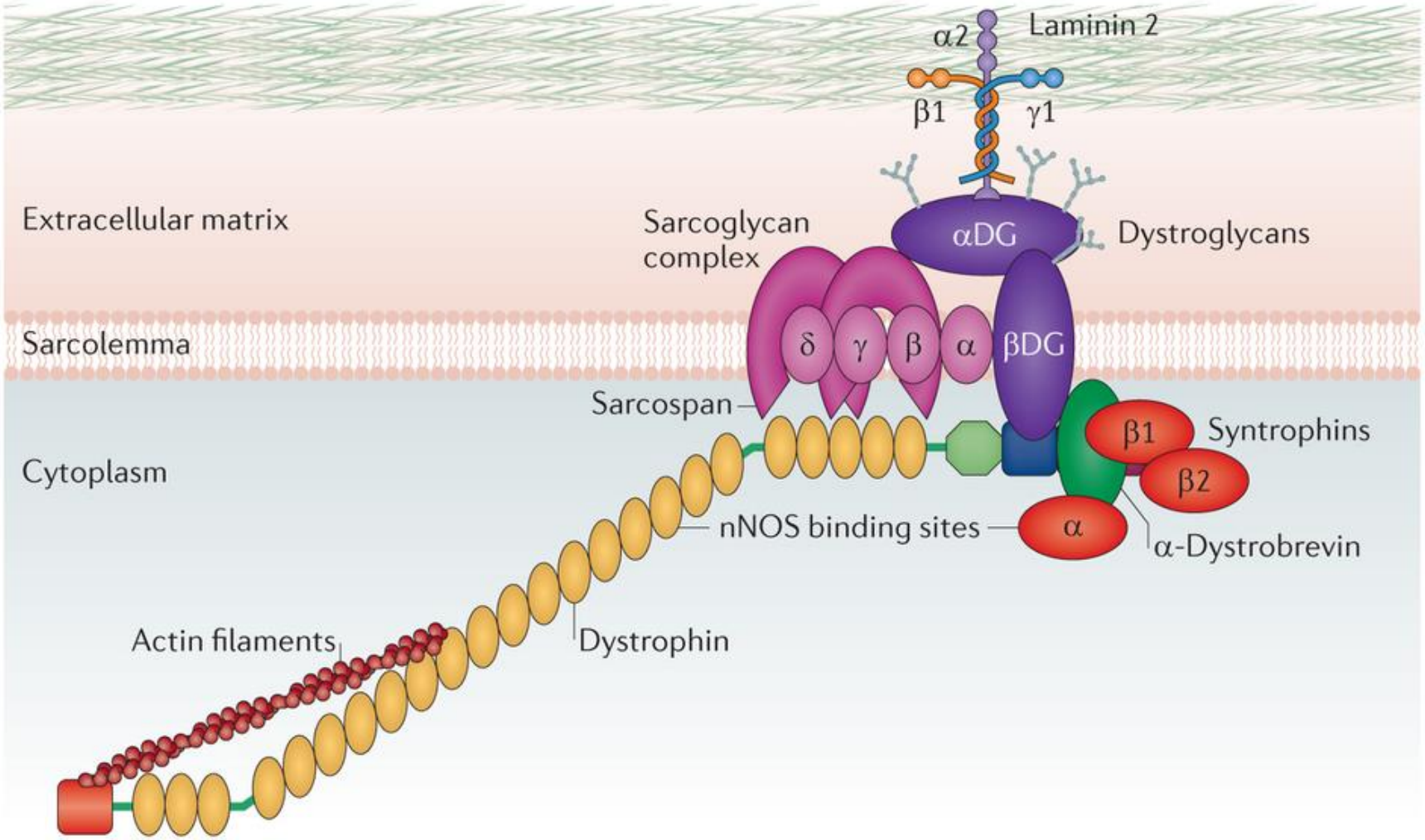
α2
Laminin 2
β1
γ1
Extracellular matrix
Sarcoglycan complex
αDG
Dystroglycans
Sarcolemma
δ
γ
β
α
βDG
Sarcospan
Cytoplasm
β1
Syntrophins
β2
nNOS binding sites
α
α-Dystrobrevin
Actin filaments
Dystrophin

Figure 1.1. Schematic diagram of the dystrophin-associated protein complex (DAPC) at the muscle membrane (sarcolemma). Dystrophin (in yellow) forms a linkage between inner actin filaments and extracellular matrix through its association with the transmembrane DAPC. Adapted from (Fairclough, Wood et al. 2013).

CHAPTER 2: DOWNREGULATION OF MICRORNA-206 IMPROVES MUSCLE VASCULARIZATION IN MDX MICE

I. Introduction

Several studies have demonstrated hemodynamic differences in muscle from normal patients and those with Duchenne muscular dystrophy (Sander, Chavoshan et al. 2000, Nelson, Rader et al. 2014). Dystrophin loss from the muscle membrane results in sarcolemmal delocalization of neuronal nitric oxide synthase (nNOS), which produces nitric oxide (NO) in response to skeletal muscle contraction. NO induces vasodilation by attenuating sympathetic vasoconstriction to allow for adequate blood flow (Grange, Isotani et al. 2001). Without proper localization of nNOS, dystrophic muscle suffers from functional ischemia, or insufficient blood flow that cannot meet metabolic demands. Compared to normal controls, *mdx* mice and DMD patients display reduced compensatory muscle oxygenation after exercise (Sander, Chavoshan et al. 2000, Latroche, Matot et al. 2015). Studies have also shown that functional ischemia is necessary for muscle necrosis in dystrophin-deficient mice, supporting a "two-hit" mechanism in dystrophic pathology (Rando 2001, Asai, Sahani et al. 2007). Therapeutic agents that induce vasodilation or increase muscle vascularization significantly improved muscle pathology as well as motor function in DMD and *mdx* mice (Ennen, Verma et al. 2013). Therefore, counteracting functional ischemia is a viable strategy for alleviating dystrophic symptoms.

Vascular endothelial growth factor A (VEGFA) is an important mediator in angiogenesis, stimulating endothelial cell proliferation, migration and survival

(Yancopoulos, Davis et al. 2000). AAV-mediated delivery of VEGFA to the *mdx* bicep significantly increased capillary density in regenerating regions and also reduced necrotic regions in muscle. VEGFA overexpression also significantly improved forelimb strength and increased muscle regeneration (Messina, Mazzeo et al. 2007). Still, VEGFA expression must be closely regulated as excessive levels may cause an imbalance of angiogenic signals. While many endothelial cells are recruited after administration of large doses of VEGFA, vessels are disorganized and leaky and may result in hemangioma formation (Carmeliet 2000). Thus, systemic application of VEGFA required to treat all of the muscle poses risks. Increasing endogenous expression of VEGFA may be a better alternative to avoid persistent overexpression from additional copies of the gene.

VEGFA is a target of microRNA-206, which is overexpressed in dystrophic muscle, yet its function in mature muscle is not well-understood. Studies in zebrafish have shown that miR-206 inhibits VEGFA expression and that disruption of miR-206 expression increased levels of VEGFA, stimulating angiogenesis (Stahlhut, Suarez et al. 2012, Lin, Lee et al. 2013). Thus, microRNA-206 may work to prevent endogenous VEGFA expression, contributing to functional ischemia in dystrophic muscle.

In this chapter, I aimed to determine whether miR-206 plays a role in DMD pathogenesis by inhibiting VEGFA expression and impeding proper muscle vascularization. First, I demonstrated that miR-206 can be effectively downregulated with an antisense construct, “anti-miR-206.” The anti-miR-206 construct was packaged into the AAV2 capsid to determine specificity *in vitro* and then into the AAV9 capsid and administered to *mdx* mice to examine therapeutic benefit. Functional improvements

were evaluated by rotarod, grip force and treadmill testing. VEGFA levels were assayed to determine the effect of treatment on miR-206 target expression. Capillary density was measured to determine the angiogenic effect of VEGFA. Finally, vessel permeability was investigated to determine the influence of VEGFA expression on endothelial cell organization and function. Findings from these studies could help to clarify the role of miR-206 and corroborate a new approach for treating DMD.

II. Materials and methods

AAV vector construction and production

Four tandem repeats of the antisense sequence against miR-206 (5'-CCACACACUUCCUUACAUUCCA-3') were previously generated through the UNC Nucleic Acids Core Facility. This sequence was cloned into the 3' untranslated region of a full length or truncated GFP coding sequence in the pEMBOL AAV vector plasmid, which contains ITRs for efficient viral packaging. The completed construct, "anti-miR-206," or the truncated GFP without miR-206 binding sites, "1/2gfp," were packaged into the AAV2 (in vitro analyses) or AAV9 (in vivo studies) capsid via triple-plasmid transfection in HEK293 cells. Briefly, 293 cells were propagated in Dulbecco's modified Eagle's medium (DMEM) in 15 cm plates supplemented with 10% fetal bovine serum (FBS) at 37°C in 10% CO_2/90% air. When cells reached 90-95% confluency, each plate was transfected with 18.7 μg vector plasmid (containing anti-miR-206 sequence), 25 μg Adenovirus helper plasmid and 6.25 μg AAV9 packaging plasmid diluted in a solution consisting of 2 ml 0.25M $CaCl_2$ and 2 ml cold HBS buffer (50 mM HEPES, 280 mM NaCl and 1.5 mM NaH_2PO_4; pH 7.1). For each virus preparation, 30 to 40 15 cm plates were used. Eight to twelve hours later, the medium was replaced with fresh DMEM supplemented with 2% FBS. At 60 to 68 hours post-transfection, cells and media were collected for AAV purification. Cells were resuspended in suspension buffer I (50mM HEPES, 150 mM NaCl, 50 mM NaH_2PO_4, 2 mM MgCl2, 2.5 mM KCl, pH 8.0) and freeze-thawed 3 times. The cell lysate was treated with DNAse (100 units/ml) and RNase A (4 units/ml) and incubated at 37°C for 1 hour. Debris was removed by centrifugation at 25,000 rpm at 4°C for 25 minutes. PEG-8000 and NaCl solution were

added to the clarified medium and incubated at 4°C overnight. For the culture medium, PEG-8000 and NaCl were added and incubated at 4°C overnight. The cell lysate and medium were centrifuged at 25,000 rpm for 30 minutes and resuspended in fresh suspension buffer. The solutions were combined and ultracentrifuged at 31,000 rpm for 16 hours in a CsCl density gradient. The AAV band was collected and subjected to a second round of CsCl density gradient ultracentrifugation at 38,000 rpm for 48 hours. The AAV band was collected in 1 ml aliquots and stored at -80°C.

AAV titer was quantified by dot blot hybridization. Ten microliters of AAV stock was added to 200 µl DMEM and treated with 50 µg/ml Dnase I at 37°C for 1 hour to degrade unencapsidated DNA. Then, 0.5 mg/ml proteinase K in 200 µl proteinase K buffer (20 mM Tris Cl pH 8.0, 20 mM EDTA pH 8.0, 1% SDS) was added and the sample was incubated at 55°C for 1 hour to degrade the capsid. The vector DNA was precipitated in 70% ethanol, 135 µmol sodium acetate and glycogen (40 µg) and centrifuged at 17,000 x g at 4°C for 10 minutes. The resultant pellet was resuspended in alkaline buffer (0.4 M NaOH and 10 mM EDTA pH 8.0) and bound to a hybridization transfer membrane (PerkinElmer). A standard of the original vector plasmid was applied to the same membrane. A biotin-labeled probe against CMV was hybridized to the membrane at 55°C overnight. Bound probe was detected using the North2South Chemiluminescent Nucleic Acid Hybridization and Detection Kit (Pierce). AAV titers were in the range of 10^{12} to 10^{13} vector genomes (vg)/ml. Virus intended for treatment were then dialyzed in dialysis buffer (2% mannitol, 6 mM $MgCl_2$ and 1X PBS) for a total of 8 hours with a buffer change every 2 hours.

In vitro specificity assay

MicroRNAs silence their target mRNAs through binding complementary sites within the 3' UTR and recruiting factors that degrade the mRNA or prevent translation. We hypothesized that the anti-miR-206 construct serves as a mock mRNA target for miR-206. To determine if miR-206 specifically bound and prevented expression of the GFP marker upstream of the anti-miR-206 sequence, we performed an in vitro specificity assay. CMV-GFP-anti-miR-206, CMV-pre-miR-206 and CMV-pre-miR-124 sequences were packaged into the AAV2 capsid by the triple transfection method described above (*AAV vector construction and production*). HEK293 cells were transduced with AAV2-CMV-GFP-anti-miR-206 (MOI: 10^6 vg/cell) alone or in combination with AAV2-pre-miR-206 (1X MOI: 10^6 vg/cell or 2X MOI: 2×10^6 vg/cell) or AAV2-pre-miR-124 (MOI for 1X: 10^6 vg/cell). After 48 hours, GFP expression was examined using a Nikon Eclipse TE300 microscope (Nikon USA) and a SPOT RT Slider camera (Diagnostic Instruments, Inc.).

Animals

Breeding pairs of homozygous females and hemizygous males for the *mdx* genotype (C57BL/10ScSn-Dmdmdx/J) were obtained from the Jackson Laboratory (Bar Harbor, ME). Male *mdx* mice were treated with PBS or 10^{12} vg of AAV9-anti-miR-206 at 8 weeks of age via tail vein injection. Wild-type C57/B6 mice were also used for comparison. Animals were anesthetized with 2.5% avertin (total dose of 250 mg/kg) and sacrificed at 1, 3 and 5 months post-treatment. Extracted muscle was snap-frozen in liquid nitrogen-cooled isopentane. Extracted muscle was stored at -80°C for future analysis. All experiments using mice were approved by the Institutional Animal Care

and Use Committee at the University of North Carolina at Chapel Hill and in accordance with the National Institute of Health guidelines.

Motor function testing

AAV9-anti-miR-206, AAV9-1/2GFP (control vector) and PBS treated mice were subjected to grip force test, rotarod testing and treadmill running to examine motor function at baseline, then 1 month after vector administration and repeated every two weeks until sacrifice. Forced exercise also increases muscle damage in *mdx* hindlimb, which otherwise shows only mild dystrophic symptoms, for better comparison of untreated and treated groups. Grip force test was used to measure the forelimb strength of the mice. A grip force meter (Chantillon, model DFIS-2) was used. Mice were held by the tail and allowed to grasp the attached bar with their front paws. The mice were then pulled back quickly to measure grip force. Rotarod testing was performed on a rotarod machine (Med Associates, Inc.) to examine balance, motor coordination and grip strength. Mice were placed on the rod and allowed to acclimate for 1 minute. The rod was then accelerated from 4 to 40 rpm over 5 minutes. The time to first fall was recorded and used for analysis. Treadmill running was performed to test endurance. Mice were allowed to acclimate to the treadmill (Harvard Apparatus) at a speed of 5 meter/min (m/min) for 60 seconds. The speed was increased to 10 m/min for 15 minutes and then increased by 5 m/min after every 10 minutes. The shock grids at the end of each lane were set to 1 mA to encourage mice to run until exhaustion. If a mouse failed to run and remained on the grid for 10 seconds, the test was terminated and the mouse was removed immediately. The total run time at each speed was recorded to calculate total distance for statistical analysis.

MicroRNA-206 quantification

Total RNA was extracted from diaphragm muscle using the TRIzol reagent (Thermo Fisher Scientific) and stored at -80°C until further use. A cDNA template for microRNAs was created using the miRNA 1st-Strand cDNA Synthesis Kit (Agilent Technologies). The resulting template was diluted 1:5 for quantitative PCR (qPCR). Reactions were set up using PowerUp SYBR Green Master Mix (Thermo Fisher Scientific) according to the manufacturer's protocol and run in an Applied Biosystems 7300 Thermocycler. MicroRNA-206 expression was quantified relative to ubiquitous miR-26b. The primers used were as follows: miR-206 (5'-GGCTGGAATGTAAGGAAGTGTGTGG-3'), endogenous miR-26b (5'-GGCCGTTCAAGTAATTCAGGATAGGT-3') and a universal reverse primer provided with the cDNA synthesis kit (proprietary sequence). Expression was depicted as fold-change over control.

VEGF-A transcript quantification

A cDNA template was reverse transcribed from total RNA using the High-Capacity Reverse Transcription kit (Thermo Fisher Scientific). The resulting template was diluted 1:5 for qPCR. Reactions were set up using PowerUp SYBR Green Master Mix (Thermo Fisher Scientific) according to the manufacturer's protocol and run in an ABI 7300 Thermocycler. VEGF-A expression was quantified relative to ubiquitous beta-actin. The primers used were as follows: VEGF-A (forward: 5'-GGCCTCCGAAACCATGAACTT-3' and reverse: 5'-TGGGACCACTTGGCATGGTG-3') and beta-actin (forward: 5'-ATCACTATTGGCAACGAGCG-3' and reverse: 5'-ACTCATCGTACTCCTGCTT-3'). Expression was depicted as fold-change over control.

Western blot

Tibialis anterior (TA) muscle was homogenized in cold RIPA buffer (150 MM NaCl, 1% Triton X-100, 0.5% sodium deoxycholate, 0.1% SDS, 50 mM Tris pH 8.0) using a tissue homogenizer (Tekmar Ultrasonic Processor model TM130). Protein concentration was determined by BCA assay (Thermo Fisher Scientific). For Western blotting, 20 µg of protein from each sample was prepared in 6X loading buffer (375 mM Tris pH 6.8, 12% SDS, 60% glycerol, 0.6 M DTT, 0.06% bromophenol blue) and heated at 95°C for 5 minutes. Proteins were separated by SDS-PAGE and wet transferred onto a PVDF membrane using the Bio-Rad Mini-PROTEAN II system. Membranes were blocked in 5% milk in 1% TBS-Tween 20 (TBS-T) for 1 hour and incubated with either rabbit polyclonal antibody against VEGF-A (Abcam, catalog #ab46154, 1:1000) or rabbit polyclonal antibody against GAPDH (Sigma-Aldrich, cat. # G9545, 1:10,000) diluted in 3% bovine serum albumin (BSA) in 1% TBS-T overnight at 4°C. Membranes were washed 3 times for 10 minutes in 1% TBS-T and then incubated with anti-rabbit IgG conjugated to horseradish peroxidase (Sigma-Aldrich, A0545, 1:5,000 for VEGF-A and 1:10,000 for GAPDH) in 5% milk. Blots were developed using the Western Lightening Pro chemiluminescence kit (PerkinElmer) and visualized using the FluorChem M imaging system (ProteinSimple).

Vessel quantification

Cryosections of diaphragm muscle 10 µm thick were made. At room temperature, slides were washed in PBS for 10 minutes then blocked in 10% horse serum for 1 hour. The muscle basal lamina was immunostained with a rat anti-laminin α2 antibody (Sigma-Aldrich, L0663, 1:500) in 1% horse serum in PBS for 1 hour and washed with

0.5% PBS-T 3 times for 5 minutes each. Anti-rat IgG conjugated to Alexa Fluor 488 dye (Molecular Probes, #A21470) and a *Griffonia simplicifolia I* lectin (GSLI) conjugated to rhodamine dye (Vector Laboratories, #RL-1102) for staining endothelial cells were diluted in 1% horse serum and used to incubate slides for 1 hour. Slides were washed with 0.5% PBS-T 3 times for 5 minutes each and mounted with aqueous mounting media (Gel/Mount, Biomeda). Slides were visualized using a Zeiss Axiovert 200M Confocal Microscope and images were taken using an AxioCam MRm camera. Images were processed using AxioVision Rel 4.6 and analyzed using ImageJ software.

Miles assay

Evans blue dye (EBD), an azo dye with high affinity for serum albumin, was used for Miles assay to test vessel function/integrity in mice. While normal vessels are impermeable to albumin, leaky vessels allow albumin and thus dye to disperse into the muscle parenchyma (Radu and Chernoff 2013). A 10 mg/ml solution of EBD was made in PBS and 2 mg total was injected in mice via the tail vein. After 30 minutes, mice were anesthetized with i.p. injection of 2.5% avertin and cervically dislocated. Muscle dissection was performed as quickly as possible to avoid increased vessel permeability after death. Each dissection was performed within 15 minutes. Muscle was weighed, placed in 500 µl formamide and incubated at 55°C for 24 hours to fully extract dye. A standard was created with EBD in formamide was run concurrently with samples in a 96 well plate. EBD absorbance was measured at 550 nm using the Perkin Elmer Victor^2 1420 Multi-label Counter/Plate-reader.

Statistical analysis

Graphs were generated and statistical analysis was performed using GraphPad 5.0 software. Unpaired, two-tailed t-tests with Welch's correction were performed when comparing two groups. One-way ANOVA was performed to determine treatment effect for Miles assay experiments. P values <0.05 were considered statistically significant.

III. Results

Anti-miR-206 specifically binds miR-206

AAV vector plasmids were generated encoding the “anti-miR-206” sequence (Fig. 1A). A CMV promoter drove the expression of either GFP or a truncated GFP gene (for *in vivo* studies, not shown), followed by four tandem repeats of the exact antisense sequence against miR-206. Specificity for miR-206 was tested by packaging the anti-miR-206 construct, the pre-miR-206 sequence and non-specific miR-124 sequence into the AAV2 capsid to transduce HEK293 cells (Fig. 1B). In AAV2-GFP-anti-miR-206 transduced cells (first row), GFP levels were high, which suggests that the construct was efficiently packaged and the AAV vector was fully functional. In addition, cells did not show any signs of stress, such as contraction or cell death, following AAV transduction. Co-transduction with an equal amount of AAV2-pre-miR-206 greatly diminished GFP expression (second row), while expression was completely inhibited with additional pre-miR-206 (third row). Conversely, co-transduction of AAV2-GFP-anti-miR-206 and non-specific AAV2-pre-miR-124 (fourth row) had no effect on GFP intensity. Thus, miR-206 specifically decreased expression of a GFP gene containing anti-miR-206 sequences in its 3’ untranslated region.

Motor function improvements with anti-miR-206 treatment

PBS, AAV9-1/2GFP or AAV9-anti-miR-206 (10^{12} vg per mouse) were tail vein injected into 8 week-old *mdx* mice. One month following treatment, motor function testing was performed every two weeks until sacrifice. Anti-miR-206 treated mice demonstrated a significant increase in rotarod run times compared to PBS treated mice at 1 month post-treatment (Fig. 2A, untreated mean = 90.95 $\pm$ 95 sec, sham vector

mean = 116.2 ± 28.83 sec, treated mean = 150.9 ± 18.61 sec, **p = 0.0105). While there was no major distinction at 3 months (Fig. 2B, PBS mean = 148.7 ± 18.78 sec, sham vector mean = 151.3 ± 12.16 sec, treated mean = 164.4 ± 16.69 sec), anti-miR-206 treated mice again performed significantly better (201.1 ± 25.86 sec) than the untreated groups (90.25 ± 20.70 sec and 95.40 ± 12.24 sec, for PBS and vector control) at 5 months post-treatment (Fig. 2C, **p = 0.0044 and **p = 0.0038 for PBS and vector control). Over the course of 5 months, rotarod run time in untreated *mdx* mice was stagnant, with only a slight increase at 3 months. On the other hand, miR-206 reduction appeared to positively impact run time within the given time span. Grip force testing did not reveal any significant differences in strength between the groups until 4 and 5 months post-treatment (Fig. 2D, 4 month PBS mean = 74.61 ± 8.379 g, vector control mean = 69.55 ± 14.05 g, treated mean = 96.24 ± 4.867 g, *p = 0.0372 and *p 0.0277 between treated and PBS and vector control, respectively. 5 month PBS mean = 79.49 + 9.808 g, sham vector mean = 67.63 ± 18.875 g, treated mean = 106.9 ± 7.345 g, *p = 0.0376 and *p = 0.0455 between treated and PBS and vector control, respectively). At 3 months, control mice began to experience a decline in strength, while treated mice continued to improve. In contrast, no obvious differences in treadmill running were seen between the groups over the course of 5 months (Fig. 2E, 2F, 2G).

MicroRNA-206 levels in the muscle

Since no differences were observed between the PBS and control vector groups, the PBS group was considered the control or “untreated” group. MicroRNA-206 levels in the diaphragm muscle were investigated by relative qPCR in WT, *mdx* and *mdx* treated with AAV9-anti-miR-206. At the 1 month timepoint, dystrophic muscle miR-206 levels

were significantly greater than the WT, with a difference of ~4-fold (Fig. 3A, **p=0.0055, n = 6). Anti-miR-206 treatment reduced the amount of miR-206 in the diaphragm by about half, but considerable variation between treated samples was observed (p=0.2891, n = 6). Two months later, WT levels were still low, yet a substantial increase in miR-206 was detected in untreated *mdx* (Fig. 3B, ***p < 0.0001, n = 6). Vector treatment significantly decreased miR-206 by almost half (*p=0.0341, n = 6). However, there was no noticeable difference between the treated and untreated *mdx* at 5 months (Fig. 3C, p=0.9753, n = 6).

VEGFA expression increases with treatment

VEGFA expression was first examined using relative qPCR to measure transcript levels in WT, *mdx* and treated *mdx* diaphragm. At 1 month, VEGF mRNA levels were significantly lower in the dystrophic diaphragm (Fig. 4A, *p = 0.0198, n = 6). With treatment, transcript levels appeared to increase albeit not significantly (untreated vs. treated, p = 0.0509, n = 6). Two months later, a significant ~2-fold increase in VEGF transcripts was found in the treated group vs. the untreated (Fig. 4B, **p = 0.0026, n = 6), surpassing expression of the WT. This 2-fold increase was sustained until the 5 month timepoint; however, this difference was not statistically significant (Fig. 4C, p = 0.0683, n = 6). Within the given timeframe, *mdx* VEGF transcript levels were consistently (~2-fold) lower than the WT. A significant decrease was again observed between WT and *mdx* muscle (Fig. 4C, ***p < .0001, n = 6) at 5 months.

The amount of VEGFA protein was assayed by Western blot at tibialis anterior muscle samples at 1 month post-treatment (Fig. 5). Bands were observed at ~35 kDa,

which is indicative of ubiquitous VEGFA-164 isoform expression. A noticeable increase in VEGFA was observed with treatment compared to WT and untreated *mdx.*

Increased capillary density with miR-206 reduction

To determine if VEGF expression induced angiogenesis, the number of capillaries per muscle fiber was quantified in the diaphragm. At 1 month, there was no obvious difference in vessel density between the untreated and treated groups (Fig. 6A). A statistically significant decrease in capillary density was found between WT (mean = 2.184 $\pm$ 0.1108) and *mdx* (mean = 1.788 $\pm$ 0.0551) muscle (*p = 0.0495, n = 6), but not in the treated sample (mean = 1.817 $\pm$ 0.0333, n = 6). Capillary density in WT and treated muscle stayed fairly consistent at 3 months (Fig. 6B). In contrast, capillary numbers were further reduced in the *mdx* (mean = 1.503 $\pm$ 0.0581) compared to WT (mean = 2.347 $\pm$ 0.1022, ***p = 0.0008, n = 6) as well as treated *mdx* muscle (mean = 1.982 $\pm$ 0.0672, ***p < 0.0001, n = 6). A significant difference was also observed between WT and treated *mdx* groups (WT mean = 2.141 $\pm$ 0.1282, *p = 0.0244, n = 6). At 5 months, vessels were again more numerous in the treated vs. untreated *mdx* muscle (2.123 $\pm$ 0.2065 vs. 1.574 $\pm$ 0.0708, *p = 0.0258, n = 6). Significantly fewer capillaries were found in the untreated muscle compared to the WT (**p = 0.0043, n = 6).

Vessel permeability is reduced with treatment

Vessel permeability in response to treatment was determined by Miles assay after 1, 3 and 5 months in quadriceps (QUAD), hamstring (HAM), gastrocnemius (GAS) and tibialis anterior (TA) muscles. In WT muscle overall, Evans blue dye (EBD) content was fairly consistent across muscle groups at all timepoints (1 month mean = 0.01753 $\pm$

0.001089 ng/mg, 3 months mean = 0.02460 ± 0.001015 ng/mg, 5 months mean = 0.01796 ± 0.001171 ng/mg). EBD content in dystrophic muscle was significantly greater than WT (1 month mean = 0.03021 ± 0.003278 ng/mg and *p = 0.0349, 3 months mean = 0.03548 ± 0.002087 ng/mg and **p = 0.0094, 5 months mean = 0.02788 ± 0.002463 ng/mg and *p = 0.0220). A significant decrease in EBD was found in treated muscle at 3 and 5 months post-treatment compared to the untreated group (3 month mean = 0.02490 ± 0.002746 ng/mg and *p = 0.0278, 5 month mean = 0.01895 ± 0.001904 ng/mg and *p = 0.0351). At 1 month post-treatment, EBD levels were lower in anti-miR-206 treated muscle (mean = 0.02073 ± 0.002114 ng/mg), but this was not statistically significant (p = 0.0592). Two-way ANOVA analysis revealed that these results were dependent on treatment only (1 month ***p = 0.0008, 3 months *p = 0.0101, 5 months *p = 0.0129) and not muscle group (1 month p = 0.0881, 3 month p = 0.3252, 5 month p = 0.5205). In addition, there was no significant interaction between treatment and muscle group (1 month p = 0.8203, 3 month p = 0.9449, 5 month p = 0.8125).

IV. Figures

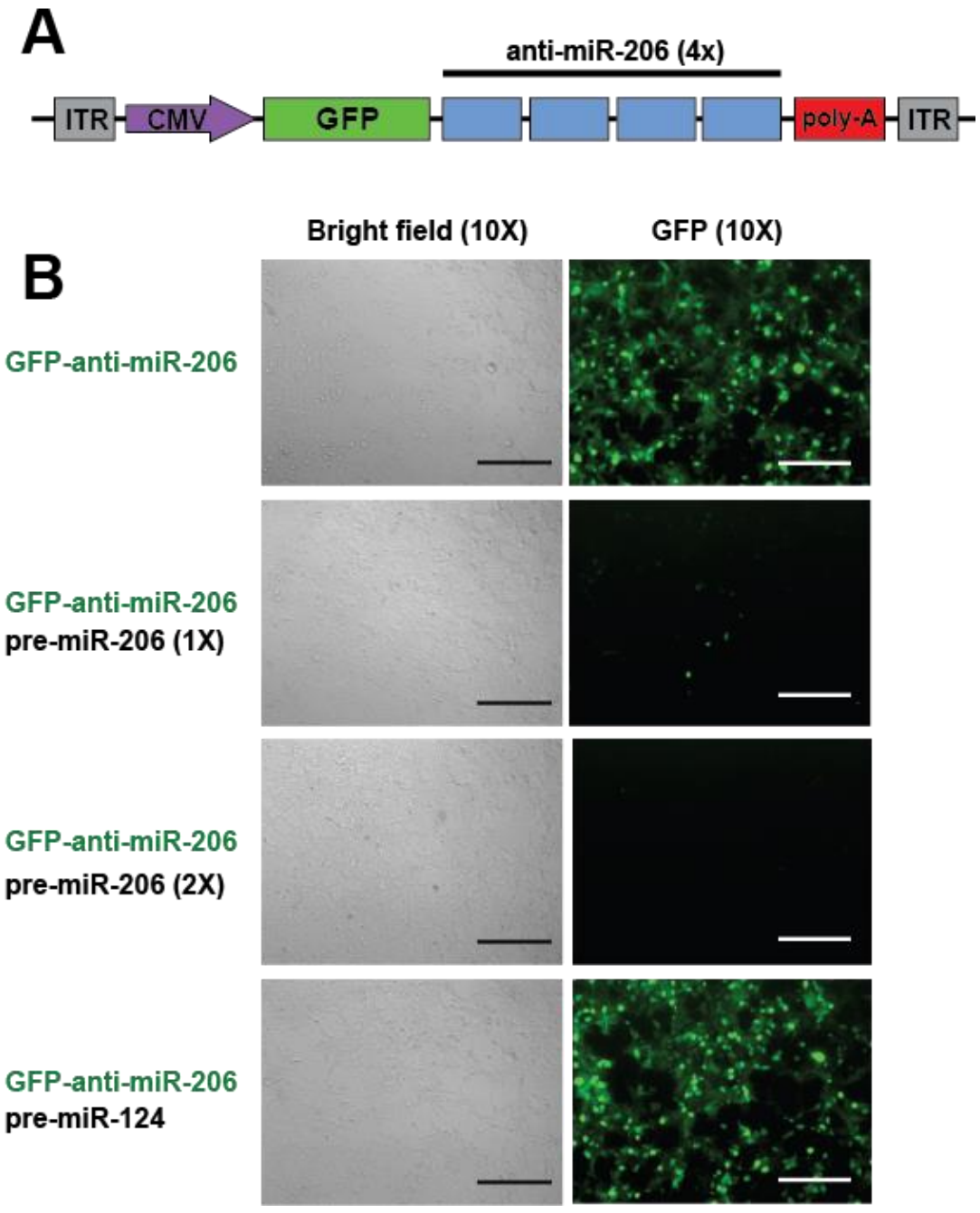

Figure 2.1. Vector construct design and miR-206 specificity. (**A**) Anti-miR-206 construct design. Four tandem repeats of the exact antisense sequence were placed in the 3' UTR of a GFP expression marker driven by a CMV promoter. The sequence was

followed by a poly-A signal and flanked by ITRs on either side for packaging into the AAV capsid. (**B**) Anti-miR-206 specificity for miR-206 was tested in vitro. CMV-GFP-anti-miR-206, CMV-pre-miR-206 and CMV-pre-miR-124 sequences were packaged into the AAV2 capsid and used to transduce HEK293 cells. AAV2-CMV-GFP-anti-miR-206 transduction alone (first row, MOI: 10^6 vg/cell) elicited high GFP expression, which was reduced by co-transduction with miR-206 precursor (second row, 1x MOI: 10^6 vg/cell and third row, 2x MOI: 2 x 10^6 vg/cell). The presence of miR-124 had no effect on GFP expression (fourth row). Magnification: 10x, scale bar = 300 μm.

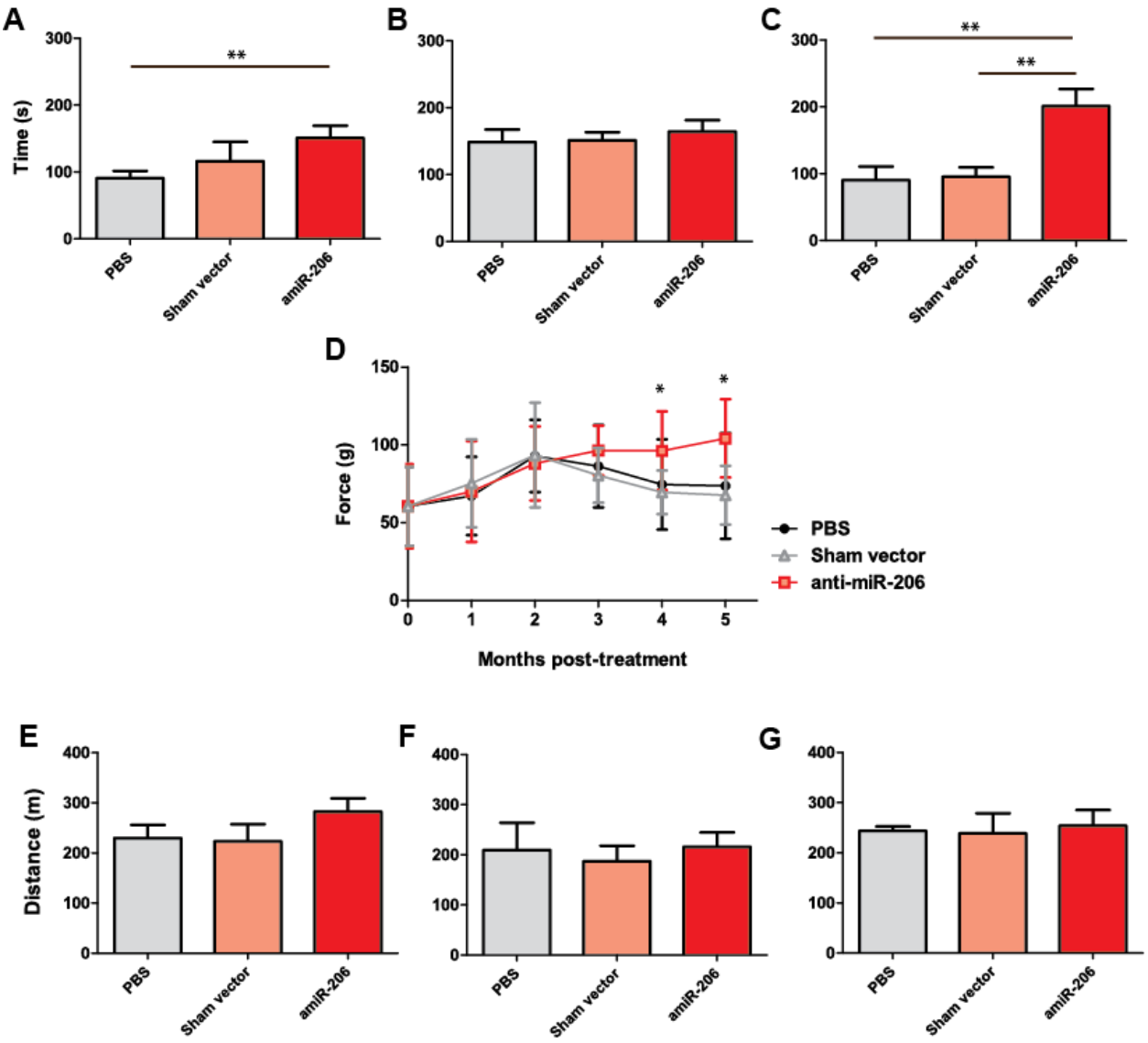

Figure 2.2. Motor function improvements with anti-miR-206 treatment. Rotarod running time was measured in PBS, control vector and AAV9-anti-miR-206 treated *mdx* mice at (**A**) 1, (**B**) 3 and (**C**) 5 months post-treatment. Significant improvements were observed with treatment at 1 and 5 months (**p = 0.0105 and **p = 0.0044 for PBS vs. treated and **p = 0.0038 for sham vector vs. treated, n = 6). Grip strength was also assessed at baseline and until 5 months post-treatment (**D**). Significant increases in strength were observed in anti-miR-206 treated mice versus the untreated group at 4 months (*p = 0.0372 and *p = 0.0227 for PBS and sham vector vs. treated, respectively)

and 5 months (*p = 0.0376 and *p = 0.0455 for PBS and sham vector vs. treated, respectively) post-treatment. No discernable differences were observed in treadmill running distance at (**E**) 1 month, (**F**) 3 months, or (**G**) 5 months post-treatment. Bars represent mean with SEM.

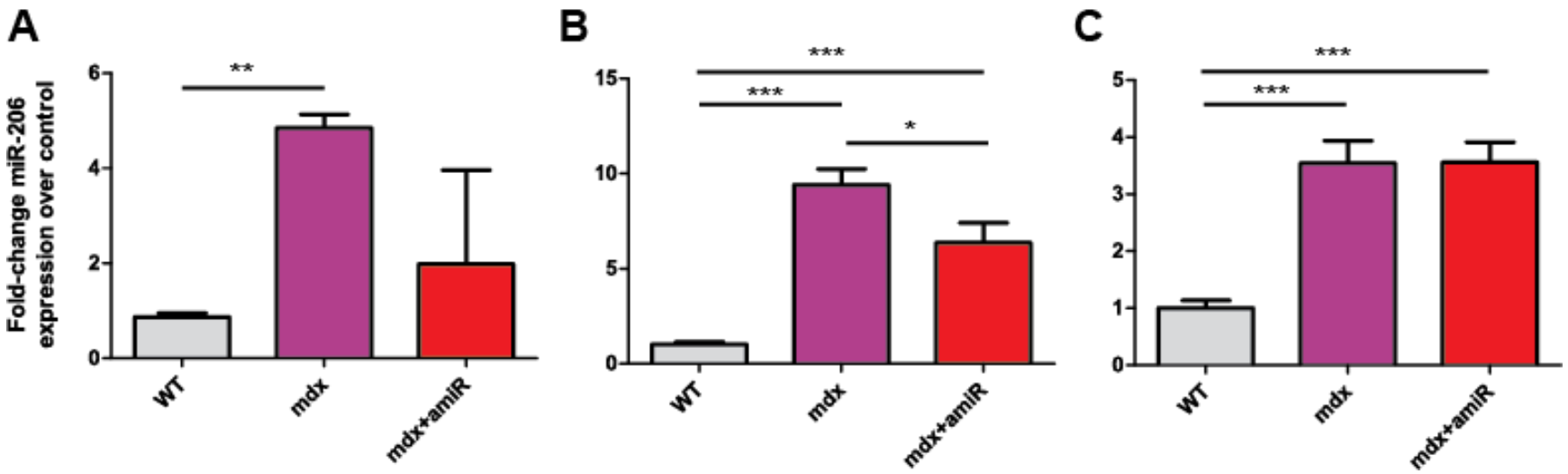

Figure 2.3. MicroRNA-206 levels in muscle. MicroRNA-206 levels were measured in the diaphragm from untreated and treated *mdx* mice as well as age-matched WT mice at (**A**) 1 month, (**B**) 3 months and (**C**) 5 months post-treatment. (**A**) At 1 month, miR-206 was significantly upregulated in untreated *mdx* muscle compared to WT (**p = 0.0055, n = 6). MicroRNA-206 levels appeared to decrease with treatment with considerable variation. (**B**) MicroRNA-206 was upregulated in dystrophic muscle and treated muscle compared to WT at 3 months (***p < 0.0001, n = 6). MicroRNA-206 significantly decreased with AAV9-anti-miR-206 treatment compared to the untreated group (*p = 0.0341). (**C**) At 5 months, treatment had no effect on miR-206 levels. In both *mdx* groups, miR-206 was again significantly more abundant than the WT (***p < 0.0001, n = 6). Bars represent mean with SEM.

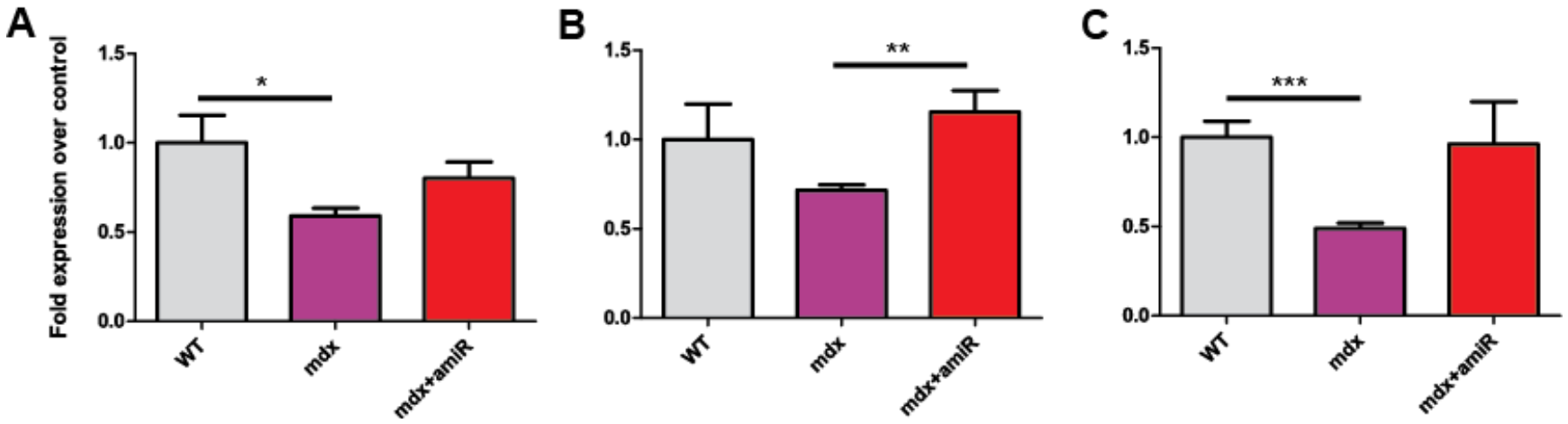

Figure 2.4. VEGF transcript levels in muscle. VEGF mRNA in diaphragm from untreated and treated *mdx* mice as well as age-matched WT mice was quantified at (**A**) 1 month, (**B**) 3 months and (**C**) 5 months post-treatment. (A) At 1 month, dystrophic muscle contained significantly less VEGF mRNA than the WT (*p = 0.0198, n = 6). With treatment, transcript levels slightly increased. (B) Two months later, VEGF mRNA was significantly upregulated in treated muscle compared to the untreated (**p = 0.0026, n = 6). (C) Again, significantly lower transcript levels were observed in untreated *mdx* muscle vs. WT (***p < 0.0001, n = 6). While treated muscle contained a greater quantity of VEGF transcripts than untreated, this result was not statistically significant (p = 0.0683, n = 6). Bars represent mean with SEM.

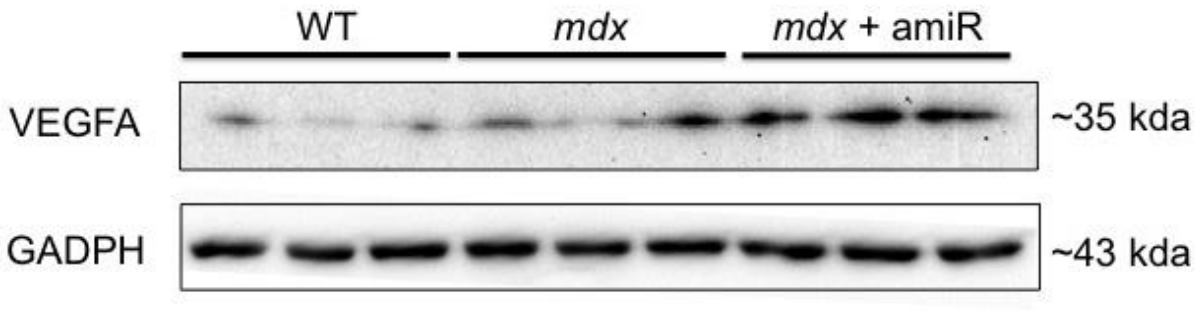

Figure 2.5. VEGFA expression in muscle. VEGFA protein levels were examined by Western blot at 1 month post-treatment in tibialis anterior muscle samples.

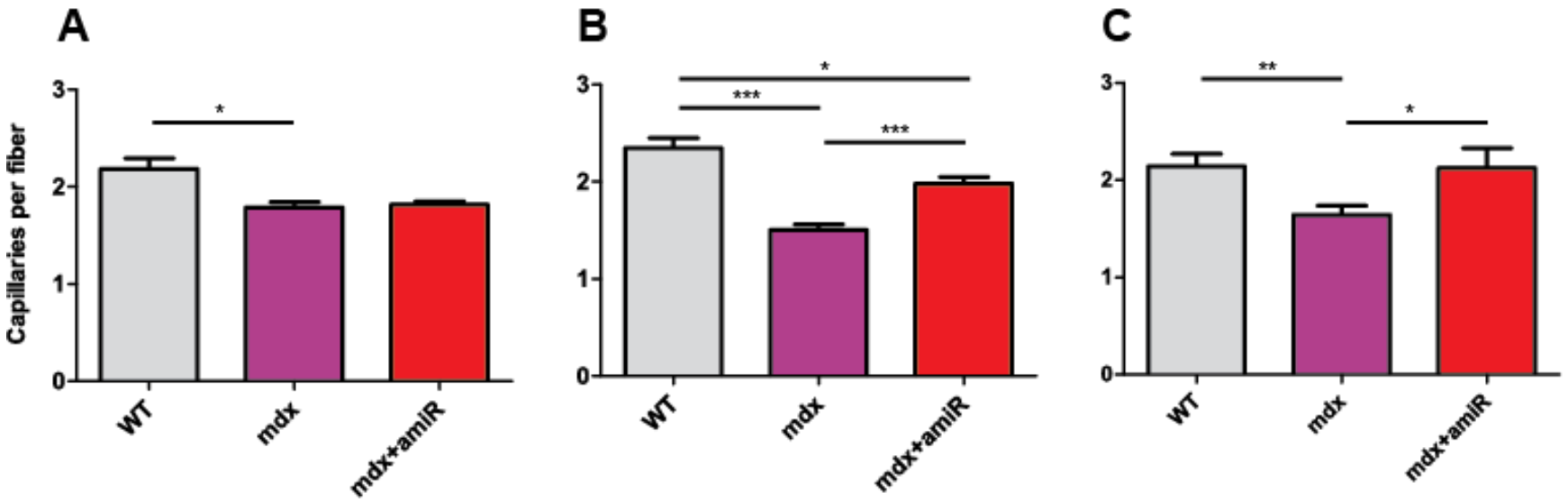

Figure 2.6. Increased capillary density in treated mdx muscle. Capillaries were quantified in diaphragm muscle from untreated and treated *mdx* mice as well as age-matched WT mice at (**A**) 1, (**B**) 3 and (**C**) 5 months post-treatment. (A) At 1 month, the number of capillaries per fiber was significantly lower in *mdx* muscle compared to WT (*p = 0.0495, n = 6). Capillary density was similar in treated muscle. (B) At 3 months, the number of capillaries per fiber in dystrophic muscle was again significantly lower than in the WT (***p = 0.0008, n = 6). A distinct increase was found after treatment (mdx vs. mdx+amiR ***p < 0.0001, n = 6). A significant increase was also observed between WT and treated *mdx* muscle (*p = 0.0244, n = 6). (C) At 5 months, capillary density was decreased in dystrophic muscle compared to WT (**p = 0.0043, n =

6). On the other hand, treatment significantly increased the number of capillaries per fiber compared to untreated *mdx* (*p = 0.0258). Bars represent mean with SEM.

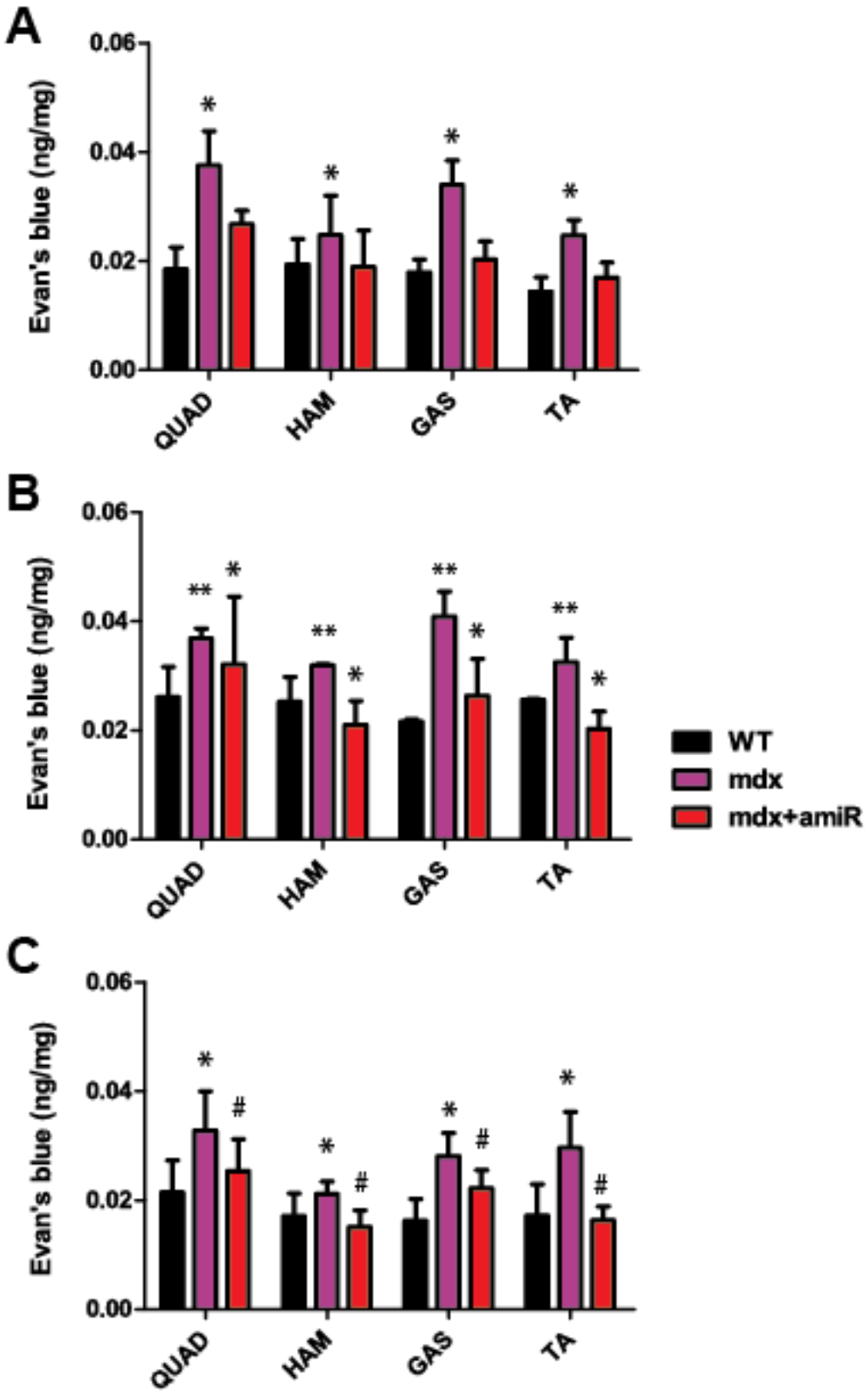
A
Evan's blue (ng/mg)
0.06
0.04
0.02
0.00
QUAD
HAM
GAS
TA
B
Evan's blue (ng/mg)
0.06
0.04
0.02
0.00
QUAD
HAM
GAS
TA
WT
mdx
mdx+amiR
C
Evan's blue (ng/mg)
0.06
0.04
0.02
0.00
QUAD
HAM
GAS
TA

Figure 2.7. Reduced vessel permeability in treated muscle. Miles assay to determine Evans blue dye content (ng/mg tissue) was performed with muscle from untreated and treated *mdx* mice as well as age-matched WT mice at (**A**) 1 month, (**B**) 3 months and (**C**) 5 months post-treatment. (A) At 1 month, a significant increase in dye permeation in dystrophic muscle was observed compared to WT (*p = 0.0349, n = 6). (B) At 3 months, *mdx* dye content was again statistically greater than WT (**p = 0.0094, n = 6). Dye levels were significantly reduced with treatment (*p = 0.0278, n = 6). (C) At 5 months, dye content was significantly greater in *mdx* muscle than WT (*p = 0.0220, n = 6). With treatment, *mdx* muscle contained considerably less dye (#, *p = 0.0351, n = 6). Bars represent mean with SEM.

V. Discussion

In this chapter, I examined the role of microRNA-206 in muscle vascularization and if downregulation of miR-206 would confer therapeutic benefit by allowing expression of VEGFA. I show for the first time that miR-206 can be bound by an antisense construct, “anti-miR-206,” which acts as a decoy target transcript or microRNA “sponge.” Excess amounts of miR-206 *in vitro* completely eliminated expression of a GFP reporter gene containing the antisense sequence in its 3’ UTR. MicroRNA sponges have been used to competitively inhibit small RNAs in mammalian cells to derepress target gene expression (Ebert, Neilson et al. 2007). This is usually accomplished *in vivo* by direct administration of complementary oligonucleotides, or antagomirs, which tend to be 2’-O-methyl, phosphorothioate or cholesterol-modified. Similar to exon skipping, these antagomirs only offer a transient effect and suffer from poor uptake unless a large dose is applied. To overcome this, microRNA inhibitory constructs have been packaged into viral vectors to enable long-term suppression (Haraguchi, Ozaki et al. 2009). Stable miR suppression has been demonstrated *in vivo* in bone marrow reconstitution and cancer xenograft models (Ebert and Sharp 2010). To accomplish this, I packaged the anti-miR-206 construct into an AAV9 vector, which displays superior muscle tropism and stable gene transfer for up to 2 years (Kornegay, Li et al. 2010, Qiao, Koo et al. 2011). Administration of the completed vector effectively reduced miR-206 levels in *mdx* mice. However, miR-206 inhibition in the diaphragm was short-lived and was not observed at 5 months post-treatment. This could be attributed to severe pathology and continuous muscle death, causing the loss of transduced tissue.

Interestingly, AAV9-anti-miR-206 treatment provided therapeutic benefit to *mdx* mice. Rotarod testing revealed significant improvements in balance and motor coordination with treatment. Additionally, grip strength was maintained in mice treated with anti-miR-206 over the experimental period. It is possible that the construct is still present in the limbs of *mdx* mice, which display milder dystrophic symptoms and muscle degeneration compared to the diaphragm (Stedman, Sweeney et al. 1991). Thus, treatment impeded eventual motor decline in the *mdx*.

Treadmill running had two purposes in this study: to assess motor function and exacerbate muscle damage for treatment comparison (Grounds, Radley et al. 2008). While no significant differences in run distance were observed, forced eccentric contraction may have amplified functional decline observed in *mdx* mice during rotarod and grip force testing. Furthermore, respiratory or cardiac impairments do not develop in the *mdx* mouse until 6 and 16 months of age, respectively. It is possible that these deficiencies are not severe enough to affect motor performance during the experimental period. Another study noted that changes in perfusion after induced ischemia were observed only in aged *mdx* mice (12 months), suggesting that vascular impairments may not develop until later (Latroche, Matot et al. 2015). Discrepancies in testing protocols and the motivation of the mice to run may also contribute to the these results.

Finally, target expression and muscle vascularization were evaluated to determine the therapeutic mechanism of miR-206 downregulation. VEGFA transcript levels in muscle significantly increased with anti-miR-206 treatment and protein levels of the ubiquitous isoform were elevated accordingly. Thus, treatment with this microRNA sponge relieved target gene inhibition. In zebrafish, angiogenesis was observed after

inhibition of miR-206, which permitted VEGFA activity (Stahlhut, Suarez et al. 2012, Lin, Lee et al. 2013). The angiogenic properties of VEGFA have been used in DMD treatments to ameliorate functional ischemia, which significantly increased capillary density in muscle as well as forelimb strength after intramuscular injection (Messina, Mazzeo et al. 2007). Transgenic mdx/Flt-1 knockout mice, which have increased ratios of capillaries to muscle fibers, have also shown improvements in muscle histology, blood flow and force production (Verma, Asakura et al. 2010). Similarly, miR-206 reduction significantly increased capillary density in dystrophic muscle. Due to concerns regarding vascular permeability with systemic VEGFA expression, vessel integrity was tested. Abnormal vasoregulation in dystrophic muscle has also been linked to diminished vessel integrity caused by dystrophin loss in smooth muscle cells. Transgenic mice expressing dystrophin solely in vascular smooth muscle cells exhibited normal hemodynamic responses after muscle contraction. While no differences in basal blood flow were seen between these mice, *mdx* and control mice, vascular dystrophin expression produced an intermediate muscle pathology. These finding suggest that vessel defects can contribute to the severity of dystrophic symptoms (Ito, Kimura et al. 2006). Miles assay revealed that dye extravasation in different muscle groups was significantly lowered with treatment and comparable to WT levels, which may be an indication of normalization of the vessel lining and the dystrophic phenotype. Alterations in microvessel endothelial cells of the blood-brain barrier have been observed in *mdx* (Nico, Frigeri et al. 2003). The open tight junctions of the microvessels caused abnormal permeability of the BBB, which may be associated with neurological dysfunction observed in DMD patients. Although the Miles assay has been typically employed in

DMD studies to look at muscle membrane integrity, mice are usually subjected to additional exercise and sacrificed 24 hours later. Mice were sacrificed 30 minutes after dye administration, which would allow transient circulation and only measure extravasation from the vessels.

Although increases in VEGFA expression were found, the question of its role in motor function improvements still remains. Prior to experimentation, it was thought that vascular improvements would influence endurance due to enhanced blood flow and aerobic capacity. In a study with muscle-specific VEGFA-deficient mice, significant decreases in capillary density and treadmill endurance were observed (Olfert, Howlett et al. 2009). However, the previously mentioned study involving AAV-mediated VEGFA delivery showed increased capillary density, but did not evaluate endurance nor blood flow (Messina, Mazzeo et al. 2007). Vascular smooth muscle and endothelial cells in *mdx* mice are still dystrophin-deficient and unable to recruit nNOS to induce proper vasoregulation in response to exercise (Loufrani, Levy et al. 2002, Ito, Kimura et al. 2006). Since our treatment does not target nNOS, the lack of blood flow regulation to affect performance during long bouts of vigorous exercise is understandable. On the other hand, defects in microvascular stress have been observed in *mdx* mice. This can be attributed to reduced endothelial diameter, which cannot withstand or mediate normal blood flow resistance (Loufrani, Levy et al. 2002). Increases in capillary density and integrity may address such issues with normal vessel stress and localized blood flow to the muscle to decrease pathology, producing the observed motor function improvements. It is also possible that treatment improves expression of B-utrophin, which localizes to the vessel endothelium (Weir, Burton et al. 2002). While utrophin

cannot sequester nNOS, it may substitute for dystrophin's structural role to improve vessel integrity similar to muscle (see *Chapter III*). Our observations of reduced Evans blue dye permeation with treatment support some degree of vessel integrity correction, which could aid in normalizing vessel stress and blood flow. Pharmacological agents work directly on the smooth muscle cells to induce vasodilation and improve exercise-related muscle aerobic capacity (Khurana and Davies 2003, Nelson, Rader et al. 2014). In contrast to gene therapies that improve vessel density and function, the effect of these treatments is temporary and may not address the progression of muscle pathology long-term. Overall, these results support a therapeutic role for miR-206 downregulation via VEGFA-induced muscle vascularization.

CHAPTER 3: DOWNREGULATION OF MICRORNA-206 IMPROVES MUSCLE PATHOLOGY IN MDX MICE

I. Introduction

Due to its similarity with dystrophin, several therapeutic strategies have aimed to provide or upregulate endogenous utrophin in dystrophic muscle. Utrophin is comparable in size to dystrophin (395 kDa) and its primary structure bears resemblance to dystrophin, especially at the NH_2 and COOH terminal domains (Blake, Weir et al. 2002). Overexpression of utrophin at the sarcolemma of transgenic *mdx* muscle prevented development of dystrophic symptoms and maintained normal muscle function (Deconinck, Tinsley et al. 1997, Tinsley, Deconinck et al. 1998). In addition, AAV delivery of a micro-utrophin protein ameliorated disease pathology, normalizing muscle fiber morphology and force generation (Odom, Gregorevic et al. 2008). Increasing utrophin levels also promoted structural integrity of the myofiber and increased resistance to contraction-induced damage. The findings from these studies underscore the compensatory role and therapeutic value of utrophin.

Studies with *mdx* mice and DMD patients have found that utrophin is upregulated in dystrophic muscle (Khurana and Davies 2003). While utrophin levels may explain the milder phenotype of *mdx*, they are not sufficient for improving muscle pathology in DMD patients (Deconinck, Rafael et al. 1997). Treatment with pharmacological agents, such as SMTC110, which work to increase endogenous utrophin expression have benefitted disease muscle (Tinsley, Fairclough et al. 2011, Tinsley, Robinson et al. 2014). Furthermore, it is believed that increasing endogenous utrophin avoids issues with

dystrophin-specific T cell targeting associated with gene replacement strategies. In one study, viral-mediated gene transfer of utrophin persisted longer and elicited a weaker immune response compared to dystrophin in immunocompetent mice (Ebihara, Guibinga et al. 2000).

MicroRNA-206 is overexpressed in DMD, but its role in disease pathology has not been defined. Utrophin is a known target of miR-206 and its expression is known to be post-transcriptionally regulated (McCarthy 2008). Overexpression of miR-206 in muscle cell culture had a strong inhibitory effect on utrophin levels, suggesting direct regulation of utrophin via its 3' UTR (Rosenberg, Georges et al. 2006). Similarly, high levels of miR-206 may contribute to insufficient utrophin expression observed in dystrophic muscle. Reducing miR-206 in the muscle may relieve its inhibitory effect, increasing endogenous expression of therapeutic booster genes, such as utrophin, and improving dystrophic pathology. To this end, I investigated whether miR-206 influences muscle pathology and expression of one of its target, utrophin. First, I measured utrophin expression, looking at both the transcript and protein level to determine if miR-206 negatively regulates utrophin. Second, I examined general muscle pathology by H&E staining in response to treatment. Third, I assessed the effect of treatment on related dystrophic symptoms, including fibrosis, fiber regeneration, serum CK, myofiber size and muscle mass. Lastly, I looked at vector persistence in the muscle to assess long-term efficacy. Findings from these studies could help to clarify the role of miR-206 in muscle pathology and define a new strategy for treating DMD.

II. Materials and methods

Utrophin transcript quantification

Total RNA was extracted from diaphragm muscle using TRIzol reagent according to the manufacturer's instructions (Thermo Fisher Scientific) and stored at -80°C until further use. A cDNA template for microRNAs was created using the miRNA 1st-Strand cDNA Synthesis Kit (Agilent Technologies). The resulting template was diluted 1:5 for quantitative PCR (qPCR). Reactions were set up using PowerUp SYBR Green Master Mix (Thermo Fisher Scientific) according to the manufacturer's protocol and run in an Applied Biosystems 7300 Thermocycler. Utrophin expression was quantified relative to ubiquitous beta-actin. The primers used were as follows: utrophin (forward: 5'-CACTGGCAGGTGAAGGATGT-3', reverse: 5'-CTTGACTGTAGGGCCTGGTG-3') and beta-actin (forward: 5'-ATCACTATTGGCAACGAGCG-3' and reverse: 5'-ACTCATCGTACTCCTGCTT-3'). Expression was depicted as fold-change over control.

Western blot

Gastrocnemius (GAS) muscle was homogenized in cold dystrophin lysis buffer (2% SDS, 6.25 mM Tris pH 8.8, 2% glycerol, PMSF, 50 mM DTT, 0.005% BPB) using a tissue homogenizer (Tekmar Ultrasonic Processor model TM130). Protein concentration was determined by BCA assay. For Western blotting, 50 µg (for utrophin detection) and 15 µg (for GAPDH detection) protein from each sample was prepared in 2X dystrophin loading buffer (5% SDS, 0.75 M Tris pH 8.8, 2% glycerol, 100 mM DTT, 1% BPB) and heated at 95°C for 5 minutes. Proteins were separated by SDS-PAGE and wet transferred onto a PVDF membrane using the Bio-rad Mini-PROTEAN II system.

Membranes were blocked in 5% milk in 1% TBS-Tween 20 (TBS-T) for 1 hour and incubated with either goat polyclonal antibody against utrophin (Santa Cruz Biotechnology, #sc-7459, 1:1000) or rabbit polyclonal antibody against GAPDH (Sigma-Aldrich, cat. # G9545, 1:10,000) diluted in 3% bovine serum albumin (BSA) in 1% TBS-T overnight at 4°C. Membranes were washed 3 times for 10 minutes in 1% TBS-T and then incubated with anti-goat or anti-rabbit IgG conjugated to horseradish peroxidase (Sigma, A5420, 1:5,000 for utrophin and Sigma-Aldrich, A0545, 1:10,000 for GAPDH) in 5% milk. Blots were developed using the Western Lightening ECL reagent (Pierce) and visualized using the FluorChem M system.

Utrophin immunostaining

GAS muscle samples were processed into 10 μm cryosections and mounted on glass slides. At room temperature, slides were blocked in 10% horse serum for 1 hour. Utrophin was immunostained with a goat utrophin antibody (Santa Cruz Biotechnology, #sc-7459, 1:100) in 1% horse serum in PBS overnight at 4°C and then washed with 0.5% PBS-T 3 times for 5 minutes each. Anti-goat IgG conjugated to Cy3 dye (1:500, Jackson ImmunoResearch Laboratories, Inc.) was diluted in 1% horse serum and used to incubate slides for 1 hour. Slides were washed with 0.5% PBS-T 3 times for 5 minutes each and mounted with aqueous mounting media (Gel/Mount, Biomeda). Slides were visualized using a Zeiss Axiovert 200M Confocal Microscope and images were taken using an AxioCam MRm camera.

Hematoxylin & eosin (H&E) staining

Frozen muscle samples were cryosectioned 10 μm in thickness and placed on glass slides. Slides were fixed in 3% acetic acid (in 95% ethanol) and washed with tap

water. They were then stained in Gill's hematoxylin solution (#24244, Polysciences, Inc.) for 30 minutes (min) to visualize cell nuclei. Slides were washed in running tap water then differentiated in 1% acid alcohol (hydrochloric acid in 70% ethanol) for about 30 seconds (sec). After washing in tap water, tissue was blued in 0.2% ammonia water for 30 sec to 1 min. Slides were then washed again and counterstained with eosin for about 5 sec to visualize eosinophilic structures (i.e. sarcoplasm). Serial dehydration was performed in 70%, 85%, 95% and 100% ethanol. Slides were then cleared in xylene 3 times for at least 5 min overall and mounted with Permount (Fisher). Images were acquired using a Nikon Eclipse TE300 microscope (Nikon USA) and a SPOT RT Slider camera (Diagnostic Instruments, Inc.). H&E images were used for centrally located nuclei quantification and analyzed in ImageJ using the *Cell Counter* function.

Collagen staining

To examine the level of fibrosis in muscle samples, two methods of collagen staining were performed. To visualize areas containing collagenic compounds, Masson trichrome staining was performed using solutions from a kit (IMEB Inc.). Slides were made by cryosectioning frozen muscle samples, which were then fixed in Bouin's solution for 15 to 20 min. After rinsing in water, sections were stained in hematoxylin solution for 10 min to visualize nuclei. After another rinse, sections were placed in Biebrich's scarlet acid fuschin solution for 15 min to stain the sarcoplasm then rinsed again. Slides were placed in Phosphotungstic/Phosphomolybdic acid solution for 15 min, then directly transferred into aniline blue stain solution to stain collagenic areas. After rinsing, slides were serially dehydrated as mentioned above (*Hematoxylin & eosin (H&E) staining*). Slides were then cleared in two changes of xylene for at least 5 min in

total. Slides were mounted with Permount. Collagen fibers and muscle were stained with Sirius red and fast green, respectively. Frozen sections were allowed to reach room temperature, then fixed in pre-warmed Bouin's solution for 15 to 20 min. Slides were washed in lukewarm running tap water until yellow color faded. They were then stained in 0.1% Fast green (in water) for 10 to 15 min and washed briefly in tap water. Slides were then placed in 1% acetic acid solution for 2 minutes and then directly into 0.1% Sirius red stain (in water) for 30 minutes. Slides were dehydrated in 100% ethanol for 2 to 3 minutes twice and xylene cleared for at least 5 min. Finally, slides were mounted with Permount. Images were acquired using a Nikon Eclipse TE300 microscope (Nikon USA) and a SPOT RT Slider camera (Diagnostic Instruments, Inc.). The percentage of fibrosis was calculated with Sirius red/fast green images using ImageJ software and the *Threshold_Colour* plugin.

Hydroxyproline quantification

Hydroxyproline, a non-proteinogenic amino acid, is particularly abundant in collagen, making up ~13.5% of the total composition. Hydroxyproline content was determined using the method described by Carlson (2009). Diaphragm samples were extracted and hydrolyzed in 5 M HCl in a 108°C dry bath overnight. After bringing samples to room temperature, 50 µg of sample was diluted in 2.25 ml ddH_2O and then neutralized with 0.1 N and 0.8 N KOH solutions. A hydroxyproline standard was also made at this time. Sodium borate buffer (0.1 M, pH 8.7) was added and then the mixture was oxidized with 2 ml of 0.2 M chloramine-T solution. After a 25 min incubation period, 1.2 ml of 3.6 M sodium thiosulfate was added to stop the oxidation reaction and vortexed briefly. Next, 2.5 ml toluene and 1.5 g KCl were added. The samples were

inverted slowly for 5 min on a test tube inverter then centrifuged at 300 x g for 1 minute. The toluene phase containing impurities was removed and the remaining aqueous layer was heated at 100°C in a dry bath for 30 min to convert the oxidized hydroxyproline (pyrrole-2-carboxylic acid) to pyrrole. After cooling to room temperature, another 2.5 ml of toluene was added and mixed with the aqueous solution to extract the pyrrole. After another round of centrifugation, 1.5 ml of the organic phase was mixed with 0.6 ml Erlich's reagent and developed for 30 min at room temperature. Sample and hydroxyproline standard absorbances were read at 560 nm. Hydroxyproline content was expressed as µg per mg muscle.

Fiber diameter

Cryosections of diaphragm muscle 10 µm thick from WT, *mdx* and treated *mdx* were made. At room temperature, slides were washed in PBS for 10 minutes then blocked in 10% horse serum for 1 hour. The muscle basal lamina was immunostained with a rat anti-laminin α2 antibody (Sigma-Aldrich, L0663, 1:500) in 1% horse serum in PBS for 1 hour and washed with 0.5% PBS-T 3 times for 5 minutes each. Anti-rat IgG conjugated to Alexa Fluor 488 dye (Molecular Probes, #A21470) was diluted in 1% horse serum and used to incubate slides for 1 hour. Slides were washed with 0.5% PBS-T 3 times for 5 minutes each and mounted with Gel/Mount. Slides were visualized using a Zeiss Axiovert 200M Confocal Microscope and images were taken using an AxioCam MRm camera. Images were analyzed using ImageJ software and the *Analyze Particles* function to measure area. Diameter was then calculated in Microsoft Excel and graphed in GraphPad Prism 5.0.

Serum creatine kinase

Muscle contains high levels of creatine kinase (CK) and if damaged, will leak CK into the blood. Measuring serum CK activity thus serves as an overall assessment of muscle injury. Whole blood samples were collected with BD Microtainer Serum Separator tubes at the time of sacrifice from the carotid artery. Tubes were spun at 10,000 rpm in a 4°C microcentrifuge for 10 min to separate serum, which was frozen at -20°C for later use. Creatine kinase reagent (Pointe Scientific) was used to catalyze the formation of NADH formation. The reaction rate of NADH production was measured at 340 nm. The serum CK in the samples catalyzes the formation of creatine and ATP from ADP and creatine phosphate. Hexokinase then catalyzes the production of glucose-6-phosphate and ADP from ATP and glucose. Finally, glucose-6-phosphate and NAD^+ are formed into 6-phopshogluconate, NADH and H^+ through glucose-6-phosphate dehydrogenase.

Body weight and muscle mass

Body weight was measured every 2 weeks after grip force testing. Muscle mass for quadriceps, hamstring, gastrocnemius, tibialis anterior and tricep muscles was measured upon dissection.

Vector persistence

DNA was extracted from diaphragm and gastrocnemius muscle samples using the DNeasy Blood and Tissue Kit (Qiagen) according to manufacturer's protocols. Absolute qPCR was performed to determine vector genome copies per cell. Two standards were created by serial dilution of the CMV-1/2gfp-anti-miR-206 vector plasmid and a previously generated plasmid containing a single copy of the mouse

glucagon gene. Reactions were set up using the GoTaq Probe qPCR Master Mix (Promega) according to the manufacturer's protocol and run in an Applied Biosystems 7300 Thermocycler. Vector genomes per cell were calculated by dividing CMV copies by half of the total glucagon copies, since one diploid nucleus contains two copies of the glucagon gene. The primers used were as follows: CMV promoter (forward: 5'-GTATGTTCCCATAGTAACGCCAATAG-3', reverse: 5'-GGCGTACTTGGCATATGATACACT-3', probe: FAM-TCAATGGGTGGAGTATTTA) and glucagon (forward: 5'-AAGGGACCTTTACCAGTGATGTG -3' and reverse: 5'-ACTTACTCTCGCCTTCCTCGG-3', probe: FAM-CAGCAAAGGAATTCA).

III. Results

Utrophin expression

Utrophin transcript levels were examined using relative qPCR in WT, *mdx* and treated *mdx* diaphragm (Fig. 1). At 1 month, utrophin expression in dystrophic muscle was significantly upregulated, nearing 3-fold, compared to WT (Fig. 1A, WT vs. *mdx* **p = 0.0016, WT vs. treated *mdx* ***p = 0.0001, n = 6), with no marked difference between the two *mdx* groups. Dystrophic muscle transcript levels were again greater (~2-fold) than the WT (***p<0.0001, n = 6) at 3 months (Fig. 1B). At the same time, a significant ~2-fold increase in utrophin transcripts was observed with treatment compared to the untreated group (***p = 0.0001, n = 6). Transcript levels in the treated group were ~4-fold greater than in WT (***p<0.0001, n = 6). A similar pattern was found two months later; however, the difference between the untreated groups was not statistically significant (Fig. 1 C, p = 0.2059, n = 6). Still, dystrophic muscle contained significantly greater levels of utrophin mRNA than the WT (WT vs. mdx *p = 0.0389, WT vs. treated mdx **p = 0.0051). Western blot was performed to examine utrophin expression at the protein level in the gastrocnemius muscle (Fig. 2). Due to cross-reactivity with dystrophin in WT samples, only *mdx* groups were compared. After incubation with a utrophin-specific antibody, a band was observed at ~400 kDa, which corresponds in size to utrophin. A noticeable increase in expression was observed with treatment at 3 months, which mirrors increases in transcript levels.

Immunofluorescent staining was performed to determine utrophin localization in gastrocnemius muscle (Fig. 3). WT and untreated *mdx* displayed sparse and punctate utrophin expression, which can be attributed to neuromuscular junction (NMJ) staining.

In anti-miR-206 treated muscle, NMJ staining was stronger and more abundant than in WT or untreated muscle. A distinct staining pattern lining the edges of the muscle fiber (highlighted in zoomed images) was also observed, likely due to utrophin expression at the sarcolemma.

Muscle pathology is normalized with treatment

Muscle pathology was examined by H&E staining in diaphragm and hamstring muscle over the course of 5 months (Fig. 4). Normal muscle is characterized by fibers that are organized, uniform in size and with nuclei located at the periphery. WT muscle generally appeared normal within the given time period. In contrast, dystrophic muscle showed signs of degeneration (irregularly shaped fibers that are pale pink with fragmented sarcoplasm or swelled, hypercontracted fibers with dark pink staining) and regeneration (smaller fibers with centrally located nuclei) with mononuclear cell infiltration (small basophilic cells without cytoplasm). Muscle damage in the *mdx* diaphragm was markedly severe compared to the hindlimb. At 3 months, regenerating fibers in untreated *mdx* appeared to be more abundant than at 1 or 5 months in both diaphragm and hamstring. In treated *mdx*, dystrinopathy was less serious. Treated diaphragm was more organized and myofibers were relatively more uniform in size and shape than in the untreated sample. In addition, there appeared to be less inflammatory cell infiltration. Over time, overall myofiber area within the *mdx* diaphragm appeared to decrease and seemingly replaced by fibrotic tissue (unstained spacing between fibers).

Decreased fibrosis in treated *mdx* mice

In dystrophic muscle, functional muscle mass is replaced by fibrotic collagen. Collagen deposition is particularly pronounced in the *mdx* diaphragm, which has been

shown to contribute to respiratory impairments that develop with age. Two methods of histological staining were used to assess fibrosis qualitatively. Masson trichrome staining was performed at 3 and 5 months post-treatment (Fig. 5A and 5B, respectively) to detect collagenic compounds. No collagen deposition was observed in the WT diaphragm at either timepoint. On the other hand, *mdx* diaphragm was severely fibrotic, with collagen occupying close to half of the muscle area. Treated *mdx* diaphragm was also fibrotic, yet to a lesser degree and in a more organized fashion compared to untreated muscle. These results were paralleled with picrosirius red/fast green staining, which is used to stain collagen fibers versus collagen constituents. In addition to diaphragm muscle (Fig. 6A and 6C), hamstring muscle was also stained to examine hindlimb fibrosis (Fig. 6B and 6D). Again, no fibrosis was observed in WT muscle at either timepoint. In dystrophic diaphragm, there was substantial collagen deposition at both times. In contrast, collagen staining was more diffuse in treated diaphragm, which suggests that fewer mature collagen fibers are present and progression of fibroses is less advanced than in the untreated sample. In the hamstring, differences in collagen deposition were less distinguishable between groups, particularly at the 5 month timepoint. Picrosirius red staining was quantified and revealed a mean of 34.45 $\pm$ 2.081 and 27.67 $\pm$ 5.711 at 3 and 5 months, respectively, in the dystrophic diaphragm (Fig. 7A and 7C). A significant reduction of fibrosis in both the *mdx* diaphragm (mean = 22.51 $\pm$ 3.274) and hamstring muscle (Fig. 7B, mean = 18.64 $\pm$ 1.673) with treatment at 3 months post-treatment (**p = 0.0043 and *p = 0.0279, respectively). At 5 months, diaphragm collagen deposition was also decreased in the treated vs. untreated group (mean = 21.56 $\pm$ 3.949); however, this was not statistically significant (p=0.3919). At the

same time, there was no apparent difference in hamstring collagen staining across all groups (Fig. 7D, WT vs. mdx p=0.6045, WT vs. treated p = 0.615, mdx vs. treated p = 0.8562).

Hydroxyproline, a major component of collagen, was also quantified in order to evaluate fibrosis in the muscle overall (Fig. 8). Consistent with the staining results, hydroxyproline content was greater in *mdx* diaphragm (mean = 5.967 $\pm$ 1.407 µg/mg) than in WT (mean = 0.5724 $\pm$ 0.2498 µg/ml, Fig. 8A). Treated diaphragm also contained less hydroxyproline (mean = 4.551 $\pm$ 1.008 µg/mg) compared to the untreated group at 3 and 5 months post-treatment. Hydroxyproline content increased in all groups at 5 months yet rose most drastically in untreated *mdx* (untreated mean = 13.68 $\pm$ 5.062 µg/mg and treated mean = 7.461 $\pm$ 1.546 µg/mg). At 3 months, hamstring muscle hydroxyproline values displayed a similar pattern to staining results, with an increase in *mdx* muscle (Fig. 8B, mean = 5.406 + 1.413 µg/mg) and a decrease with anti-miR-206 treatment (mean = 4.410 $\pm$ 1.011 µg/mg). Hydroxyproline assay results for hamstring at 5 months were inconclusive and not shown.

Normalization of fiber diameter

Immature fibers, which are smaller in diameter than mature fibers, are more abundant in dystrophic muscle due to active degeneration and regeneration. Fiber diameter was calculated in WT, *mdx* and treated *mdx* gastrocnemius muscle to determine fiber stability at 1, 3 and 5 months post-treatment (Fig. 9). The majority of WT fibers ranged between 45 and 75 µm, with a peak at 60 µm, which was consistent at all timepoints. However, the percentages of different fiber diameters within this range became more evenly distributed with increasing age and a less prominent peak at 60

μm was observed by 5 months. Muscle fibers in the untreated group were concentrated in the lower size range, with a peak at 10 μm and a gradual decline with increasing diameter. After treatment, *mdx* fiber distribution still peaked at 10 μm, but appeared to shift slightly to larger diameters. Unlike WT muscle, there were no apparent changes in fiber size distribution in either *mdx* groups with age. Fiber diameter in the diaphragm was also examined and exhibited a similar pattern to the gastrocnemius muscle (results not shown).

Centronucleation in dystrophic muscle

Newly regenerated fibers are recognized by their centrally located nuclei, or centronucleation, and are used as another indicator of fiber instability. Muscle fibers containing centrally located nuclei were quantified in WT, *mdx* and treated *mdx* diaphragm muscle at 3 and 5 months post-treatment (Fig. 10A and 10B). Centronucleation was not observed in WT muscle at either timepoint. In contrast, a large percentage of *mdx* fibers were centrally nucleated (33.20 $\pm$ 1.984% and 29.34 $\pm$ 3.285%, at 3 and 5 months, respectively). A significant decrease was observed with treatment at 3 months (mean = 24.63 $\pm$ 1.949%, **p=0.0065, n = 6). Centronucleation also markedly decreased with anti-miR-206 treatment at 5 months, yet this result was not statistically significant (mean = 21.46 $\pm$ 1.671%, p = 0.0698, n = 6). Slightly less centronucleation was observed at 5 months compared to 3 months post-treatment for both untreated and treated *mdx*.

Reduction of serum muscle creatine kinase in anti-miR-206 treated mice

Striated muscle contains high levels of creatine kinase (CK), which is released into the serum in response to damage. Serum CK was measured in WT, *mdx* and

treated *mdx* to evaluate overall muscle damage (Fig. 11). At the 3 month timepoint, WT serum contained an average of 240.6 ± 74.75 u/L CK, which decreased to 176.3 ± 22.46 u/L two months later. Compared to WT, *mdx* serum contained much greater levels of CK (up to 17,083 u/L, **p = 0.0224, and 12,531 u/L, *p = 0.0365, respectively) at 3 months and 5 months. Mean CK values for *mdx* serum were 8,512 ± 2535 u/L and 6,134 ± 1,927 u/L at 3 and 5 months, respectively. Serum CK values in *mdx* varied greatly, with a range of ~15,000 u/L at 3 months and ~10,000 u/L at 5 months. In response to anti-miR-206 treatment, CK values were reduced, with a mean of 4,412 ± 1,123 u/L and 5,295 ± 1148 u/L at 3 and 5 months post-treatment. However, compared to untreated *mdx*, this result was not significant (p = 0.1896 and p = 0.7214 at 3 and 5 months, respectively). Still, treated *mdx* exhibited a much smaller range of CK values versus the untreated group, with a range of ~6,000 u/L and ~7,000 u/L at 3 and 5 months, respectively. Compared to WT, treated *mdx* levels were nonetheless significantly greater at both timepoints (*p = 0.0139 and *p=0.0112 for 3 and 5 months, respectively).

Bodyweight & muscle mass

Bodyweight was measured in untreated and treated mice between 1 and 5 months post-treatment (Fig. 12). While bodyweight increased steadily in untreated and treated mice, no major differences in weight were found between the two groups. Similarly, no notable changes were observed in muscle mass with treatment (Fig. 13). Hamstring mass very slightly increased between 1 and 5 months in the treated group.

Vector persistence

To determine if the AAV vector genome remained in the muscle over time, absolute qPCR was performed with diaphragm and gastrocnemius samples from AAV9-anti-miR-206 treated mice (Fig. 14). At one month, ~0.3 vector genomes (vg) were detected per cell in the gastrocnemius muscle, which stayed constant two months later. The amount of vector genomes decreased by 5 months to ~0.2 vg/cell. In contrast, diaphragm muscle harbored up to 10 vg/cell with an average of 5 vg/cell at 1 month. Vector concentration was reduced by about half at 3 months. Finally, vector concentration was 0.5 vg/cell at 5 months. Overall, the diaphragm was highly transduced yet experienced considerable vector genome loss within the time period compared to the gastrocnemius muscle.

IV. Figures

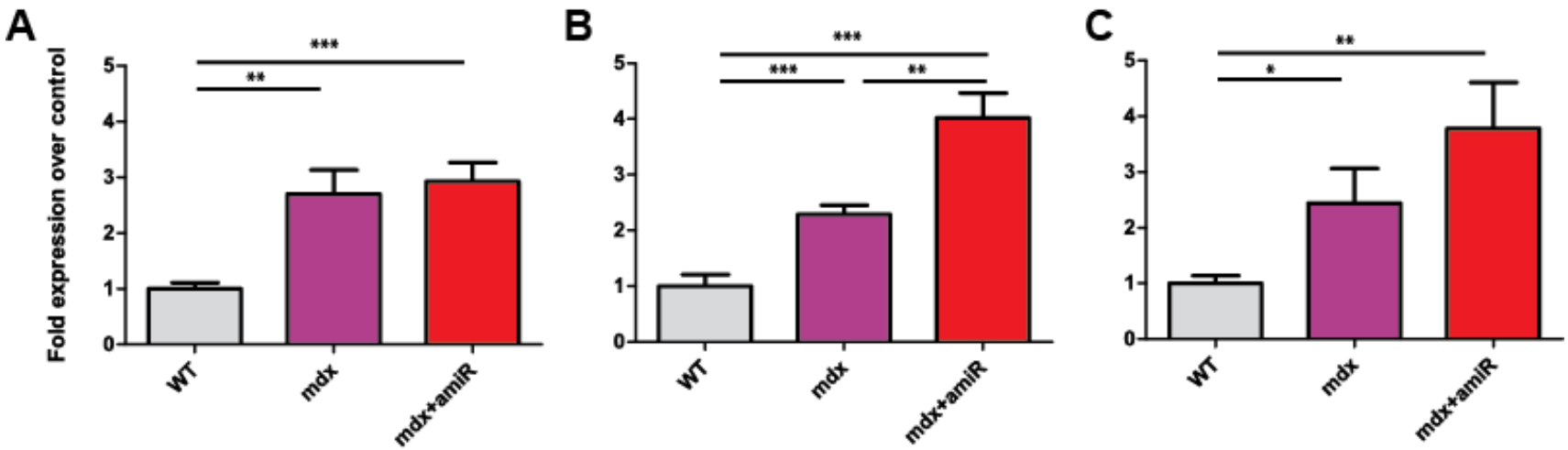

Figure 3.1. Upregulation of utrophin transcripts with treatment. Utrophin mRNA was quantified in diaphragm from untreated and treated *mdx* mice as well as age-matched WT mice at (**A**) 1, (**B**) 3 and (**C**) 5 months post-treatment. (A) Utrophin transcript levels were significantly greater at 1 month in both untreated *mdx* and treated *mdx* muscle versus WT (**p = 0.0016 and ***p = 0.0001, respectively, n = 6). (B) At 3 months, a significant increase in transcripts was again observed in *mdx* and treated *mdx* compared to WT (***p < 0.0001, n = 6). Utrophin mRNA in treated muscle was considerably upregulated compare to untreated muscle (**p = 0.0012, n = 6). (C) Two months later, *mdx* and treated *mdx* levels were consistently greater than WT (*p = 0.0389 and **p = 0.0051, respectively, n = 6). Treatment increased utrophin levels, but this difference was not statistically significant. Bars represent mean with SEM.

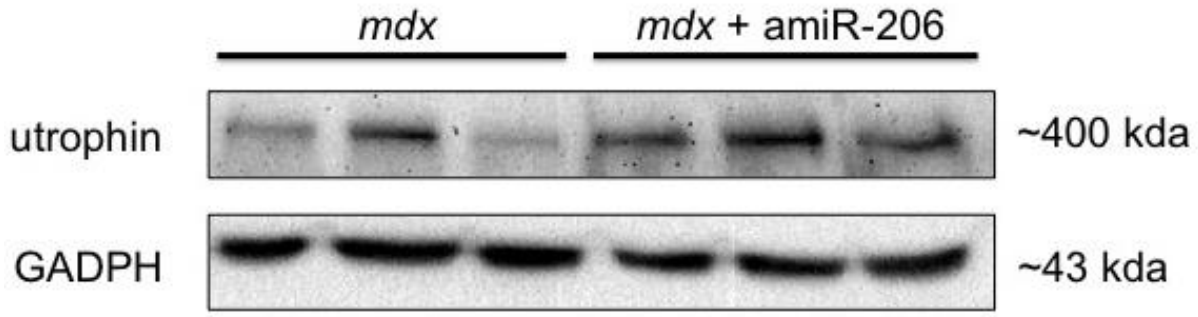

Figure 3.2. Upregulation of utrophin protein with treatment. Utrophin expression was examined in the gastrocnemius muscle from untreated and treated *mdx* mice at 3 months post-treatment.

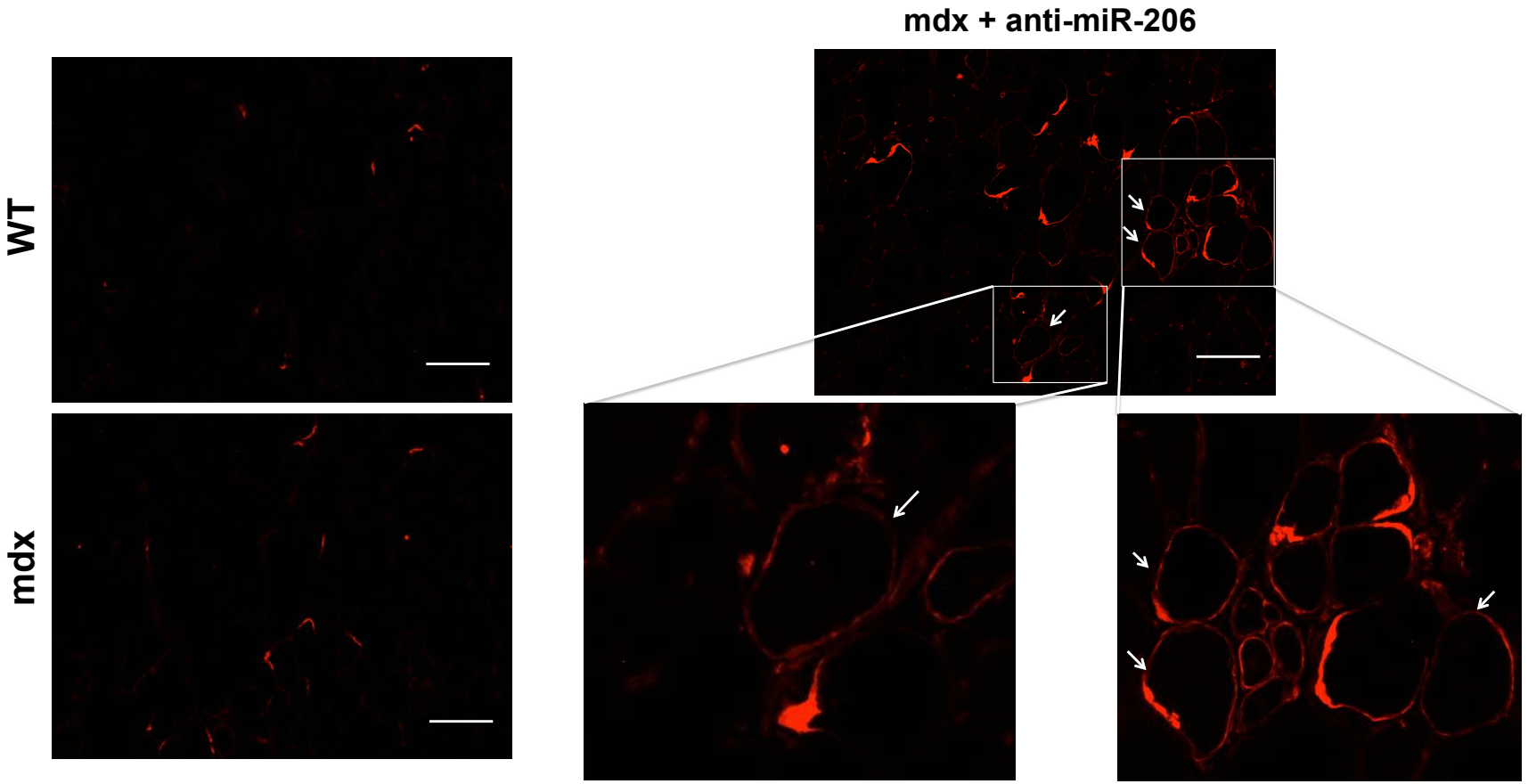

Figure 3.3. Utrophin localization at the muscle membrane. Immunofluorescent staining was performed in gastrocnemius muscle from WT, *mdx* and treated *mdx* mice at 3 months. WT and *mdx* muscle had sparse, punctate utrophin staining while utrophin appeared to localize at the muscle membrane in the treated muscle. Bar = 100 μm, magnification: 10X.

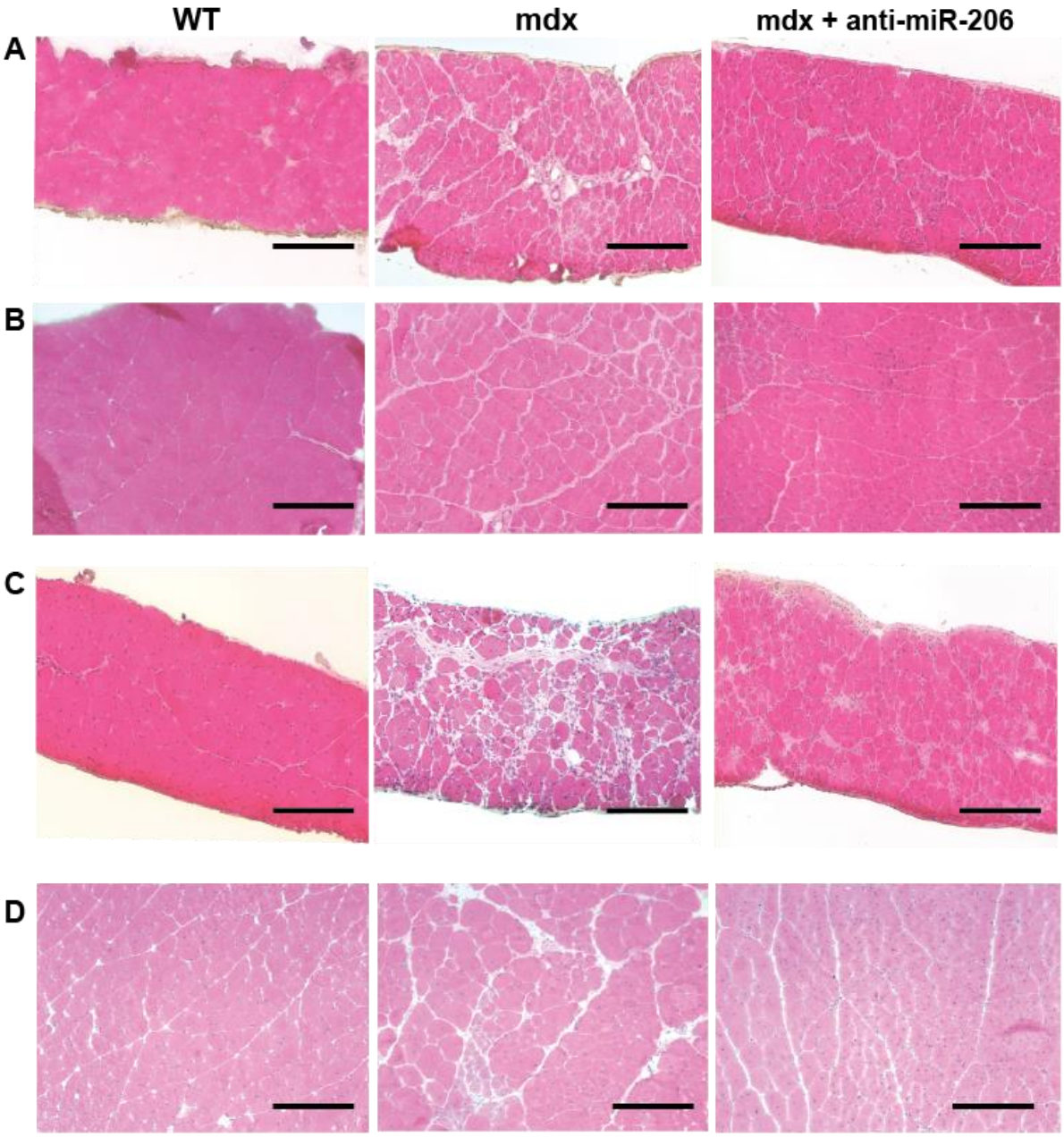
WT
mdx
mdx + anti-miR-206
A
B
C
D

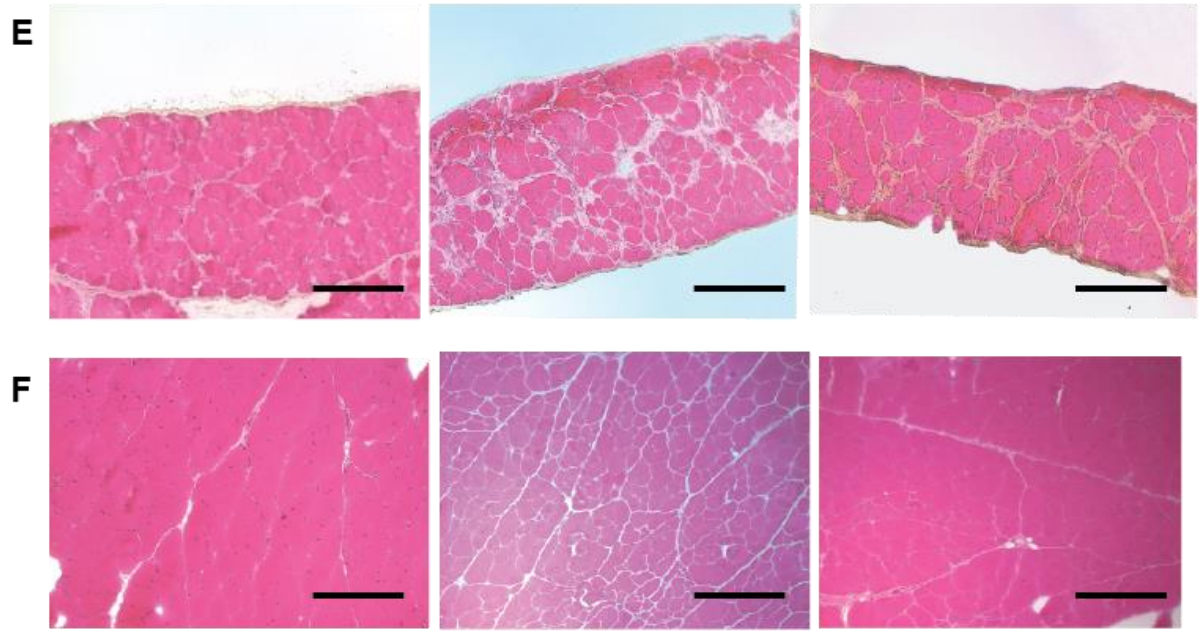

Figure 3.4. Improvement in muscle pathology with AAV9-anti-miR-206 treatment. Pathology was observed at 1 month in (A) diaphragm and (B) hamstring muscle. Dystrophic pathology was more severe in *mdx* muscle than in WT or with treatment. Staining showed that dystrinopathy became more severe at 3 months in (C) diaphragm as well as (D) hamstring. Treatment once again appeared to lessen severity. Finally, muscle condition was observed at 5 months in (E) diaphragm and (F) hamstring. Again, dystrophic symptoms were worse in the *mdx* diaphragm than in the WT or untreated. Pathology was not as pronounced in the hamstring across all groups. Bar = 300 μm, magnification: 10X.

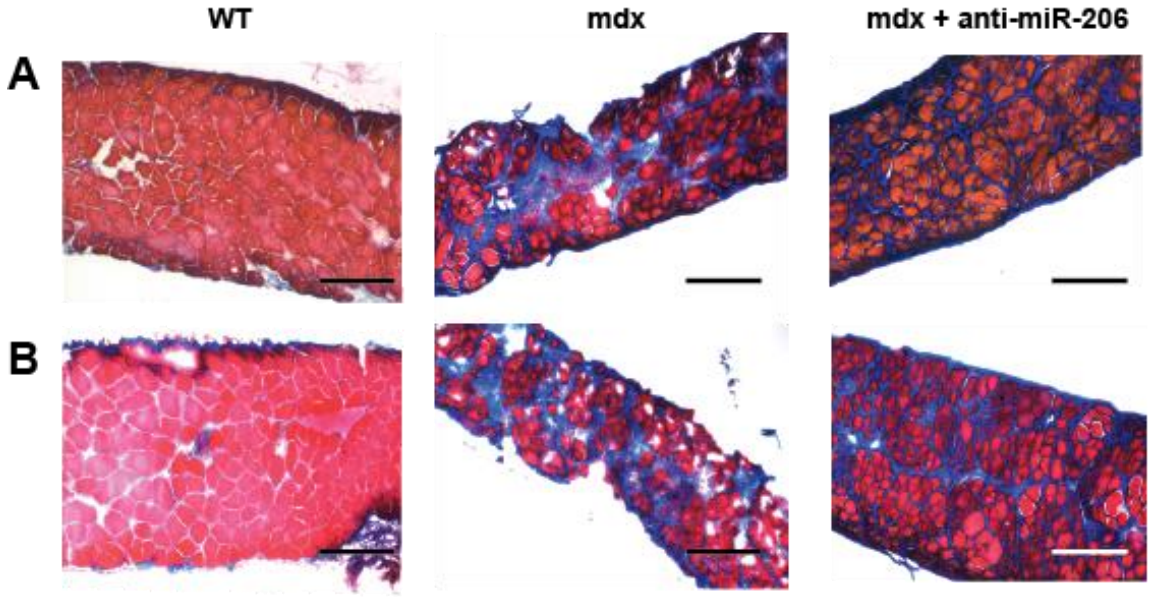

Figure 3.5. Decreased collagen deposition with treatment. Masson trichrome staining was performed to examine fibrosis in diaphragm at (A) 3 months and (B) 5 months post-treatment. Collagen deposition is represented in blue and sarcoplasm in red. Little to no collagen was found within WT muscle. In contrast, collagen deposition was greatly increased in dystrophic muscle. While fibrosis was still observed with treatment, it was decreased overall and occupied a smaller area than without treatment. Bar = 300 μm, magnification: 10X.

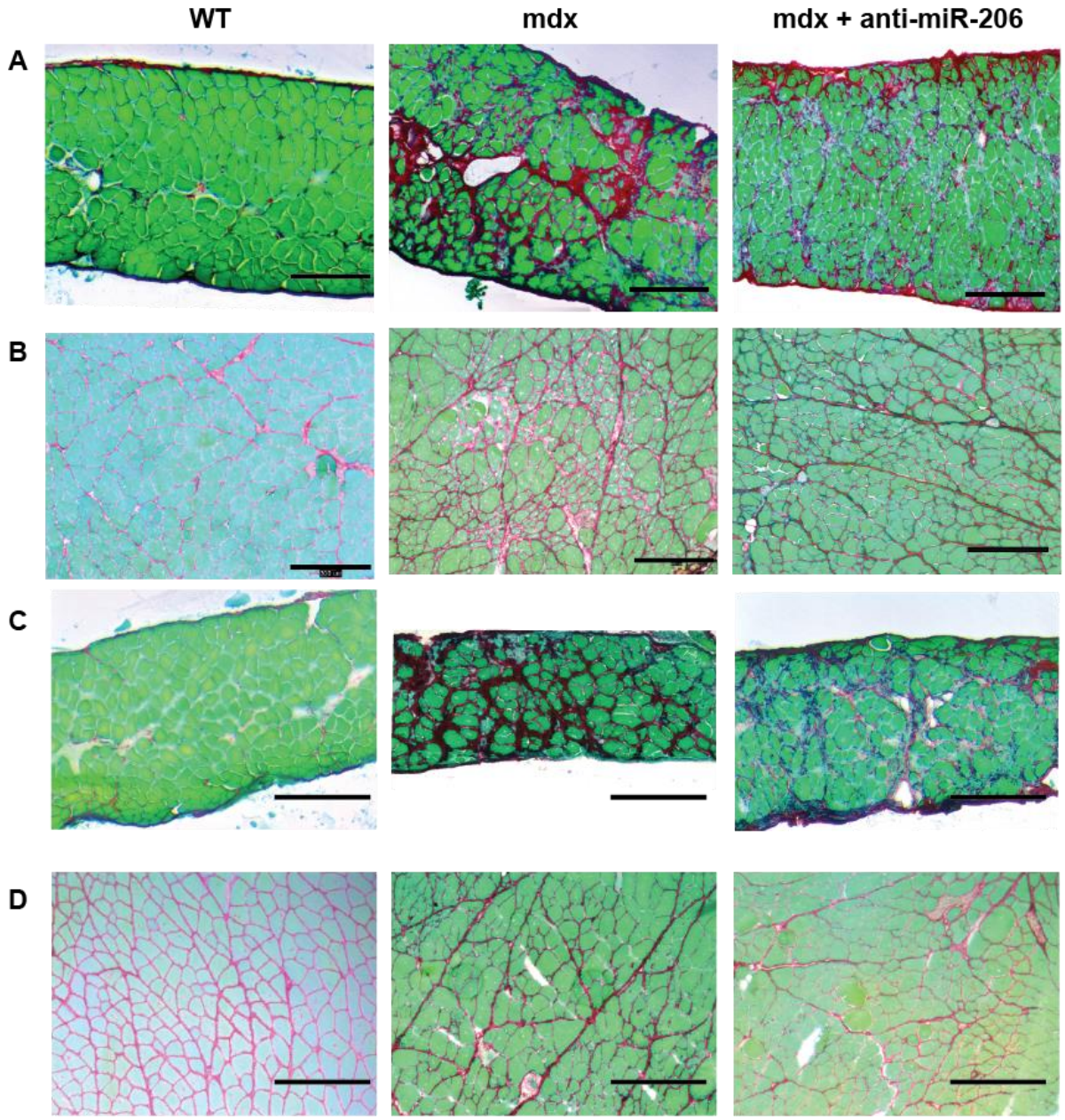

Figure 3.6. Reduced fibrosis in treated muscle. Picrosirius red/fast green staining was performed to detect collagen fibers at 3 months in (**A**) diaphragm and (**B**) hamstring and 5 months in (**C**) diaphragm and (**D**) hamstring. Collagen fibers are shown in red, while sarcoplasm is stained green. Fibrosis was greatly increased in dystrophic diaphragm, but more diffuse in the treated sample, suggestive of fewer mature collagen

fibers. WT did not show any fibrosis. While an increase in fibrosis was observed in dystrophic muscle compared to normal muscle, no discernable changes were seen in the hamstring between groups.

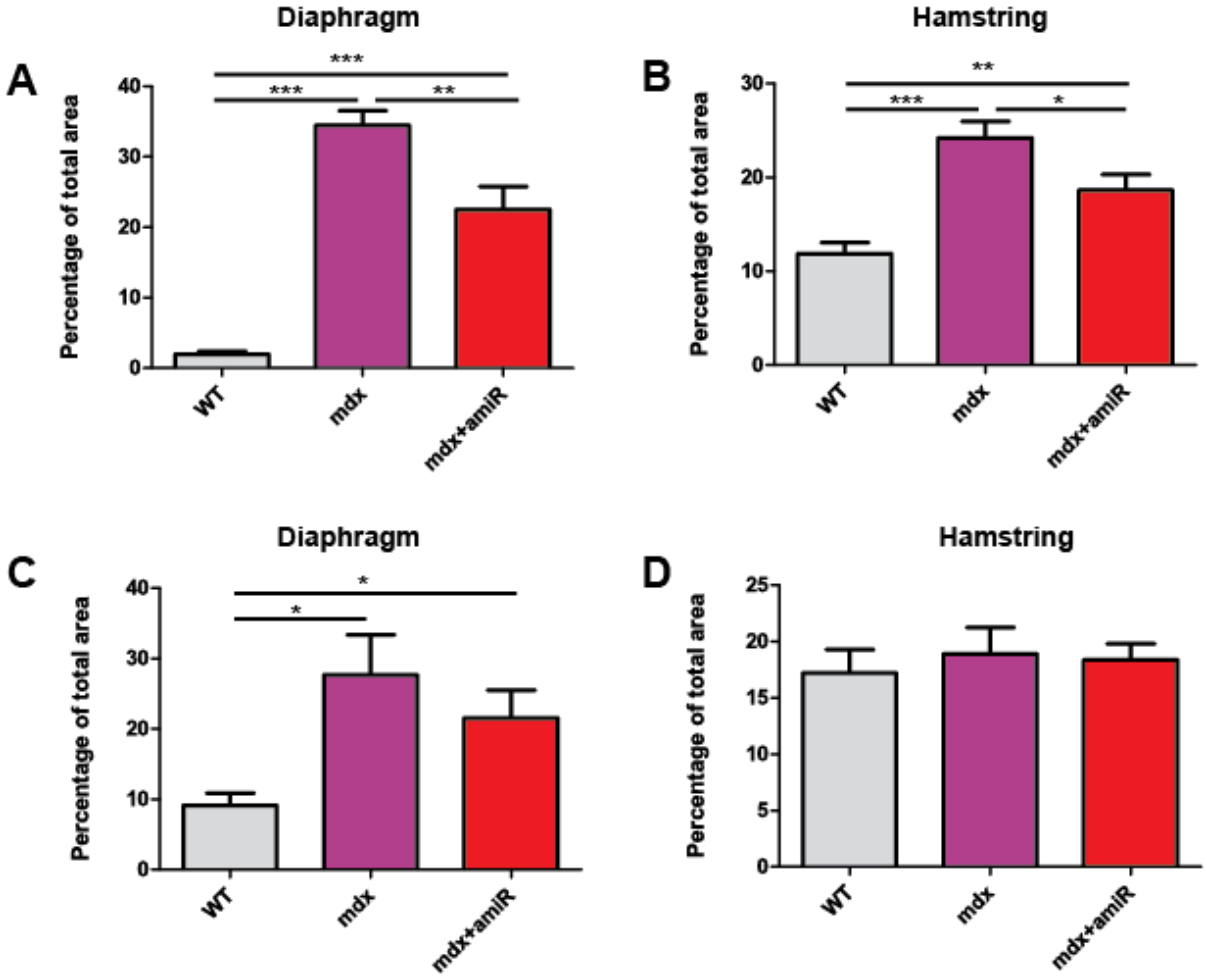

Figure 3.7. Reduced fibrotic area in treated muscle. Picrosirius red staining was quantified at 3 months in (A) diaphragm and (B) hamstring and at 5 months in (C) diaphragm and (D) hamstring. (A) Compared to WT diaphragm, both *mdx* groups displayed a significant increase in fibrotic area (***$p < 0.0001$, $n = 6$). With treatment, fibrotic area was greatly reduced (**$p = 0.0043$, $n = 6$). (B) A similar pattern was observed in the hamstring, with a significant increase in fibrosis between WT and dystrophic muscle (WT vs. *mdx* ***$p < 0.0001$ and WT vs. treated *mdx* **$p = 0.0046$, $n = 6$). Treated hamstring also contained considerably less fibrosis compared to the untreated (*$p = 0.0279$). (C) At 5 months, a significant increase in fibrotic area in

dystrophic muscle from WT was again found (WT vs. *mdx* *p = 0.0112 and WT vs. mdx+amIR *p = 0.0139, n = 6). Fibrosis decreased with treatment yet this was not statistically significant. (D) No distinct differences could be found between groups in the hamstring at 5 months. Bars represent mean with SEM.

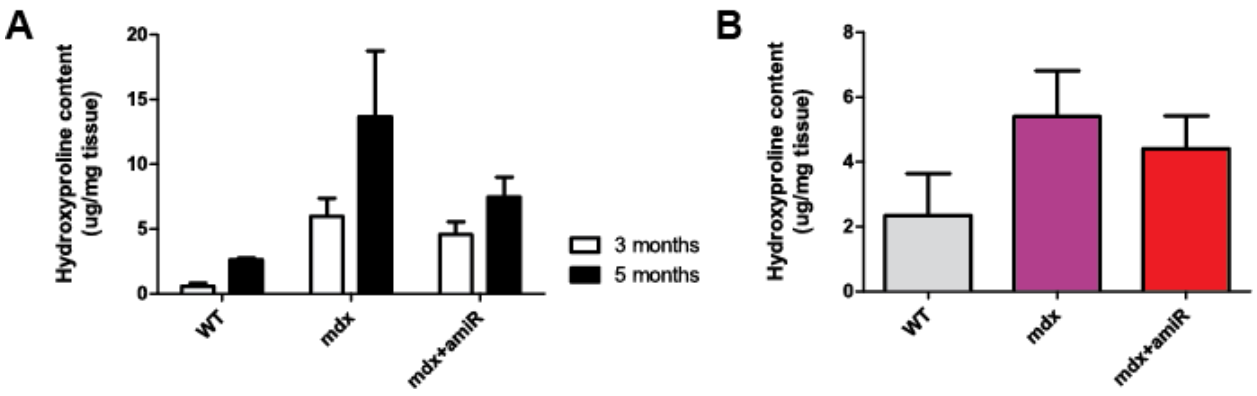

Figure 3.8. Decreased hydroxyproline content with treatment. Hydroxyproline was quantified (A) diaphragm at 3 and 5 months and (B) hamstring at 3 months. (A) Hydroxyproline concentration was lower in WT diaphragm than either *mdx* group. All groups showed an increase in hydroxyproline from 3 to 5 months. While a small improvement was observed with treatment at 3 months, untreated *mdx* showed a much greater increase in hydroxyproline with time. (B) Hamstring muscle displayed a similar pattern, as dystrophic muscle contained higher levels of hydroxyproline, which was reduced with treatment. Bars represent mean with SEM.

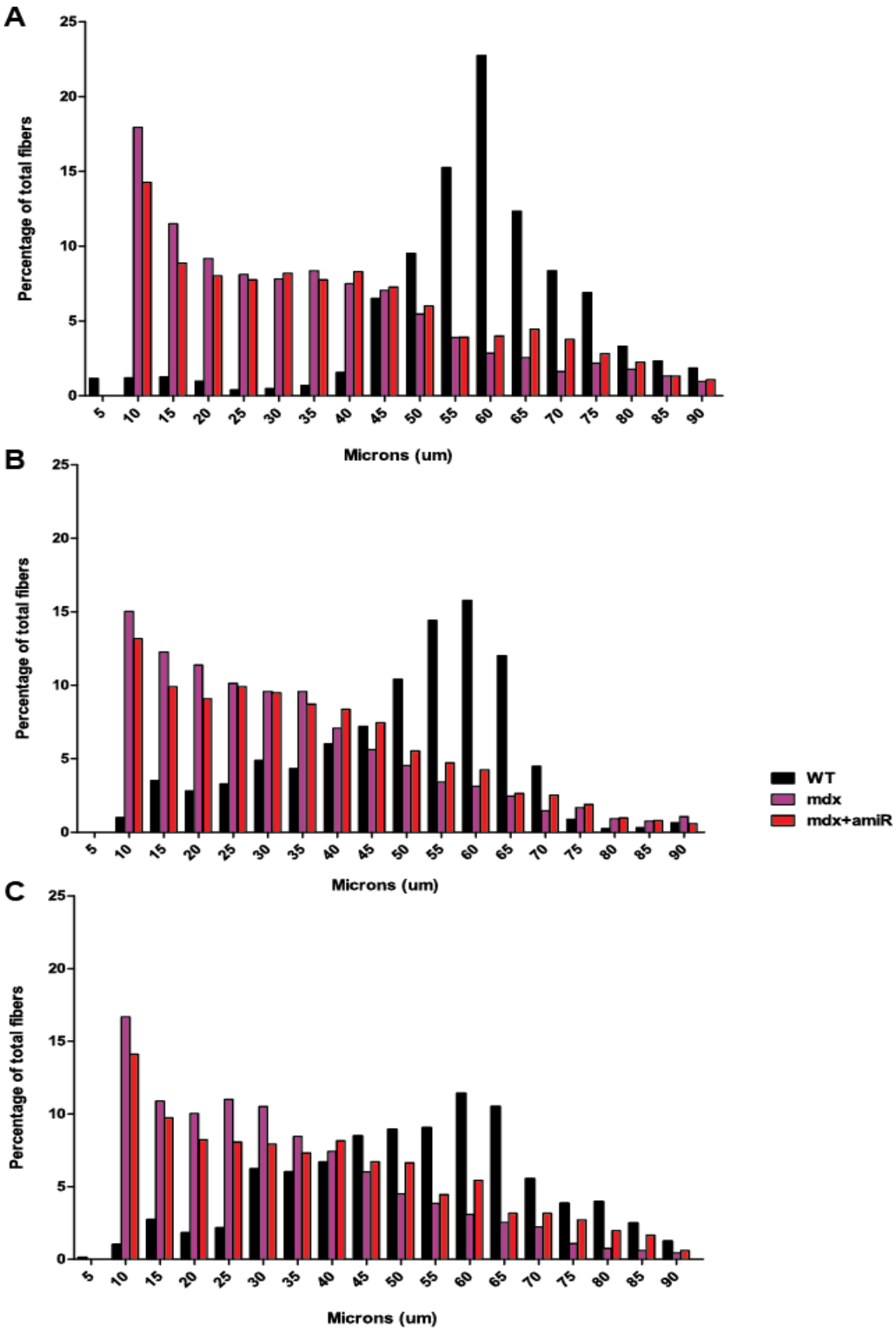
A
B
C
Percentage of total fibers
Microns (um)
0
5
10
15
20
25
30
35
40
45
50
55
60
65
70
75
80
85
90
WT
mdx
mdx+amiR

Figure 3.9. Normalization of fiber diameter. Fiber diameter was measured at (**A**) 1 month, (**B**) 3 months and (**C**) 5 months post-treatment. In WT muscle, a prominent peak at 60 μm across all timepoints. In contrast, the majority of dystrophic muscle fibers were small in size, with a peak at 10 μm. A slight shift toward normal sizes was observed with treatment, yet fibers were still smaller than WT overall. Bars represent mean.

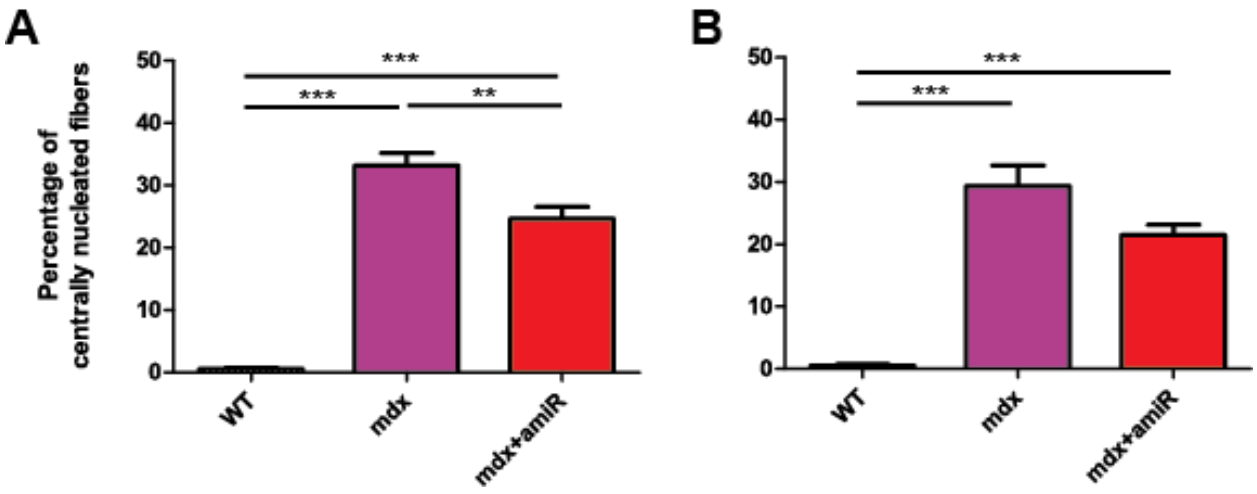

Figure 3.10. Reduced fiber regeneration with treatment. Centronucleation was measured in diaphragm at (**A**) 3 months and (**B**) 5 months post-treatment. (A) Dystrophic muscle contained significantly more centrally nucleated fibers than the WT (WT vs. *mdx* and treated *mdx* ***p < 0.0001, n = 6 for all groups). A substantial decrease in centronucleation was found with treatment (*mdx* vs. *mdx*+amiR **p = 0.0065, n = 6). (B) Similarly, a significant increase in the number of centrally nucleated fibers was found between WT and dystrophic muscle (WT vs. *mdx* ***p = 0.0003 and WT vs. *mdx*+amiR ***p < 0.0001, n = 6). Bars represent mean with SEM.

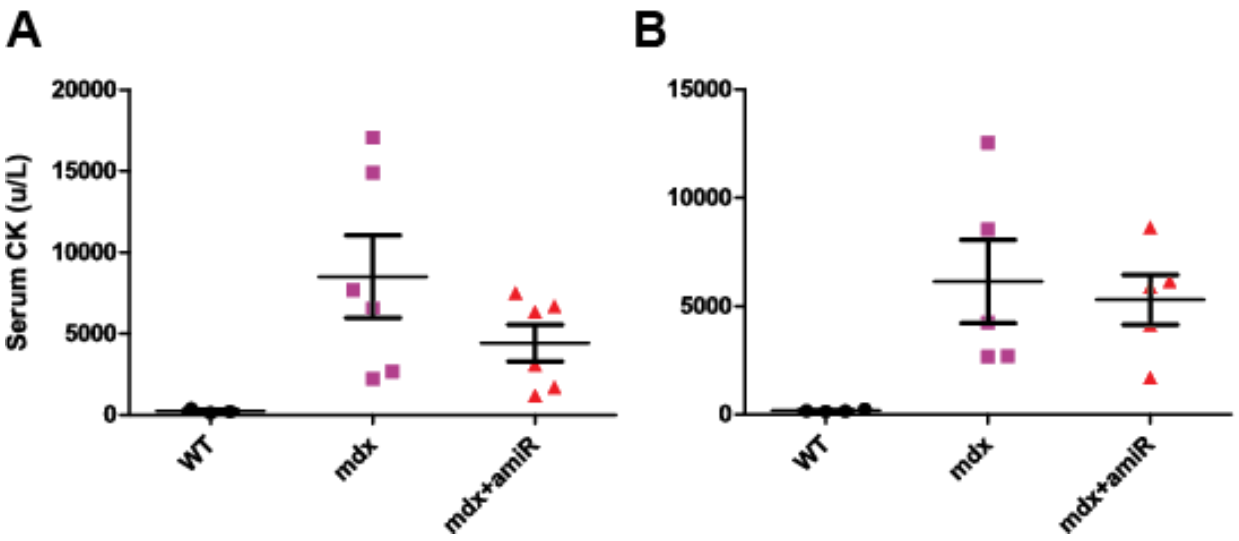

Figure 3.11. Improvements in overall muscle damage with treatment. Serum CK levels were measured at (**A**) 3 months and (**B**) 5 months post-treatment. WT CK levels were consistently low, suggestive of minimal muscle damage at both timepoints. In contrast, *mdx* CK levels were generally much higher, with a considerable range amongst samples. (A) At 3 months post-treatment, treated *mdx* CK levels appeared to be lower, with less variation. (B) At 5 months, a similar pattern was observed in treated mice but there was less of a distinction between untreated mice. Points represent individual measurements, horizontal center bars represent means and vertical bars signify ± SEM.

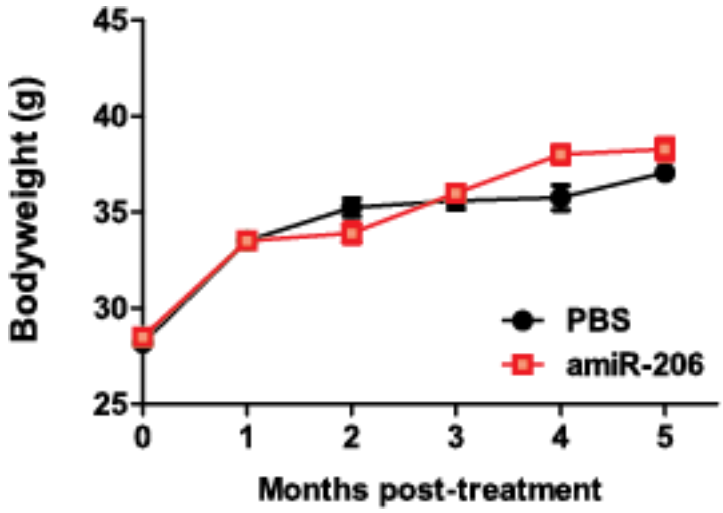

Figure 3.12. Bodyweight in mdx mice. Bodyweight was measured in untreated and treated *mdx* mice, which steadily increased with time. No significant differences were observed with treatment.

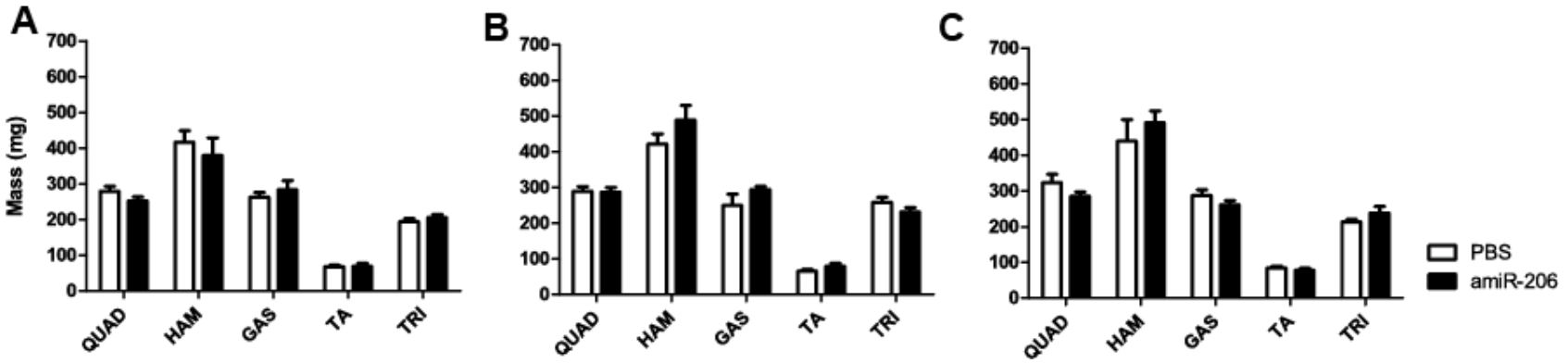

Figure 3.13. Muscle mass in mdx mice. Muscle mass was measured for different muscle groups at (**A**) 1 month, (**B**) 3 months and (**C**) 5 months post-treatment. Treatment did not have a significant effect on mass for any muscle group. Bars represent mean with SEM.

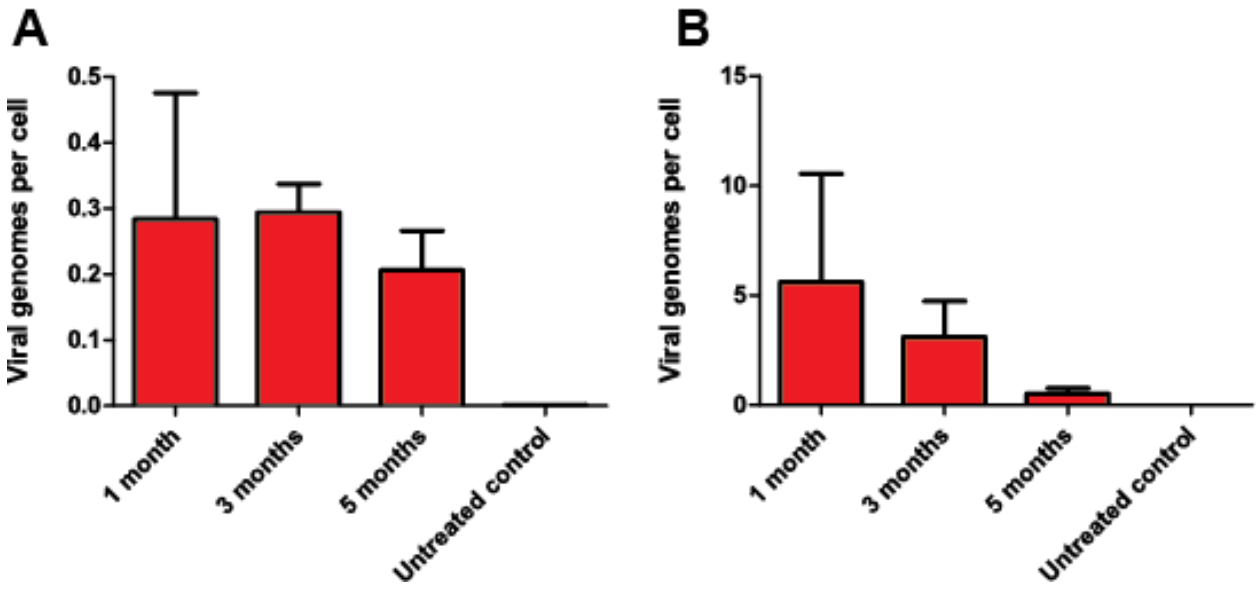

Figure 3.14. Vector persistence in treated mdx mice. The number of viral genomes per cell were detected in (**A**) gastrocnemius and (**B**) diaphragm over time. (A) The number of vector genomes in gastrocnemius was maintained from 1 to 3 months, with a decrease at 5 months. (B) Viral genomes in the diaphragm were greatly reduced with time. Bars represent mean with SEM.

V. Discussion

In this chapter, I examined the role of microRNA-206 in muscle pathology and if downregulation of miR-206 provides therapeutic benefit via expression of utrophin. First, I showed that administration of AAV9-anti-miR-206 significantly improved utrophin transcript levels in *mdx* mice and increased protein levels as well. Thus, downregulation of miR-206 diminishes its inhibitory effect on utrophin expression. After anti-miR-206 treatment, muscle pathology in the *mdx* mice appeared to improve, with a normalization of muscle fiber morphology and organization and also a decrease in inflammatory cell infiltration. Lowered serum CK levels also reflected a reduction in overall muscle damage with treatment. A significant decrease in centronucleation signified improvements in muscle fiber stability, since regeneration occurs in response to active myofiber necrosis. A slight shift in myofiber size was observed with treatment; however, most fibers were still smaller and likely less mature than in the WT. Fiber size in the diaphragm showed a similar pattern (not shown). Coupled with the centronucleation results, it is possible that the treatment may prevent mature myofiber death, but has no effect on myoblast proliferation. Treatment also did not appear to affect body or muscle mass.

Reducing microRNA-206 also appeared to influence a prominent aspect of the dystrophic phenotype, fibrosis. Masson trichrome staining revealed a significant decrease in collagen deposition. The presence of collagen fibers was examined by Picrosirius red/fast green staining, which showed that there were fewer mature fibers with treatment. Furthermore, increases in hydroxyproline content observed in the *mdx* diaphragm with time were stunted by treatment. These data suggest that

downregulation of miR-206 may delay progression of secondary disease pathways resulting from myofiber necrosis, such as fibrosis.

While utrophin is a known therapeutic target and can prevent muscle damage and fibrosis associated with DMD pathology, it is important to note that any changes could be influenced by expression of additional miR-206 targets and through a variety of different mechanisms. As mentioned in *Chapter II*, increased VEGFA expression can improve muscle vascularization to better dystrophic pathology. IGF-1 is another therapeutic miR-206 target whose expression may be hampered as well (Engvall and Wewer 2003). It is possible that miR-206 downregulation depresses targets that work together to produce the improvements observed in this study.

Nonetheless, there were obvious shortcomings with anti-miR-206 treatment. As discussed in *Chapter II*, miR-206 downregulation was short-lived and a marked reduction in viral genome was observed in the diaphragm. Interestingly, even though AAV transduction was initially lower in the hindlimb, motor function increases were still observed and may suggest that not all muscle fibers need to be transduced for therapeutic effect. Unlike utrophin gene replacement, sarcolemmal distribution in the majority of fibers was not observed. Studies suggest that only a two or three-fold increase is necessary to improve the dystrophic phenotype, so increased utrophin expression may only need occur in a fraction of fibers (Khurana and Davies 2003). Stronger staining in the neuromuscular junction with treatment also does not rule its contribution in improved function. In *mdx; utrophin*$^{-/-}$ mice, utrophin expression at the NMJ is greatly reduced and results in a decrease in the number of acetylcholine receptors by as much as 40%, suggesting that proper NMJ function is also affected in

DMD (Gramolini and Jasmin 1997). Furthermore, overexpression of PGC-1α, a transcriptional coactivator, enhanced NMJ function by improving motor neuron activity, resulting in improved muscle pathology and running performance in *mdx* mice (Handschin, Kobayashi et al. 2007). While dystrophic symptoms were greatly improved, miR-206 downregulation was not sufficient to completely alleviate pathology and prevent further muscle degeneration. Still, these data demonstrated that downregulation of miR-206 improve muscle pathology, supporting a deleterious role for miR-206 in DMD. In conclusion, this study draws attention to a previously unappreciated aspect of DMD and defines a new therapeutic avenue for muscular dystrophy.

CHAPTER 4: FUTURE DIRECTIONS

I. Overall impact of the current study

The goal of this study was to examine the role of microRNA-206 in mature muscle in secondary disease pathways that contribute to the dystrophic phenotype. The data presented here support a pathological role for miR-206, which is alleviated to some degree after miR-206 knockdown. This body of work also highlights the influence of secondary disease pathways on DMD pathology and their function in exacerbating the primary defect. Targeting dystrophin alone may not be sufficient to fully resolve symptoms and it is possible that concurrent disease mechanisms need to be addressed for complete recovery.

Although treatment with AAV9-anti-miR-206 improved dystrophic symptoms, the effect is less striking compared to direct gene replacement therapies with mini- or micro-dystrophin. Still, the lack of persistent gene expression and discovery of dystrophin-targeted T cell responses observed in DMD patients have halted progression of such therapies, spurring investigation into alternative AAV serotypes and strategies for increasing efficacy (Kornegay, Li et al. 2010, Mendell , Campbell et al. 2010). DMD patients may develop an immune response to the therapeutic dystrophin gene or to dystrophin expressed by revertant fibers. Therefore, strategies that seek to increase endogenous expression of booster genes may fare better. One example is treatment with an utrophin upregulator, which works by increasing expression of endogenous utrophin and has shown promise in clinical trials (Tinsley, Fairclough et al. 2011).

A major obstacle in DMD treatments is the size limit of presently available vectors. The full-length dystrophin gene is 2.4 Mbp with a cDNA length of 14 kb. Current gene therapy strategies rely on producing a truncated dystrophin protein to produce a milder phenotype similar to Becker muscular dystrophy. Using short sequences to affect microRNA-mediated regulation are more amenable to size constraints and are more versatile through their ability to target multiple pathways. Here, I have shown for the first time that using AAV-mediated microRNA downregulation has therapeutic potential for DMD, supporting further exploration into aberrant microRNA expression in other diseases that may benefit from a similar approach.

II. Possible future studies

MicroRNA-206 is known to be upregulated in both *mdx* mice and DMD patients, suggesting that this therapy could eventually be translated to human use (Greco, De Simone et al. 2009). Additional investigation to quantify miR-206 and miR-206 target expression in humans is needed to determine if patients would benefit from this therapy. Verification of miR-206 target binding in humans is also necessary. While miR-206 is upregulated in humans, it is possible that the amount of miR-206 or anti-miR-206 binding is not similar to mice, which would affect therapeutic efficacy of this treatment. Adjustments could be made to the anti-miR-206 sequence to increase miR-206 sequestration in humans.

The full potential of this therapy may also be obscured by insufficient depletion of miR-206. Although no attempt was made during this study to maximize microRNA binding efficacy, another group showed that up to 7 binding sites for another microRNA can be placed on a decoy target, after which the knockdown effect was saturated

(Haraguchi, Ozaki et al. 2009). This warrants further exploration into dosing and additional miR-206 binding sites on the decoy target.

Presently available AAV vectors also do not efficiently transduce satellite, or muscle precursor, cells, which highly express miR-206 (Arnett, Konieczny et al. 2014). This may be an advantage, since one major concern of targeting the satellite cells would be interference with normal muscle maturation. However, it has been hypothesized that muscle precursors are unable to differentiate due to inhibitory factors in the diseased microenvironment (Oexle and Kohlschütter 2001). Since miR-206 levels decrease as muscle cells mature, it would be interesting to see if miR-206 reduction would affect differentiation or aid in repopulating the muscle with differentiated fibers. While miR-206 is known to inhibit transcription factor Pax7 expression during early stages of differentiation, it is unclear what role miR-206 plays at later timepoints. Further study into the expression profile of miR-206 over time and whether this pattern is perturbed in DMD would be very useful for understanding the best way to utilize this therapy.

III. Considerations for DMD therapies

While we now have a better understanding of miR-206 function in DMD, the current results indicate that miR-206 reduction would not have an immediate impact on functional deficits. Because this treatment affects secondary disease mechanisms and does not appear to increase sarcolemmal utrophin expression globally, it can only work to lessen the severity of pathology and cannot prevent membrane instability and eventual muscle death. As mentioned previously, improvements to the current therapeutic design could be made. However, anti-miR-206 treatment may be useful in

combination with gene therapies that increase dystrophin levels. For example, AAVs carrying mini-dystrophin and anti-miR-206 could be co-delivered to target both primary and secondary disease mechanisms. Direct administration of an oligonucleotide with the anti-miR-206 sequence, similar to AONs for exon skipping therapies, could also easily be incorporated into existing therapies and allow for changes in dosing or even repeated dosing.

IV. Conclusions

Although additional verification is needed for eventual clinical application of anti-miR-206 treatment, I have shown for the first time that miR-206 can be targeted to elicit a therapeutic effect. I also show that miR-206 affects beneficial gene expression, supporting its pathological role. In summary, I have uncovered evidence for a previously unappreciated disease mechanism as well as a novel therapeutic paradigm for Duchenne muscular dystrophy, bringing us another step closer to a cure.

BIBLIOGRAPHY

Aartsma and A. Rus (2009). "Theoretic applicability of antisense - mediated exon skipping for Duchenne muscular dystrophy mutations." Human mutation **30**(3): 293-299.

Adamo, C. M., D.-F. Dai, J. M. Percival, E. Minami, M. S. Willis, E. Patrucco, S. C. Froehner and J. A. Beavo (2010). "Sildenafil reverses cardiac dysfunction in the mdx mouse model of Duchenne muscular dystrophy." Proceedings of the National Academy of Sciences **107**(44): 19079-19083.

Alexakis, C., T. Partridge and G. Bou-Gharios (2007). "Implication of the satellite cell in dystrophic muscle fibrosis: a self-perpetuating mechanism of collagen overproduction." American Journal of Physiology - Cell Physiology **293**(2): C661.

Anderson, J. E., K. Garrett, A. Moor, L. McIntosh and K. Penner (1998). "Dystrophy and myogenesis in mdx diaphragm muscle." Muscle & nerve **21**(9): 1153-1165.

Arnett, A. L. H., P. Konieczny, J. N. Ramos, J. Hall, G. Odom, Z. Yablonka-Reuveni, J. R. Chamberlain and J. S. Chamberlain (2014). "Adeno-associated viral vectors do not efficiently target muscle satellite cells." Molecular Therapy - Methods & Clinical Development **1**: 14038.

Asai, A., N. Sahani, M. Kaneki, Y. Ouchi, J. A. J. Martyn and S. E. Yasuhara (2007). "Primary Role of Functional Ischemia, Quantitative Evidence for the Two-Hit Mechanism, and Phosphodiesterase-5 Inhibitor Therapy in Mouse Muscular Dystrophy." PLoS ONE **2**(8): e806.

Asokan, A., D. V. Schaffer and R. Jude Samulski (2012). "The AAV Vector Toolkit: Poised at the Clinical Crossroads." Mol Ther **20**(4): 699-708.

Bainbridge, J. W., M. S. Mehat, V. Sundaram, S. J. Robbie, S. E. Barker, C. Ripamonti, A. Georgiadis, F. M. Mowat, S. G. Beattie, P. J. Gardner, K. L. Feathers, V. A. Luong, S. Yzer, K. Balaggan, A. Viswanathan, T. J. de Ravel, I. Casteels, G. E. Holder, N. Tyler, F. W. Fitzke, R. G. Weleber, M. Nardini, A. T. Moore, D. A. Thompson, S. M. Petersen-Jones, M. Michaelides, L. I. van den Born, A. Stockman, A. J. Smith, G. Rubin and R. R. Ali (2015). "Long-term effect of gene therapy on Leber's congenital amaurosis." N Engl J Med **372**(20): 1887-1897.

Bainbridge, J. W. B., A. J. Smith, S. S. Barker, S. Robbie, R. Henderson, K. Balaggan, A. Viswanathan, G. E. Holder, A. Stockman, N. Tyler, S. Petersen-Jones, S. S. Bhattacharya, A. J. Thrasher, F. W. Fitzke, B. J. Carter, G. S. Rubin, A. T. Moore and R. R. Ali (2008). "Effect of Gene Therapy on Visual Function in Leber's Congenital Amaurosis." New England Journal of Medicine **358**(21): 2231-2239.

Blake, D. J., A. Weir, S. E. Newey and K. E. Davies (2002). "Function and Genetics of Dystrophin and Dystrophin-Related Proteins in Muscle." Physiological Reviews **82**(2): 291-329.

Boutin, S. "Prevalence of Serum IgG and Neutralizing Factors Against Adeno-Associated Virus (AAV) Types 1, 2, 5, 6, 8, and 9 in the Healthy Population: Implications for Gene Therapy Using AAV Vectors." Human gene therapy **21**(6): 704-712.

Bowles, D. E., S. W. McPhee, C. Li, S. J. Gray, J. J. Samulski, A. S. Camp, J. Li, B. Wang, P. E. Monahan, J. E. Rabinowitz, J. C. Grieger, L. Govindasamy, M. Agbandje-McKenna, X. Xiao and R. J. Samulski (2012). "Phase 1 gene therapy for Duchenne muscular dystrophy using a translational optimized AAV vector." Mol Ther **20**(2): 443-455.

Burnett, J. R. and A. J. Hooper (2009). "Alipogene tiparvovec, an adeno-associated virus encoding the Ser(447)X variant of the human lipoprotein lipase gene for the treatment of patients with lipoprotein lipase deficiency." Curr Opin Mol Ther **11**(6): 681-691.

Cacchiarelli, D., J. Martone, E. Girardi, M. Cesana, T. Incitti, M. Morlando, C. Nicoletti, T. Santini, O. Sthandier, L. Barberi, A. Auricchio, A. Musaro and I. Bozzoni (2010). "MicroRNAs involved in molecular circuitries relevant for the Duchenne muscular dystrophy pathogenesis are controlled by the dystrophin/nNOS pathway." Cell Metab **12**(4): 341-351.

Calcedo, R., L. H. Vandenberghe, G. Gao, J. Lin and J. M. Wilson (2009). "Worldwide Epidemiology of Neutralizing Antibodies to Adeno-Associated Viruses." Journal of Infectious Diseases **199**(3): 381-390.

Calos, M. P. (2016). "The CRISPR Way to Think about Duchenne's." The New England journal of medicine **374**(17): 1684-1686.

Campbell, K. P. and J. T. Stull (2003). "Skeletal Muscle Basement Membrane-Sarcolemma-Cytoskeleton Interaction Minireview Series." Journal of Biological Chemistry **278**(15): 12599-12600.

Carmeliet, P. (2000). "VEGF gene therapy: stimulating angiogenesis or angioma-genesis?" Nat Med **6**(10): 1102-1103.

Chargé, S. B. P. and M. A. Rudnicki (2004). "Cellular and Molecular Regulation of Muscle Regeneration." Physiological Reviews **84**(1): 209.

Chen, J.-F., Y. Tao, J. Li, Z. Deng, Z. Yan, X. Xiao and D.-Z. Wang (2010). "microRNA-1 and microRNA-206 regulate skeletal muscle satellite cell proliferation and differentiation by repressing Pax7." The Journal of cell biology **190**(5): 867-879.

Chiriboga, C. A., K. J. Swoboda, B. T. Darras, S. T. Iannaccone, J. Montes, D. C. De Vivo, D. A. Norris, C. F. Bennett and K. M. Bishop (2016). "Results from a phase 1 study of nusinersen (ISIS-SMNRx) in children with spinal muscular atrophy." Neurology **86**(10): 890-897.

Cirak, S., V. Arechavala-Gomeza, M. Guglieri, L. Feng, S. Torelli, K. Anthony, S. Abbs, M. E. Garralda, J. Bourke, D. J. Wells, G. Dickson, M. J. A. Wood, S. D. Wilton, V. Straub, R. Kole, S. B. Shrewsbury, C. Sewry, J. E. Morgan, K. Bushby and F. Muntoni (2011). "Exon skipping and dystrophin restoration in patients with Duchenne muscular dystrophy after systemic phosphorodiamidate morpholino oligomer treatment: an open-label, phase 2, dose-escalation study." The Lancet **378**(9791): 595-605.

Clement, N., D. R. Knop and B. J. Byrne (2009). "Large-Scale Adeno-Associated Viral Vector Production Using a Herpesvirus-Based System Enables Manufacturing for Clinical Studies." Human Gene Therapy **20 SRC - GoogleScholar**: 796-806.

Cohn, R. D. (2000). "Molecular basis of muscular dystrophies." Muscle & nerve **23**(10): 1456-1471.

Dalkilic, I. and L. M. Kunkel (2003). "Muscular dystrophies: genes to pathogenesis." Current opinion in genetics & development **13**(3): 231-238.

Deconinck, A. E., J. A. Rafael, J. A. Skinner, S. C. Brown, A. C. Potter, L. Metzinger, D. J. Watt, J. G. Dickson, J. M. Tinsley and K. E. Davies (1997). "Utrophin-Dystrophin-Deficient Mice as a Model for Duchenne Muscular Dystrophy." Cell **90**(4): 717-727.

Deconinck, N. and B. Dan (2007). "Pathophysiology of Duchenne Muscular Dystrophy: Current Hypotheses." Pediatric Neurology **36**(1): 1-7.

Deconinck, N., J. Tinsley, F. De Backer, R. Fisher, D. Kahn, S. Phelps, K. Davies and J. M. Gillis (1997). "Expression of truncated utrophin leads to major functional improvements in dystrophin-deficient muscles of mice." Nat Med **3**(11): 1216-1221.

Dolgin, E. (2017). Spinal muscular atrophy approval boosts antisense drugs, Nature Research.

Ebert, M. S., J. R. Neilson and P. A. Sharp (2007). "MicroRNA sponges: competitive inhibitors of small RNAs in mammalian cells." Nat Meth **4**(9): 721-726.

Ebert, M. S. and P. A. Sharp (2010). "MicroRNA sponges: progress and possibilities." Rna **16**(11): 2043-2050.

Ebihara, S., G.-H. Guibinga, R. Gilbert, J. Nalbantoglu, B. Massie, G. Karpati and B. J. Petrof (2000). "Differential effects of dystrophin and utrophin gene transfer in immunocompetent muscular dystrophy (mdx) mice." Physiological Genomics **3**(3): 133.

Emery, A. E. (2002). "The muscular dystrophies." The Lancet **359**(9307): 687-695.

Engvall, E. and U. M. Wewer (2003). "The new frontier in muscular dystrophy research: booster genes." The FASEB Journal **17**(12): 1579-1584.

Ennen, J. P., M. Verma and A. Asakura (2013). "Vascular-targeted therapies for Duchenne muscular dystrophy." Skeletal muscle **3**(1): 9.

Fabb, S. A., D. J. Wells, P. Serpente and G. Dickson (2002). "Adeno-associated virus vector gene transfer and sarcolemmal expression of a 144 kDa micro-dystrophin effectively restores the dystrophin-associated protein complex and inhibits myofibre degeneration in nude/mdx mice." Human Molecular Genetics **11**(7): 733-741.

Fairclough, R. J., M. J. Wood and K. E. Davies (2013). "Therapy for Duchenne muscular dystrophy: renewed optimism from genetic approaches." Nat Rev Genet **14**(6): 373-378.

Fletcher, S. S. (2006). "Dystrophin expression in the mdx mouse after localised and systemic administration of a morpholino antisense oligonucleotide." The journal of gene medicine **8**(2): 207-216.

Foster, H., L. Popplewell and G. Dickson (2012). "Genetic therapeutic approaches for Duchenne muscular dystrophy." Hum Gene Ther **23**(7): 676-687.

Gambardella, S., F. Rinaldi, S. M. Lepore, A. Viola, E. Loro, C. Angelini, L. Vergani, G. Novelli and A. Botta (2010). "Overexpression of microRNA-206 in the skeletal muscle from myotonic dystrophy type 1 patients." Journal of Translational Medicine **8**(1): 48.

Gramolini, A. O. and B. J. Jasmin (1997). "Duchenne muscular dystrophy and the neuromuscular junction: the utrophin link." Bioessays **19**(9): 747-750.

Grange, R. W., E. Isotani, K. S. Lau, K. E. Kamm, P. L. Huang and J. T. Stull (2001). "Nitric oxide contributes to vascular smooth muscle relaxation in contracting fast-twitch muscles." Physiological Genomics **5**(1): 35-44.

Greco, S., M. De Simone, C. Colussi, G. Zaccagnini, P. Fasanaro, M. Pescatori, R. Cardani, R. Perbellini, E. Isaia, P. Sale, G. Meola, M. C. Capogrossi, C. Gaetano and F. Martelli (2009). "Common micro-RNA signature in skeletal muscle damage and regeneration induced by Duchenne muscular dystrophy and acute ischemia." FASEB J **23**(10): 3335-3346.

Grounds, M. D., H. G. Radley, G. S. Lynch, K. Nagaraju and A. De Luca (2008). "Towards developing standard operating procedures for pre-clinical testing in the mdx mouse model of Duchenne muscular dystrophy." Neurobiology of disease **31**(1): 1-19.

Guglieri, M., V. Straub, K. Bushby and H. Lochmüller (2008). "Limb–girdle muscular dystrophies." Current opinion in neurology **21**(5): 576-584.

Handschin, C., Y. M. Kobayashi, S. Chin, P. Seale, K. P. Campbell and B. M. Spiegelman (2007). "PGC-1α regulates the neuromuscular junction program and ameliorates Duchenne muscular dystrophy." Genes & development **21**(7): 770-783.

Haraguchi, T., Y. Ozaki and H. Iba (2009). "Vectors expressing efficient RNA decoys achieve the long-term suppression of specific microRNA activity in mammalian cells." Nucleic Acids Research **37**(6): e43-e43.

Howell, J. M., H. Lochmuller, A. O'Hara, S. Fletcher, B. A. Kakulas, B. Massie, J. Nalbantoglu and G. Karpati (1998). "High-level dystrophin expression after adenovirus-mediated dystrophin minigene transfer to skeletal muscle of dystrophic dogs: prolongation of expression with immunosuppression." Hum Gene Ther **9**(5): 629-634.

Ito, K., S. Kimura, S. Ozasa, M. Matsukura, M. Ikezawa, K. Yoshioka, H. Ueno, M. Suzuki, K. Araki, K.-i. Yamamura, T. Miwa, G. Dickson, G. D. Thomas and T. Miike (2006). "Smooth muscle-specific dystrophin expression improves aberrant vasoregulation in mdx mice." Human Molecular Genetics **15**(14): 2266-2275.

Jain, R. K. (2003). "Molecular regulation of vessel maturation." Nat Med **9**(6): 685-693.

Jarmin, S., H. Kymalainen, L. Popplewell and G. Dickson (2014). "New developments in the use of gene therapy to treat Duchenne muscular dystrophy." Expert Opin Biol Ther **14**(2): 209-230.

Khurana, T. S. and K. E. Davies (2003). "Pharmacological strategies for muscular dystrophy." Nat Rev Drug Discov **2**(5): 379-390.

Kinali, M., V. Arechavala-Gomeza, L. Feng, S. Cirak, D. Hunt, C. Adkin, M. Guglieri, E. Ashton, S. Abbs, P. Nihoyannopoulos, M. E. Garralda, M. Rutherford, C. McCulley, L. Popplewell, I. R. Graham, G. Dickson, M. J. A. Wood, D. J. Wells, S. D. Wilton, R. Kole, V. Straub, K. Bushby, C. Sewry, J. E. Morgan and F. Muntoni (2009). "Local restoration of dystrophin expression with the morpholino oligomer AVI-4658 in Duchenne muscular dystrophy: a single-blind, placebo-controlled, dose-escalation, proof-of-concept study." The Lancet Neurology **8**(10): 918-928.

Kobayashi, Y. M., E. P. Rader, R. W. Crawford, N. K. Iyengar, D. R. Thedens, J. A. Faulkner, S. V. Parikh, R. M. Weiss, J. S. Chamberlain, S. A. Moore and K. P. Campbell (2008). "Sarcolemma-localized nNOS is required to maintain activity after mild exercise." Nature **456**(7221): 511-515.

Kornegay, J. N., D. J. Bogan Jr Fau - Bogan, M. K. Bogan Dj Fau - Childers, J. Childers Mk Fau - Li, P. Li J Fau - Nghiem, D. A. Nghiem P Fau - Detwiler, C. A. Detwiler Da Fau - Larsen, R. W. Larsen Ca Fau - Grange, R. K. Grange Rw Fau - Bhavaraju-Sanka, S. Bhavaraju-Sanka Rk Fau - Tou, B. P. Tou S Fau - Keene, J. F. Keene Bp Fau - Howard, Jr., J. Howard Jf Jr Fau - Wang, Z. Wang J Fau - Fan, S. J. Fan Z Fau - Schatzberg, M. A. Schatzberg Sj Fau - Styner, K. M. Styner Ma Fau - Flanigan, X. Flanigan Km Fau - Xiao, E. P. Xiao X Fau - Hoffman and E. P. Hoffman "Canine models of Duchenne muscular dystrophy and their use in therapeutic strategies." (1432-1777 (Electronic)).

Kornegay, J. N., J. Li, J. R. Bogan, D. J. Bogan, C. Chen, H. Zheng, B. Wang, C. Qiao, J. F. Howard and X. Xiao (2010). "Widespread Muscle Expression of an AAV9 Human Mini-dystrophin Vector After Intravenous Injection in Neonatal Dystrophin-deficient Dogs." Mol Ther **18**(8): 1501-1508.

Kotterman, M. A. and D. V. Schaffer (2014). "Engineering adeno-associated viruses for clinical gene therapy." Nature Reviews Genetics **15**(7): 445-451.

Latroche, C., B. Matot, A. Martins-Bach, D. Briand, B. Chazaud, C. Wary, P. G. Carlier, F. Chrétien and G. Jouvion (2015). "Structural and Functional Alterations of Skeletal Muscle Microvasculature in Dystrophin-Deficient mdx Mice." The American Journal of Pathology **185**(9): 2482-2494.

Lin, C.-Y., H.-C. Lee, C.-Y. Fu, Y.-Y. Ding, J.-S. Chen, M.-H. Lee, W.-J. Huang and H.-J. Tsai (2013). "miR-1 and miR-206 target different genes to have opposing roles during angiogenesis in zebrafish embryos." Nat Commun **4**.

Liu, N., A. H. Williams, J. M. Maxeiner, S. Bezprozvannaya, J. M. Shelton, J. A. Richardson, R. Bassel-Duby and E. N. Olson (2012). "microRNA-206 promotes skeletal muscle regeneration and delays progression of Duchenne muscular dystrophy in mice." J Clin Invest **122**(6): 2054-2065.

Long, C., J. R. McAnally, J. M. Shelton, A. A. Mireault, R. Bassel-Duby and E. N. Olson (2014). "Prevention of muscular dystrophy in mice by CRISPR/Cas9–mediated editing of germline DNA." Science (New York, N.Y.) **345**(6201): 1184-1188.

Loufrani, L., B. I. Levy and D. Henrion (2002). "Defect in Microvascular Adaptation to Chronic Changes in Blood Flow in Mice Lacking the Gene Encoding for Dystrophin." Circulation Research **91**(12): 1183-1189.

Lu, Q. L., C. J. Mann, F. Lou, G. Bou-Gharios, G. E. Morris, S.-a. Xue, S. Fletcher, T. A. Partridge and S. D. Wilton (2003). "Functional amounts of dystrophin produced by skipping the mutated exon in the mdx dystrophic mouse." Nature medicine **9**(8): 1009-1014.

Lu, Y., Y. K. Choi, M. Campbell - Thompson, C. Li, Q. Tang, J. M. Crawford, T. R. Flotte and S. Song (2006). "Therapeutic level of functional human alpha 1 antitrypsin (hAAT) secreted from murine muscle transduced by adeno - associated virus (rAAV1) vector." The journal of gene medicine **8**(6): 730-735.

McCarthy, J. J. (2008). "MicroRNA-206: the skeletal muscle-specific myomiR." Biochimica et Biophysica Acta (BBA)-Gene Regulatory Mechanisms **1779**(11): 682-691.

McCarthy, J. J., K. A. Esser and F. H. Andrade (2007). "MicroRNA-206 is overexpressed in the diaphragm but not the hindlimb muscle of mdx mouse." American Journal of Physiology - Cell Physiology **293**(1): C451-C457.

Mendell , J. R., K. Campbell , L. Rodino-Klapac , Z. Sahenk , C. Shilling , S. Lewis , D. Bowles , S. Gray , C. Li , G. Galloway , V. Malik , B. Coley , K. R. Clark , J. Li , X. Xiao , J. Samulski , S. W. McPhee , R. J. Samulski and C. M. Walker (2010). "Dystrophin Immunity in Duchenne's Muscular Dystrophy." New England Journal of Medicine **363**(15): 1429-1437.

Mendell, J. R., W. K. Engel and E. C. Derrer (1971). "Duchenne Muscular Dystrophy: Functional Ischemia Reproduces Its Characteristic Lesions." Science **172**(3988): 1143-1145.

Messina, S., A. Mazzeo, A. Bitto, M. h. Aguennouz, A. Migliorato, M. G. De Pasquale, L. Minutoli, D. Altavilla, L. Zentilin, M. Giacca, F. Squadrito and G. Vita (2007). "VEGF overexpression via adeno-associated virus gene transfer promotes skeletal muscle regeneration and enhances muscle function in mdx mice." The FASEB Journal **21**(13): 3737-3746.

Mezzina, M. and O.-W. Merten (2011). "Adeno-associated viruses." Methods in molecular biology (Clifton, N.J.) **737**: 211-234.

Moser, H. (1984). "Duchenne muscular dystrophy: pathogenetic aspects and genetic prevention." Human genetics **66**(1): 17-40.

Muntoni, F., S. Torelli and A. Ferlini (2003). "Dystrophin and mutations: one gene, several proteins, multiple phenotypes." The Lancet Neurology **2**(12): 731-740.

Nathwani, A. C., E. G. D. Tuddenham, S. Rangarajan, C. Rosales, J. McIntosh, D. C. Linch, P. Chowdary, A. Riddell, A. J. Pie, C. Harrington, J. O'Beirne, K. Smith, J. Pasi, B. Glader, P. Rustagi, C. Y. C. Ng, M. A. Kay, J. Zhou, Y. Spence, C. L. Morton, J. Allay, J. Coleman, S. Sleep, J. M. Cunningham, D. Srivastava, E. Basner-Tschakarjan, F. Mingozzi, K. A. High, J. T. Gray, U. M. Reiss, A. W. Nienhuis and A. M. Davidoff (2011). "Adenovirus-Associated Virus Vector–Mediated Gene Transfer in Hemophilia B." New England Journal of Medicine **365**(25): 2357-2365.

Nelson, C. E., C. H. Hakim, D. G. Ousterout, P. I. Thakore, E. A. Moreb, R. M. C. Rivera, S. Madhavan, X. Pan, F. A. Ran and W. X. Yan (2016). "In vivo genome editing improves muscle function in a mouse model of Duchenne muscular dystrophy." Science **351**(6271): 403-407.

Nelson, M. D., F. Rader, X. Tang, J. Tavyev, S. F. Nelson, M. C. Miceli, R. M. Elashoff, H. L. Sweeney and R. G. Victor (2014). "PDE5 inhibition alleviates functional muscle ischemia in boys with Duchenne muscular dystrophy." Neurology **82**(23): 2085-2091.

Nico, B., A. Frigeri, G. P. Nicchia, P. Corsi, D. Ribatti, F. Quondamatteo, R. Herken, F. Girolamo, A. Marzullo, M. Svelto and L. Roncali (2003). "Severe alterations of endothelial and glial cells in the blood-brain barrier of dystrophic mdx mice." Glia **42**(3): 235-251.

Nonaka, I. (1998). "Animal Models of Muscular Dystrophies." Comparative Medicine **48**(1): 8-17.

Odom, G. L., P. Gregorevic, J. M. Allen, E. Finn and J. S. Chamberlain (2008). "Microutrophin delivery through rAAV6 increases lifespan and improves muscle function in dystrophic dystrophin/utrophin-deficient mice." Mol Ther **16**(9): 1539-1545.

Oexle, K. and A. Kohlschütter (2001). "Cause of Progression in Duchenne Muscular Dystrophy: Impaired Differentiation More Probable Than Replicative Aging." Neuropediatrics **32**(03): 123-129.

Ohlendieck, K. and K. P. Campbell (1991). "Dystrophin-associated proteins are greatly reduced in skeletal muscle from mdx mice." J Cell Biol **115**(6): 1685-1694.

Ohlendieck, K., K. Matsumura, V. V. Ionasescu, J. A. Towbin, E. P. Bosch, S. L. Weinstein, S. W. Sernett and K. P. Campbell (1993). "Duchenne muscular dystrophy: Deficiency of dystrophin - associated proteins in the sarcolemma." Neurology **43**(4): 795.

Olfert, I. M., R. A. Howlett, K. Tang, N. D. Dalton, Y. Gu, K. L. Peterson, P. D. Wagner and E. C. Breen (2009). "Muscle-specific VEGF deficiency greatly reduces exercise endurance in mice." The Journal of Physiology **587**(8): 1755-1767.

Qiao, C., T. Koo, J. Li, X. Xiao and J. G. Dickson (2011). "Gene therapy in skeletal muscle mediated by adeno-associated virus vectors." Methods Mol Biol **807**: 119-140.

Radu, M. and J. Chernoff (2013). "An in vivo Assay to Test Blood Vessel Permeability." (73): e50062.

Rando, T. A. (2001). "Role of nitric oxide in the pathogenesis of muscular dystrophies: a "two hit" hypothesis of the cause of muscle necrosis." Microscopy research and technique **55**(4): 223-235.

Rosenberg, A. S., M. Puig, K. Nagaraju, E. P. Hoffman, S. A. Villalta, V. A. Rao, L. M. Wakefield and J. Woodcock (2015). "Immune-mediated pathology in Duchenne muscular dystrophy." Science Translational Medicine **7**(299): 299rv294.

Rosenberg, M. I., S. A. Georges, A. Asawachaicharn, E. Analau and S. J. Tapscott (2006). "MyoD inhibits Fstl1 and Utrn expression by inducing transcription of miR-206." The Journal of Cell Biology **175**(1): 77.

Sakamoto, M., K. Yuasa, M. Yoshimura, T. Yokota, T. Ikemoto, M. Suzuki, G. Dickson, Y. Miyagoe-Suzuki and S. i. Takeda (2002). "Micro-dystrophin cDNA ameliorates dystrophic phenotypes when introduced into mdx mice as a transgene." Biochemical and Biophysical Research Communications **293**(4): 1265-1272.

Salva, M. Z., C. L. Himeda, P. W. L. Tai, E. Nishiuchi, P. Gregorevic, J. M. Allen, E. E. Finn, Q. G. Nguyen, M. J. Blankinship, L. Meuse, J. S. Chamberlain and S. D. Hauschka (2007). "Design of Tissue-specific Regulatory Cassettes for High-level rAAV-mediated Expression in Skeletal and Cardiac Muscle." Mol Ther **15**(2): 320-329.

Sander, M., B. Chavoshan, S. A. Harris, S. T. Iannaccone, J. T. Stull, G. D. Thomas and R. G. Victor (2000). "Functional muscle ischemia in neuronal nitric oxide synthase-deficient skeletal muscle of children with Duchenne muscular dystrophy." Proceedings of the National Academy of Sciences **97**(25): 13818-13823.

Serrano, A. L. and P. Muñoz-Cánoves (2010). "Regulation and dysregulation of fibrosis in skeletal muscle." Experimental Cell Research **316**(18): 3050-3058.

Soifer, H. S., J. J. Rossi and P. Sætrom (2007). "MicroRNAs in Disease and Potential Therapeutic Applications." Molecular Therapy **15**(12): 2070-2079.

Stahlhut, C., Y. Suarez, J. Lu, Y. Mishima and A. J. Giraldez (2012). "miR-1 and miR-206 regulate angiogenesis by modulating VegfA expression in zebrafish." Development **139**(23): 4356-4364.

Stedman, H. H., H. L. Sweeney, J. B. Shrager, H. C. Maguire, R. A. Panettieri, B. Petrof, M. Narusawa, J. M. Leferovich, J. T. Sladky and A. M. Kelly (1991). "The mdx

mouse diaphragm reproduces the degenerative changes of Duchenne muscular dystrophy." Nature **352**(6335): 536-539.

Stein, C. A. (2016). "Eteplirsen approved for Duchenne muscular dystrophy: The FDA faces a difficult choice." Molecular Therapy **24**(11): 1884-1885.

Tidball, J. G. (1995). "Inflammatory cell response to acute muscle injury." Medicine and science in sports and exercise **27**(7): 1022-1032.

Tidball, J. G. (2005). "Inflammatory processes in muscle injury and repair." American Journal of Physiology - Regulatory, Integrative and Comparative Physiology **288**(2): R345.

Tinsley, J., N. Deconinck, R. Fisher, D. Kahn, S. Phelps, J. M. Gillis and K. Davies (1998). "Expression of full-length utrophin prevents muscular dystrophy in mdx mice." Nat Med **4**(12): 1441-1444.

Tinsley, J., N. Robinson, F. Wilson, G. Horne and K. Davies (2014). "Future Clinical And Biomarker Development For SMT C1100, The First Utrophin Modulator To Enter Clinical Trials For Duchenne Muscular Dystrophy (DMD)(S6. 004)." Neurology **82**(10 Supplement): S6. 004.

Tinsley, J. M., R. J. Fairclough, R. Storer, F. J. Wilkes, A. C. Potter, S. E. Squire, D. S. Powell, A. Cozzoli, R. F. Capogrosso, A. Lambert, F. X. Wilson, S. P. Wren, A. De Luca and K. E. Davies (2011). "Daily Treatment with SMTC1100, a Novel Small Molecule Utrophin Upregulator, Dramatically Reduces the Dystrophic Symptoms in the <italic>mdx</italic> Mouse." PLoS ONE **6**(5): e19189.

Verma, M., Y. Asakura, H. Hirai, S. Watanabe, C. Tastad, G.-H. Fong, M. Ema, J. A. Call, D. A. Lowe and A. Asakura (2010). "Flt-1 haploinsufficiency ameliorates muscular dystrophy phenotype by developmentally increased vasculature in mdx mice." Human Molecular Genetics **19**(21): 4145-4159.

Vila, M. C., M. B. Klimek, J. S. Novak, S. Rayavarapu, K. Uaesoontrachoon, J. F. Boehler, A. A. Fiorillo, M. W. Hogarth, A. Zhang and C. Shaughnessy (2015). "Elusive sources of variability of dystrophin rescue by exon skipping." Skeletal muscle **5**(1): 44.

Wallace, G. Q. and E. M. McNally (2009). "Mechanisms of muscle degeneration, regeneration, and repair in the muscular dystrophies." Annu Rev Physiol **71**: 37-57.

Wang, B., J. Li and X. Xiao (2000). "Adeno-associated virus vector carrying human minidystrophin genes effectively ameliorates muscular dystrophy in mdx mouse model." Proceedings of the National Academy of Sciences **97**(25): 13714-13719.

Wang, Z., R. Storb, C. L. Halbert, G. B. Banks, T. M. Butts, E. E. Finn, J. M. Allen, A. D. Miller, J. S. Chamberlain and S. J. Tapscott (2012). "Successful regional delivery and long-term expression of a dystrophin gene in canine muscular dystrophy: a preclinical model for human therapies." Molecular Therapy **20**(8): 1501-1507.

Watchko, J. J. (2004). "Adeno-associated virus vector-mediated minidystrophin gene therapy improves dystrophic muscle contractile function in mdx mice." Human gene therapy **13**(12): 1451-1460.

Wehling, M., M. J. Spencer and J. G. Tidball (2001). "A nitric oxide synthase transgene ameliorates muscular dystrophy in mdx mice." The Journal of Cell Biology **155**(1): 123-132.

Weir, A. P., E. A. Burton, G. Harrod and K. E. Davies (2002). "A- and B-utrophin Have Different Expression Patterns and Are Differentially Up-regulated in mdx Muscle." Journal of Biological Chemistry **277**(47): 45285-45290.

Williams, A. H., N. Liu, E. Van Rooij and E. N. Olson (2009). "MicroRNA control of muscle development and disease." Current opinion in cell biology **21**(3): 461-469.

Williams, A. H., G. Valdez, V. Moresi, X. Qi, J. McAnally, J. L. Elliott, R. Bassel-Duby, J. R. Sanes and E. N. Olson (2009). "MicroRNA-206 delays ALS progression and promotes regeneration of neuromuscular synapses in mice." Science **326**(5959): 1549-1554.

Willmann, R., S. Possekel, J. Dubach-Powell, T. Meier and M. A. Ruegg (2009). "Mammalian animal models for Duchenne muscular dystrophy." Neuromuscular Disorders **19**(4): 241-249.

Wozniak, A. C., J. Kong, E. Bock, O. Pilipowicz and J. E. Anderson (2005). "Signaling satellite-cell activation in skeletal muscle: Markers, models, stretch, and potential alternate pathways." Muscle & Nerve **31**(3): 283-300.

Yancopoulos, G. D., S. Davis, N. W. Gale, J. S. Rudge, S. J. Wiegand and J. Holash (2000). "Vascular-specific growth factors and blood vessel formation." Nature **407**(6801): 242-248.

Yokota, T., Q. l. Lu, T. Partridge, M. Kobayashi, A. Nakamura, S. Takeda and E. Hoffman (2009). "Efficacy of systemic morpholino exon - skipping in duchenne dystrophy dogs." Annals of neurology **65**(6): 667-676.